The LINNEAN SOCIETY of London ZOOLOGICAL Journal of the Linnean Society

Zoological Journal of the Linnean Society, 2014, **170**, 400–466. With 40 figures

Herpetocetus morrowi (Cetacea: Mysticeti), a new species of diminutive baleen whale from the Upper Pliocene (Piacenzian) of California, USA, with observations on the evolution and relationships of the Cetotheriidae

JOSEPH J. EL ADLI[1,2]*, THOMAS A. DEMÉRÉ[1] and ROBERT W. BOESSENECKER[3,4]

[1]*Department of Paleontology, P.O. Box 121390, San Diego Natural History Museum, San Diego, California, 92112, USA*
[2]*Department of Earth and Environmental Sciences, University of Michigan, 1109 Geddes Avenue, Ann Arbor, Michigan, 48109, USA*
[3]*Department of Geology, University of Otago, P.O. Box 56, Dunedin, 9054, New Zealand*
[4]*University of California Museum of Paleontology, University of California, 1101 Valley Life Sciences Building, Berkeley, California, 94720, USA*

Received 24 August 2013; revised 18 October 2013; accepted for publication 21 October 2013

The extinct edentulous mysticete family Cetotheriidae historically has been viewed as a notoriously paraphyletic group, and only recently have rigorous studies been executed to rectify this issue. These problems do not necessarily just stem from lack of phylogenetic analyses, but are in part because of a general lack of complete specimens, poor descriptions of taxa, and long-lived taxonomic instability issues. The fossil mysticete genus *Herpetocetus* is a poster child of these problems as it is primarily only known from a few relatively incomplete and poorly described specimens. A new species of *Herpetocetus* from the upper Pliocene of California, ***Herpetocetus morrowi* sp. nov.**, provides an archetypal model for the genus based on a multitude of well-preserved specimens. These specimens reveal a diminutive mysticete characterized by an elongate rostrum and roughly quadrate cranium. A mosaic of primitive and derived features preserved in this new species underscores its potential value in helping to resolve a number of taxonomic and phylogenetic problems. The occurrence of specimens assignable to juvenile through to mature adult individuals provides a basis for investigating ontogenetic changes. Functional analysis of the unusual craniomandibular anatomy of *H. morrowi* suggests a limited degree of mandibular gape and an enhanced capacity for longitudinal rotation of the dentary, features that support a hypothesis of suction feeding convergent with that of living grey whales. A phylogenetic analysis provides support for recognition of a redefined and monophyletic Cetotheriidae and Herpetocetinae, and also serves as a basis for evaluating the recent proposal that the pygmy right whale (*Caperea marginata*) is a living cetothere. Morphological features of *Herpetocetus morrowi*, including features of the cranium and petrosal, suggest that a number of the purported synapomorphies supporting a *Caperea*–cetothere grouping are either symplesiomorphies, nonhomologous features, or are highly variable.

doi: 10.1111/zoj.12108

ADDITIONAL KEYWORDS: *Caperea* – functional morphology – palaeontology – phylogeny – systematics.

INTRODUCTION

The genus *Herpetocetus* has had a chequered nomenclatural history, and like most of the fossil cetacean taxa named by Van Beneden in the late 19th century, its status as a diagnosable taxon is questionable. Whitmore & Barnes (2008) provided the most recent review of the nomenclatural history of *Herpetocetus*, and relying on a complex series of assumptions and referred specimens of uncertain provenance, these

*Corresponding author. E-mail: jeladli@umich.edu

authors chose to retain the genus and assign to it several new species. Whitmore & Barnes (2008) also recognized a group of closely related small-bodied fossil mysticetes that they placed into a new subfamily, the Herpetocetinae. Unfortunately, as defined by these authors, herpetocetine membership was largely based on authority and was not formulated in the context of a cladistic phylogenetic analysis.

As defined by Whitmore & Barnes (2008), the genus *Herpetocetus* encompasses a relatively diverse and speciose group of fossil mysticetes that have been described from upper Miocene and Pliocene marine facies exposed on the east and west coasts of both the north Pacific and north Atlantic oceans. In 1872, Pierre-Joseph Van Beneden described the type species of *Herpetocetus*, *Herpetocetus scaldiensis* Van Beneden, 1872, based on a series of unassociated mysticete fossil remains from Antwerp, Belgium. These specimens, commissioned for collection by Bernard du Bus, were excavated by soldiers during construction of fortifications at Antwerp years before Van Beneden began work on the collections (Deméré, Berta & McGowen, 2005: 104). Several of the fossil specimens originally assigned to *H. scaldiensis* by Van Beneden have been found to actually represent different undescribed mysticete taxa (Deméré *et al*., 2005).

Unfortunately, Van Beneden did not select a type specimen for *Herpetocetus* either in his original manuscript or in his subsequent, beautifully illustrated monograph series published in 1882. It was not until Abel (1938) that IRSNB M.379 (formerly catalogued as IRSNB 14; O. Lambert pers. comm., February 2013), a left dentary included by Van Beneden in his original description of *H. scaldiensis*, was designated as the lectotype of *H. scaldiensis*. Whitmore & Barnes (2008) recently provided an extensive historical account of the specimens assigned by various authors to this species and noted that three specimens studied by Van Beneden (1882), a partial squamosal, a partial dentary, and an atlas, are possibly from the same individual and could serve as cotypes of *H. scaldiensis*. If correct, these specimens (IRSNB 405, 137, and 355, respectively) would make it possible to associate the unique mandibular morphology of the lectotype dentary with portions of the cranium and axial skeleton. However, because of the poorly documented and apparently haphazard method of collection of all of these specimens, it does not seem likely that they belong to the same individual and it is just as scientifically erroneous now, as it was in the original description by Van Beneden, to assign them to the same taxon in the absence of clear association.

Owing to the current lack of specimens of *H. scaldiensis* from Belgium possessing clearly associated cranial and mandibular material, referral of isolated cranial and postcranial material from these strata is unreasonable. Therefore, referred specimens of *H. scaldiensis* must be critically reassessed. The authors do not, however, doubt that referred specimens of *H. scaldiensis* (IRSNB 405 and USNM 336361) should be designated as herpetocetines based on similar morphological features documented in more complete herpetocetine specimens that do possess cranial material and associated dentaries (i.e. UCMP 124950). However, given the dubious history regarding the lectotype specimen it is unreasonable to assume that these referred specimens are assignable to *H. scaldiensis*. This study will consider specimens referred to *H. scaldiensis* by other workers (i.e. IRSNB 405 and USNM 336361 by Whitmore & Barnes, 2008) as not belonging to *H. scaldiensis*, and therefore will discuss them, and their position within Herpetocetinae, independently from IRSNB M.379. This approach was followed in order to allow for comparison with other herpetocetines, which merits consideration even if it is possible that referral of these specimens to *H. scaldiensis* is inaccurate.

The type locality of *H. scaldiensis* is equivocal and its ultimate designation has major implications for the age of the specimen. The marine sedimentary facies in the vicinity of Antwerp, Belgium, and from which IRSNB M.379 may have been collected, are of the obsolete Diestian and Scaldisian stages. These stages correspond to the Late Tortonian to Messinian (Louwye & Laga, 1998) and Zanclean to Early Piacenzian, respectively. Dollo (1909: 116) listed *H. scaldiensis* in the fauna recovered from marine sandstones of the local Bolderian Stage, assumed at the time to be Late Miocene in age but now assigned to the lower to middle Miocene (Louwye *et al*., 2000; Laga, Louwye & Geets, 2001), whereas Abel (1938: 22) indicated that the lectotype dentary was collected from Upper Miocene deposits (Anversian). Whitmore & Barnes (2008) concluded that the locality of the lectotype for *H. scaldiensis* was most likely Scaldisian in age based on Van Beneden's reference to the 'sable gris' (Van Beneden, 1882) as the locality for *H. scaldiensis*. In their paper, Whitmore & Barnes interpreted the 'sable gris' to be the sables à *Isocardia cor* (Scaldisian in age), but dismissed, without evidence, the possibility that IRSNB M.379 may have originated from another layer of grey sands described by de Heinzelin (1955) that correspond to the latest Diestian Stage. Van Beneden (in Mourlon, 1876) expressed that *Herpetocetus* was recovered from Diestian age rock units based on association with other macrofauna. Referred specimens of *H. scaldiensis* (e.g. USNM 336361) collected by Paul L. Gigase and discussed by Whitmore & Barnes (2008) have been found in Pliocene age deposits, the

Kattendijk sands (Zanclean) and Ooederen sands (Piacenzian) at Antwerp, Belgium. This clearly demonstrates that herpetocetines were present in the north-east Atlantic during the Pliocene. Regardless of the lack of reliable provenance for the *H. scaldiensis* lectotype, it is reasonable to assume that species of *Herpetocetus* were present within the late Miocene to Early Pliocene and that the precise locality where IRSNB M.379 was collected has been lost in time.

A second species of *Herpetocetus* has been described from the Zanclean age Tatsunokuchi Formation of Sendai, Japan, by Hatai, Hayasaka & Masuda (1963) as '*Mitzuhoptera*' *sendaicus*, the holotype of which is an isolated, partial tympanic bulla (IGPS 78423). Oishi & Hasegawa (1994) reassigned '*M.*' *sendaicus* to *Herpetocetus* based on comparison of the holotype tympanic bulla to a referred partial skeleton (NSMT-PV 19540) collected from the Lower Pliocene Yushima Formation of Iwate Prefecture, Japan. Although NSMT-PV 19540 is undoubtedly a herpetocetine mysticete, the assignment of this specimen to *Herpetocetus sendaicus* is problematic because of the incompleteness of the holotype tympanic bulla. The fact that the tympanic bullae of *Herpetocetus* do not allow for clear differentiation amongst species suggests that description of a new species within the genus based solely on a partial, isolated tympanic bulla should be discouraged. Therefore the authors agree with the opinion of Boessenecker (2011a: 2) and suggest the consideration of *H. sendaicus* as a *nomen dubium*. However, although the taxonomic name *H. sendaicus* will not be further considered, the NSMT-PV 19540 skeleton will be discussed because of its completeness relative to other known herpetocetine skeletons.

Whitmore & Barnes (2008) described two new species of *Herpetocetus* from the east and west coast of the USA. *Herpetocetus transatlanticus* was discovered *ex situ* in a spoil pile at the Lee Creek phosphate mine in Aurora, North Carolina (Whitmore & Barnes, 2008). Whitmore & Barnes (2008) suggested, through written communications from T. G. Gibson, that the matrix containing the holotype of *H. transatlanticus* originated from the Sunken Meadow member of the Yorktown Formation (Lower Pliocene, Zanclean). The holotype specimen itself (USNM 182962) is a partial cranium that is missing the rostrum, the distal portions of the supraorbital processes of the frontals, and all but the anterior-most portions of the supraoccipital and the right parietal. USNM 182962 contains both tympanic bullae, as well as both petrosals. Several isolated squamosals, bullae, and petrosals were also referred to the species by Whitmore & Barnes (2008).

Herpetocetus bramblei, a second species described by Whitmore & Barnes (2008), is represented by UCMP 82465, which contains the left portion of the braincase, left petrosal, distal portion of the left supraorbital process of the frontal, fragment of the descending process of the right maxilla, and an incomplete right dentary. The type locality of *H. bramblei* is the Mio-Pliocene aged Purisima Formation at Opal Cliffs in Santa Cruz County, California. Whitmore & Barnes (2008) noted that UCMP 82465 was collected from above the basal unconformity of the Purisima Formation, which has yielded a glauconite K/Ar date of 6.9 ± 0.5 Mya, and that the *H. bramblei* type locality was 'probably somewhat younger'. Therefore, these authors suggested a latest Miocene to earliest Pliocene age. Furthermore, UCMP 82465 was collected from UCMP locality V6875, a widespread shell-rich bonebed with abundant crustacean elements and wood fragments, which Powell *et al*. (2007) identified based on palaeomagnetism and microfossils as the 5.33 Mya Miocene–Pliocene boundary.

Recently, several well-preserved, referred specimens of *H. bramblei* including several crania, isolated petrosals, tympanic bullae, and dentaries have been recovered from UCMP localities V6875, V90042, and V99854 in the Purisima Formation near Santa Cruz and San Gregorio (Boessenecker & Geisler, 2008; Boessenecker, in press), which have greatly expanded the morphological information available on the species. These new specimens from the Purisima Formation indicate a latest Miocene (6.4–5.33 Mya) age for *H. bramblei*. Additionally, new specimens from the Pliocene parts of the San Gregorio and Santa Cruz sections of the Purisima Formation near Half Moon Bay and Santa Cruz, respectively, have produced fossil material of a new species of *Herpetocetus* (Boessenecker, in press). Finally, an unexpected record of *Herpetocetus* has recently been reported from the early–middle Pleistocene Falor Formation of Humboldt County in northern California, indicating that herpetocetines nearly survived to modern times (Boessenecker, 2013).

It is clear that *Herpetocetus* is plagued by a multitude of nomenclatural problems stemming from designation of new species based on poorly preserved specimens and isolated elements that cast doubt upon the diagnosability of the genus. Recent studies of mandibular morphology in herpetocetines (Boessenecker, 2011a) have shown conservatism amongst the morphology of different species of *Herpetocetus*. Boessenecker (2011a) suggested that the similar morphology of herpetocetine dentaries from the Santa Margarita Sandstone of California, which are considerably older (i.e. Tortonian) than any demonstrable specimens of *Herpetocetus*, could indicate that the general dentary morphology of *Herpetocetus* actually evolved prior to divergence of *Herpetocetus* from its sister taxa (*Nannocetus* Kellogg, 1929; and *Piscobalaena* Pilleri & Siber, 1989). Thus, the distinctive

morphology of the dentary may be only apomorphic at higher taxonomic levels and therefore pleisiomorphic at the genus and species level. This hypothesis will be further demonstrated in future publications of undescribed mysticetes from the Miocene of southern California.

The association of '*Herpetocetus*-like' dentaries with clearly distinct, non-*Herpetocetus* herpetocetine skulls is exceptionally problematic for the stability of the genus because of the establishment of an isolated dentary as the lectotype of the type species of *Herpetocetus*. Furthermore, if the specimens referred to *H. scaldiensis* by Van Beneden (1872) and Whitmore & Barnes (2008) cannot be reasonably assigned to that species (because of the stratigraphical, temporal, and taxonomic uncertainty associated with the lectotype and referred specimens), then it is questionable to refer any new specimens and taxa to *Herpetocetus* that do not at least include a dentary. The severity of this taxonomic and nomenclatural problem is deepened with the increasing body of evidence that the 'unique' dentary morphology of the lectotype of *H. scaldiensis* may not only be undiagnostic at the species level, but may not even be diagnostic at the genus level.

Given this more than century-long nomenclatural and taxonomic conundrum, there are several solutions available. One solution would be to petition the ICZN for the designation of a neotype, as has been suggested by previous authors (e.g. Deméré *et al*., 2005), whereas another solution would be to declare *H. scaldiensis* a *nomen dubium* and erect a new genus to contain the current diversity of *Herpetocetus* species. Either of these solutions would be a drawn-out affair, and are beyond the scope of this paper. Therefore, the more pressing (and arguably more interesting) topics of phylogenetic relationships, character evolution, and functional anatomy will be the focus of this study. As a way of highlighting the significance of these topics, species of *Herpetocetus* have played a central role in several recent studies (Fordyce & Marx, 2012) of mysticete evolution and the phylogenetic relationships of the enigmatic neobalaenid, *Caperea marginata* Gray, 1864. For these reasons we have chosen to provisionally accept the conclusions of Whitmore & Barnes (2008) concerning the phylogenetic definition of *Herpetocetus* (i.e. taxonomic membership of the genus) in our description and discussion of a new species of herpetocetine mysticete from the Pliocene marine deposits of southern California, USA.

MATERIAL AND METHODS

Measurements under 300 mm were made to the nearest tenth of a millimetre with Carrera Precision digital callipers, whereas measurements larger than 300 mm were made to the nearest millimetre with larger vernier callipers. Angular measurements were taken to the nearest degree using a handheld goniometer and the image processing program ImageJ (Rasband, 1997). Some aspects of the holotype skull of *H. morrowi* were studied using computed tomography (CT).

Institutional acronyms for housed specimens utilized in this study are as follows: AMNH, American Museum of Natural History, New York City, New York, USA; CASG, California Academy of Sciences, Department of Geology, San Francisco, California, USA; ChM PV, Charleston Museum, Charleston, North Carolina, USA; FMNH, Field Museum of Natural History, Chicago, Illinois, USA; HSU, Humboldt State University Vertebrate Museum, Arcata, California, USA; IGPS, Institute of Geology and Paleontology, Tohoku University, Sendai, Japan; IRSNB, Institut Royal des Sciences Naturelles de Belgique, Brussels, Belgium; LACM, Natural History Museum of Los Angeles County, Los Angeles, USA; MMG, Museu Mineralógico e Geológico da Universidade de Lisboa, Lisbon, Portugal; MNHN, Muséum National d'Histoire Naturelle, Paris, France; MR, Royal Museum of Natural History, Brussels, Belgium; MSNM, Museo di Storia Naturale di Milano, Milan, Italy; MSNT, Museo di Storia Naturale e del Territorio dell'universita di Pisa, Pisa, Italy; MVZ, University of California, Berkeley Museum of Vertebrate Zoology, Berkeley, California, USA; NMV, National Museum of Victoria, Melbourne, Australia; NSMT-PV, Section of Vertebrate Paleontology, Department of Geology, National Science Museum, Tokyo, Japan; SAM, South Australian Museum, Adelaide, Australia; SDNHM, San Diego Natural History Museum, San Diego, California, USA; UCMP, University of California Museum of Paleontology, Berkeley, California, USA; UO, Museum of Natural History, University of Oregon, Eugene, Oregon, USA; USNM, National Museum of Natural History, Smithsonian Institution, Washington, DC, USA.

SYSTEMATICS

CETACEA BRISSON, 1762

MYSTICETI GRAY, 1864

CHAEOMYSTICETI MITCHELL, 1989

CETOTHERIIDAE BRANDT, 1872

HERPETOCETINAE STEEMAN, 2007; *SENSU* WHITMORE AND BARNES, 2008

HERPETOCETUS VAN BENEDEN, 1872

Type species

Herpetocetus scaldiensis Van Beneden, 1872

Distribution
Late Miocene and Pliocene of California, North Carolina, Belgium, and Japan

Included species
Herpetocetus transatlanticus (Whitmore & Barnes, 2008), *Herpetocetus bramblei* (Whitmore & Barnes, 2008), *Herpetocetus morrowi* sp. nov., and *Herpetocetus* sp. nov. (Oishi & Hasegawa, 1994).

Diagnosis
A genus of small-bodied mysticete with a narrowly elongated angular process of the dentary that projects well posterior to the posterior surface of the mandibular condyle; with a postparietal foramen penetrating the posteroventral corner of the parietal on the temporal wall at a triple junction amongst the parietal, squamosal, and alisphenoid; with an anteroposteriorly large alisphenoid that makes up a significant portion of the temporal wall and is exposed along the entire ventral border of the parietal; with ascending processes of the maxilla that medially abut and dorsally cover the posterior segments of the nasals; with postglenoid process that is strongly rotated anterolaterally to be aligned with the lateral edge of the skull and resulting in an anteromedially orientated glenoid fossa (synapomorphies of species of *Herpetocetus*).

HERPETOCETUS MORROWI SP. NOV.

Diagnosis
A species of *Herpetocetus* with premaxillary eminences that dorsally overlap the maxilla, with a facial nerve sulcus on the posterior process of the petrosal that is completely enclosed to form a facial nerve canal, with a distinct notch for the lingual nerve posteroventral to the mandibular foramen on the dentary (autapomorphies of *H. morrowi*).

Holotype
UCMP 129450 – nearly complete skull including both tympanic bullae, both petrosals, a right malleus, a nearly complete left dentary, ten associated vertebrae including the atlas and axis, rib fragments, and a humerus. Collected by James Pitt and Lawrence G. Barnes, 14.vii.1971 (Fig. 1). Skull reprepared by J. J. El Adli in 2009 at SDNHM. Collected from UCMP Locality V-73130, Texas Street 1, San Diego, San Diego County, California, USA; San Diego Formation, Late Pliocene (Piacenzian, ~2.5–3.5 Mya).

Paratypes
SDNHM 65781 – nearly complete skull missing the supraoccipital shield, parietals, frontals, nasals, and posterior portions of maxillae and premaxillae. Collected by Bradford O. Riney, 2.vii.1990 from SDNHM Locality 3553, Rancho Del Rey, SPA 1, Chula Vista, San Diego County, California, USA; San Diego Formation, member 4, Late Pliocene (Piacenzian, ~2.5–3.5 Mya).

SDNHM 130390 – nearly complete skull missing the supraoccipital shield and left squamosal. Collected by Richard A. Cerutti and Bradford O. Riney, 14.viii.1990 from SDNHM Locality 3575, Rancho Del Rey, SPA 1, Chula Vista, San Diego County, California, USA; San Diego Formation, member 4, Late Pliocene (Piacenzian, ~2.5–3.5 Mya).

Referred specimens
SDNHM 34155 – partial skull consisting of left half of cranium, left petrosal and tympanic bulla, and major portions of the posterior regions of the rostrum. Collected by Richard A. Cerutti and Donald R. Swanson, 6.v.1987 from SDNHM Locality 3397, H Street Widening, Chula Vista, San Diego County, California, USA; San Diego Formation, member 5, Late Pliocene (Piacenzian, ~2.5–3.5 Mya).

SDNHM 90484 – partial basicranium preserving the basioccipital, basisphenoid, and portions of the right exoccipital, the right and left squamosals, and right and left pterygoids. Collected by Richard A. Cerutti, 3.x.2001 from SDNHM Locality 4873, Otay Ranch, Village 1, Chula Vista, San Diego County, California, USA; San Diego Formation, member 4, Late Pliocene (Piacenzian, ~2.5–3.5 Mya).

SDNHM 125833 – left squamosal. Collected by Richard A. Cerutti and Donald R. Swanson, 6.v.1987 from SDNHM Locality 3397, H Street Widening, Chula Vista, San Diego County, California, USA; San Diego Formation, member 5, Late Pliocene (Piacenzian, ~2.5–3.5 Mya).

SDNHM 35907 – partial right squamosal. Collected by Margo C. Rausch, 2.iv.1983 from SDNHM Locality 3158C, Hidden Vista Village, Chula Vista, San Diego County, California, USA; San Diego Formation, member 3 or 4, Late Pliocene (Piacenzian, ~2.5–3.5 Mya).

SDNHM 38213 – partial left squamosal. Collected by Matthew W. Cerutti, 30.xii.1988, from SDNHM Locality 3460, Walrus Channel, National City, San Diego County, California, USA; San Diego Formation, Late Pliocene (Piacenzian, ~2.5–3.5 Mya).

SDNHM 42758 – associated presphenoid and vomer. Collected by Bradford O. Riney and Richard A. Cerutti, 11.ii.1988 from SDNHM Locality 3418, Bel Air Ridge, Chula Vista, San Diego County, California, USA; San Diego Formation, member 4, Late Pliocene (Piacenzian, ~2.5–3.5 Mya).

SDNHM 59976 – partial rostrum. Collected by Richard A. Cerutti, 15.viii.1981 from SDNHM Locality 3158, Hidden Vista Village, Chula Vista, San

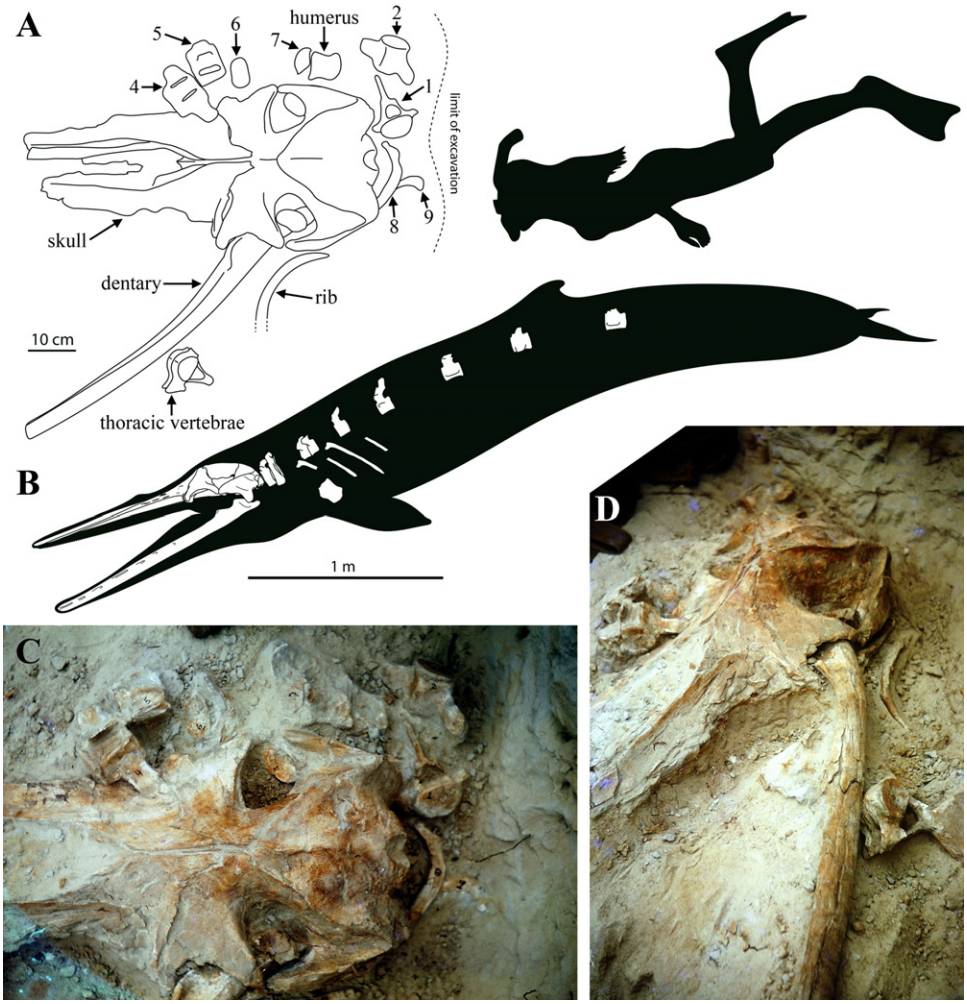

Figure 1. ***Herpetocetus morrowi*** **sp. nov.** A, illustrated quarry map of UCMP 124950 as discovered in the field showing the configuration of visible bone elements; B, inferred position of known bone elements of *H. morrowi* within the body; C, overhead view of the field excavation of UCMP 124950; D, oblique view of the field excavation of UCMP 124950. Numbers in A are those assigned in the field during excavation of the specimen as referred to in the text: 1, lumbar(?) vertebra; 2, lumbar vertebra; 4, lumbar vertebra; 5, lumbar vertebra; 6, thoracic vertebra; 7, vertebral epiphysis; 8, rib; 9, rib.

Diego County, California, USA; San Diego Formation, Late Pliocene (Piacenzian, ~2.5–3.5 Mya).

SDNHM 38689 – associated right petrosal and tympanic bulla. Collected by Richard A. Cerutti, 11.ii.1988 from SDNHM Locality 3418, Bel Air Ridge, Chula Vista, San Diego County, California, USA; San Diego Formation, member 4, Late Pliocene (Piacenzian, ~2.5–3.5 Mya).

SDNHM 63690 – left petrosal lacking posterior process. Collected by Museum field party, 18.vii.1996 from SDNHM Locality 4047, Rancho Del Rey, SPA 4, Chula Vista, San Diego County, California, USA; San Diego Formation, member 4, Late Pliocene (Piacenzian, ~2.5–3.5 Mya).

SDNHM 23633 – right tympanic bulla missing medial margin. Collected by Norman Brown, v.1977 from SDNHM Locality 2970A, Washington Street-Western Cut, San Diego, San Diego County, California, USA; San Diego Formation, Late Pliocene (Piacenzian, ~2.5–3.5 Mya).

SDNHM 35280 – right tympanic bulla (immature). Collected by Bradford O. Riney, 18.ii.1988 from SDNHM Locality 3418, Bel Air Ridge, Chula Vista, San Diego County, California, USA; San Diego Formation, member 4, Late Pliocene (Piacenzian, ~2.5–3.5 Mya).

SDNHM 42754 – partial involucrum of right tympanic bulla. Collected by Ray Havens, 1959 from SDNHM Locality 690, Haven's Cave, San Diego, San Diego County, California, USA; San Diego Formation, Late Pliocene (Piacenzian, ~2.5–3.5 Mya).

SDNHM 63691 – right tympanic bulla with damaged medial margin. Collected by SDNHM field party, 18.vii.1996 from SDNHM Locality 4047, Rancho Del Rey, SPA 3, Chula Vista, San Diego County, California, USA; San Diego Formation, member 4, Late Pliocene (Piacenzian, ~2.5–3.5 Mya).

SDNHM 23373 – involucrum of left tympanic bulla. Collected by Richard A. Cerutti, 1980 from SDNHM Locality 3016, Paradise Valley, National City, San Diego County, California, USA; San Diego Formation, Late Pliocene (Piacenzian, ~2.5–3.5 Mya).

SDNHM 35875 – involucrum of left tympanic bulla. Collected by Richard A. Cerutti and Donald R. Swanson, 8.v.1987 from SDNHM Locality 3397, H Street Widening, Chula Vista, San Diego County, California, USA; San Diego Formation, member 5, Late Pliocene (Piacenzian, ~2.5–3.5 Mya).

SDNHM 42657 – involucrum of damaged left tympanic bulla. Collected by SDNHM field party, 1990 from SDNHM Locality 3506, Rancho Del Rey, SPA 1, Chula Vista, San Diego County, California, USA; San Diego Formation, member 4, Late Pliocene (Piacenzian, ~2.5–3.5 Mya).

SDNHM 63255 – left tympanic bulla missing medial margin. Collected by Gino Calvano, 31.v.1995 from SDNHM Locality 3982, Rancho Del Rey, SPA 3, Chula Vista, San Diego County, California, USA; San Diego Formation, member 4, Late Pliocene (Piacenzian, ~2.5–3.5 Mya).

SDNHM 77272 – left tympanic bulla (immature). Collected by Richard A. Cerutti, 15.vi.1981 from SDNHM Locality 3158B, Blue Bonnet Court, National City, San Diego County, California, USA; San Diego Formation, Late Pliocene (Piacenzian, ~2.5–3.5 Mya).

SDNHM 24600 – partial right dentary missing anterior 5% of ramus, and entire mandibular condyle and angular process. Collected by Robert L. Clark, xii.1982 from SDNHM Locality 2969, Washington Street, San Diego, San Diego County, California, USA; San Diego Formation, Late Pliocene (Piacenzian, ~2.5–3.5 Mya).

SDNHM 25071 – partial right dentary missing posterior 50% of ramus. Collected by Richard A. Cerutti, 1981 from SDNHM Locality 3006, Hidden Vista Village, Chula Vista, San Diego County, California, USA; San Diego Formation, member 2, Late Pliocene (Piacenzian, ~2.5–3.5 Mya).

SDNHM 25117 – partial horizontal ramus of right dentary. Collected by Richard A. Cerutti, 13.v.1981 from SDNHM Locality 3182, Hidden Vista Village, Chula Vista, San Diego County, California, USA; San Diego Formation, Late Pliocene (Piacenzian, ~2.5–3.5 Mya).

SDNHM 30746 – anterior tip of right dentary. Collected by Richard A. Cerutti, xi.1983 from SDNHM Locality 4392, El Rancho Del Rey, Unit 6A, Chula Vista, San Diego County, California, USA; San Diego Formation, member 6, Late Pliocene (Piacenzian, ~2.5–3.5 Mya).

SDNHM 35294 – damaged right dentary missing middle portion of ramus. Collected by Bradford O. Riney and Richard A. Cerutti, 16.ii.1988 from SDNHM Locality 3419, Bel Air Ridge, Chula Vista, San Diego County, California, USA; San Diego Formation, member 2, Late Pliocene (Piacenzian, ~2.5–3.5 Mya).

SDNHM 35985 – partial right dentary missing posterior 10% of ramus. Collected by Richard A. Cerutti, 19.ii.1988 from SDNHM Locality 3418, Belair Ridge, Chula Vista, San Diego County, California, USA; San Diego Formation, member 4, Late Pliocene (Piacenzian, ~2.5–3.5 Mya).

SDNHM 38679 – partial right dentary missing posterior 20% of ramus. Collected by Richard A. Cerutti, 18.xi.1989 from SDNHM Locality 3489, Rancho Del Rey, SPA 1, Chula Vista, San Diego County, California, USA; San Diego Formation, member 4, Late Pliocene (Piacenzian, ~2.5–3.5 Mya).

SDNHM 63096 –right dentary missing angular process and portion of mandibular condyle. Collected by Robert Q. Gutzler, 22.iii.1995 from SDNHM Locality 3986, Rancho Del Rey, SPA 3, Chula Vista, San Diego County, California, USA; San Diego Formation, member 4, Late Pliocene (Piacenzian, ~2.5–3.5 Mya).

SDNHM 63127 – partial ramus of right dentary. Collected by Richard A. Cerutti, 2.xii.1996 from SDNHM Locality 4055, Rancho Del Rey, SPA 3, Chula Vista, San Diego County, California, USA; San Diego Formation, member 4, Late Pliocene (Piacenzian, ~2.5–3.5 Mya).

SDNHM 63256 – partial right dentary missing coronoid crest, mandibular condyle, and angular process. Collected by Richard A. Cerutti and Gino Calvano, 31.v.1995 from SDNHM Locality 3982, Rancho Del Rey, SPA 3, Chula Vista, San Diego County, California, USA; San Diego Formation, member 4, Late Pliocene (Piacenzian, ~2.5–3.5 Mya).

SDNHM 63257 – partial right dentary missing angular process and portion of mandibular condyle. Collected by Richard A. Cerutti, 26.v.1995 from SDNHM Locality 3982, Rancho Del Rey, SPA 3, Chula Vista, San Diego County, California, USA; San Diego Formation, member 4, Late Pliocene (Piacenzian, ~2.5–3.5 Mya).

SDNHM 65780 – partial ramus of right dentary. Collected by Richard A. Cerutti, 15.v.1990 from SDNHM Locality 3628, Rancho Del Rey, SPA 1, Chula Vista, San Diego County, California, USA; San Diego Formation, member 5, Late Pliocene (Piacenzian, ~2.5–3.5 Mya).

SDNHM 83694 – nearly complete right dentary missing anterior 25% of ramus. Collected by Chad Herrington and Scott Musick, 1.viii.2000 from SDNHM Locality 4519, Sunbow, Phase 1C, Chula Vista, San Diego County, California, USA; San Diego Formation, member 2, Late Pliocene (Piacenzian, ~2.5–3.5 Mya).

SDNHM 22386 – partial left dentary. Collected by Richard A. Cerutti, 19.i.1992 from SDNHM Locality 3088C, Philipino Gardens, National City, San Diego County, California, USA; San Diego Formation, Late Pliocene (Piacenzian, ~2.5–3.5 Mya).

SDNHM 23057 – partial left dentary missing anterior 75% of ramus. Collected by Richard A. Cerutti, 21.iii.1981 from SDNHM Locality 2970A, Washington Street, San Diego, San Diego County, California, USA; San Diego Formation, Late Pliocene (Piacenzian, ~2.5–3.5 Mya).

SDNHM 32138 – partial left dentary missing anterior 10% of ramus and apex of angular process. Collected by Richard A. Cerutti and Bradford O. Riney, 11.vi.1982 from SDNHM Locality 4404, El Rancho Del Rey, Chula Vista, San Diego County, California, USA; San Diego Formation, member 8, Late Pliocene (Piacenzian, ~2.5–3.5 Mya).

SDNHM 38293 – partial left dentary missing angular process and mandibular condyle. Collected by Donald R. Swanson, 7.ix.1988 from SDNHM Locality 3581, Rancho Del Rey, SPA 1, Chula Vista, San Diego County, California, USA; San Diego Formation, member 4, Late Pliocene (Piacenzian, ~2.5–3.5 Mya).

SDNHM 63258 – partial left dentary, missing posterior half. Collected by Richard A. Cerutti and Robert Q. Gutzler, 31.v.1995 from SDNHM Locality 3982, Rancho Del Rey SPA 3, Chula Vista, San Diego County, California, USA; San Diego Formation, member 4, Late Pliocene (Piacenzian, ~2.5–3.5 Mya).

SDNHM 68530 – partial left dentary missing angular process and anterior 50% of ramus. Collected by Bradford O. Riney, 16.ix.1998 from SDNHM Locality 4181, Chula Vista Veteran's Home, Chula Vista, San Diego County, California, USA; San Diego Formation, member 4, Late Pliocene (Piacenzian, ~2.5–3.5 Mya).

SDNHM 124132 – anterior 25% of left dentary. Collected by Patrick J. Sena, 21.iii.2007 from SDNHM Locality 6066, Otay Ranch Village 2 North, Chula Vista, San Diego County, California, USA; San Diego Formation, member 1, Late Pliocene (Piacenzian, ~2.5–3.5 Mya).

SDNHM 68537–15 associated vertebrae and ribs. Collected by Bradford O. Riney, 15.vii.1998 from SDNHM Locality 4183, Chula Vista Veteran's Home, Chula Vista, San Diego County, California, USA; San Diego Formation, member 4, Late Pliocene (Piacenzian, ~2.5–3.5 Mya).

SDNHM 90509 – associated cervical, thoracic, and lumbar vertebrae and ribs. Collected by Patrick J. Sena, 29.x.2001 from SDNHM Locality 4878, Otay Ranch Village 1 West, Chula Vista, San Diego County, California, USA; San Diego Formation, member 1, Late Pliocene (Piacenzian, ~2.5–3.5 Mya).

Morphological description

Skull

General features of the skull: Except where noted, the following description of the skull of *H. morrowi* is based on features preserved in the holotype, UCMP 124950. The holotype skull consists of a relatively complete cranium and a nearly complete rostrum (Figs 2–8). Some portions of the skull are missing and presumably were damaged either during diagenesis and/or during recovery of the specimen. These missing areas include the anterior portions of both maxillae and premaxillae; major portions of the extreme lateral margins of both maxillae; the anterior

Figure 2. ***Herpetocetus morrowi*** **sp. nov.**, UCMP 124950, holotype skull in dorsal view. Scale bar = 10 cm.

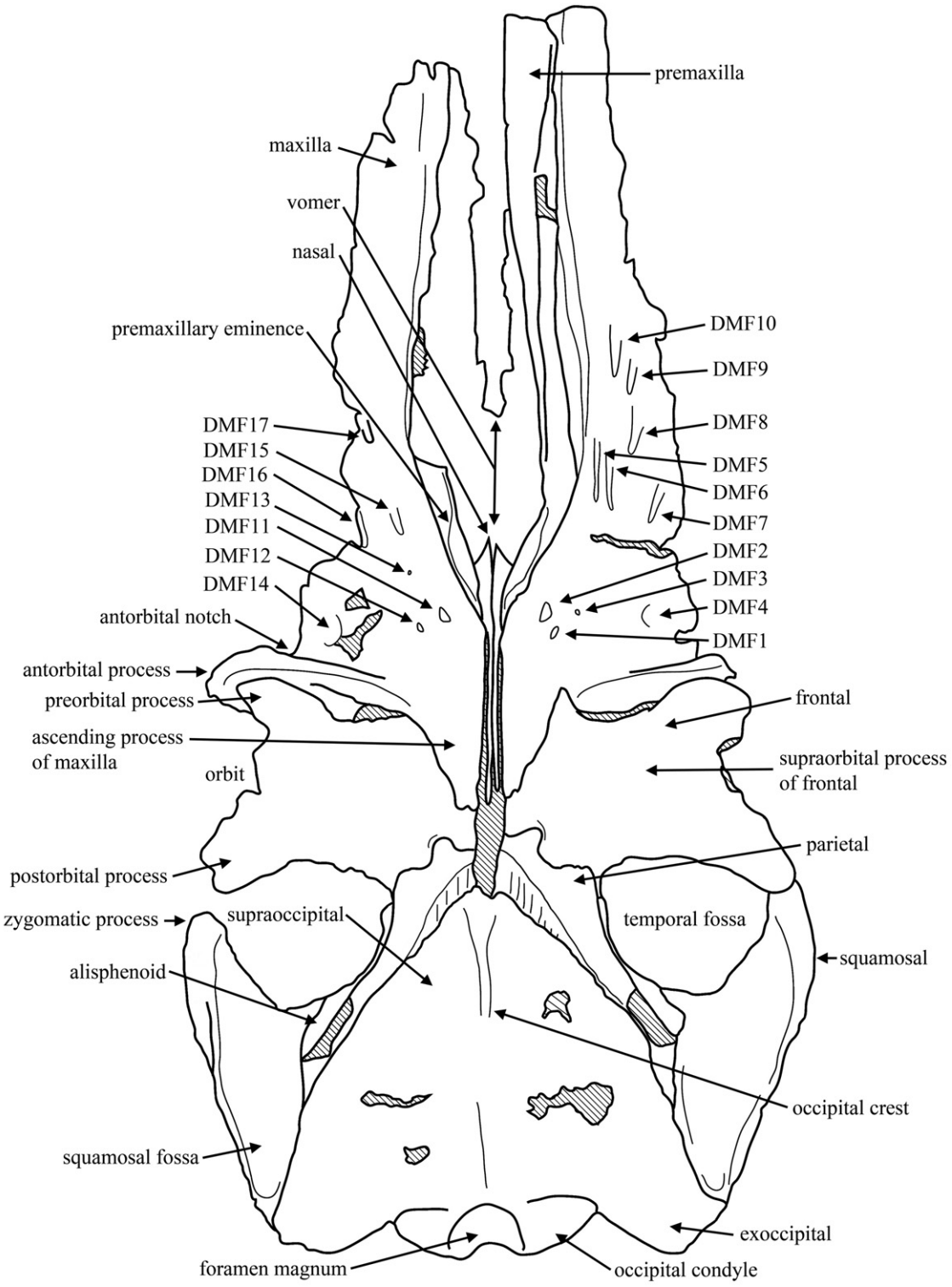

Figure 3. ***Herpetocetus morrowi*** **sp. nov.**, UCMP 124950, illustrated holotype skull in dorsal view showing anatomical features. DMF, dorsal maxillary foramen. Scale bar = 10 cm.

Figure 4. ***Herpetocetus morrowi*** **sp. nov.**, UCMP 124950, holotype skull in ventral view. Scale bar = 10 cm.

portion of the vomer; the distal portion of the antorbital process of the right maxilla; the orbital rim of both supraorbital processes of the frontal; the distal portion of the postorbital process of the left frontal; the right and left lacrimals and jugals; the apex of the supraoccipital shield; the anterior tip of both zygomatic processes of the squamosal; the anterior portion of both pterygoid hamuli; the anteromedial portion of both falciform processes of the squamosal; the ventral margin of both postglenoid processes of the squamosal; much of the right tympanic bulla, as well as the sigmoid processes of both tympanic bullae. The right and left maxillae, premaxillae, nasals, frontals, and parietals have separated along the sagittal plane, post-mortem, forming a gap between corresponding adjacent bones. The ascending process of the left maxilla has shifted anteriorly, creating a slight separation between the posterior edge of the descending process of the maxilla and the anterior border of the supraorbital process of the frontal. In dorsal aspect, the cranial elements have undergone some degree of counter-clockwise torque, which has resulted in offset of the anterior edge of the supraoccipital shield from its *in vivo* position, separation of the anterior edge of the left parietal and alisphenoid away from the frontal, and displacement of the left zygomatic process of the squamosal from its natural contact with the left postorbital process of the frontal. This minor offset has left the majority of the right side of the skull intact, maintaining much of the original cranial architecture. The anterior portion of the left premaxilla has been removed just beyond the anterior extension of the nasals for study. The right tympanic bulla was also removed to reveal the associated petrosal.

Herpetocetus morrowi is one of the smallest known edentulous mysticetes, with a reconstructed condylobasal length for the holotype skull of ~908 mm and a bizygomatic width of 356 mm (Fig. 1B). The estimated condylobasal length is based on an assumed morphometric relationship between condylobasal length and bizygomatic width and utilizes measurements from the paratype skull, SDNHM 65781, which has a preserved condylobasal length of 1008 mm and a bizygomatic width of 395 mm (Fig. 9). The largest known skull of *H. morrowi*, SDNHM 130390, has a condylobasal length of ~1200 mm and an estimated bizygomatic width of ~400 mm (Figs 10, 11). For comparison, specimens of *Piscobalaena nana* have estimated skull lengths that range from ~833 to ~1050 mm and bizygomatic widths of 324 to 433 mm, respectively (Bouetel & de Muizon, 2006). The holotype skull of *H. morrowi* is absolutely smaller in zygomatic and exoccipital width than the holotype crania of *H. transatlanticus* and *H. bramblei*. It is noteworthy that the holotype skull of *H. morrowi* is probably a subadult based on the degree of closure of cranial sutures, as is the holotype cranium of *H. transatlanticus* (Whitmore & Barnes, 2008). In contrast, the holotype of *H. bramblei* is thought to represent a fully mature individual (Whitmore & Barnes, 2008).

Perhaps the most obvious general aspects of the overall skull are its relatively attenuated and dorsoventrally flatted rostrum and its quadrate cranium. The attenuated and flattened rostrum and quadrate cranium are features shared with *Pi. nana*, as well as certain other small-bodied cetotheriids like *Cephalotropis coronatus* Cope, 1896 and *Cetotherium rathkii* Brandt, 1843. Other named species of *Herpetocetus* probably also had similarly configured rostra and crania.

The level of telescoping exhibited by *H. morrowi*, as with all herpetocetines, represents a mosaic of both plesiomorphic and apomorphic features. Plesiomorphic features include: the anterior position of the narial fossa well anterior to the antorbital

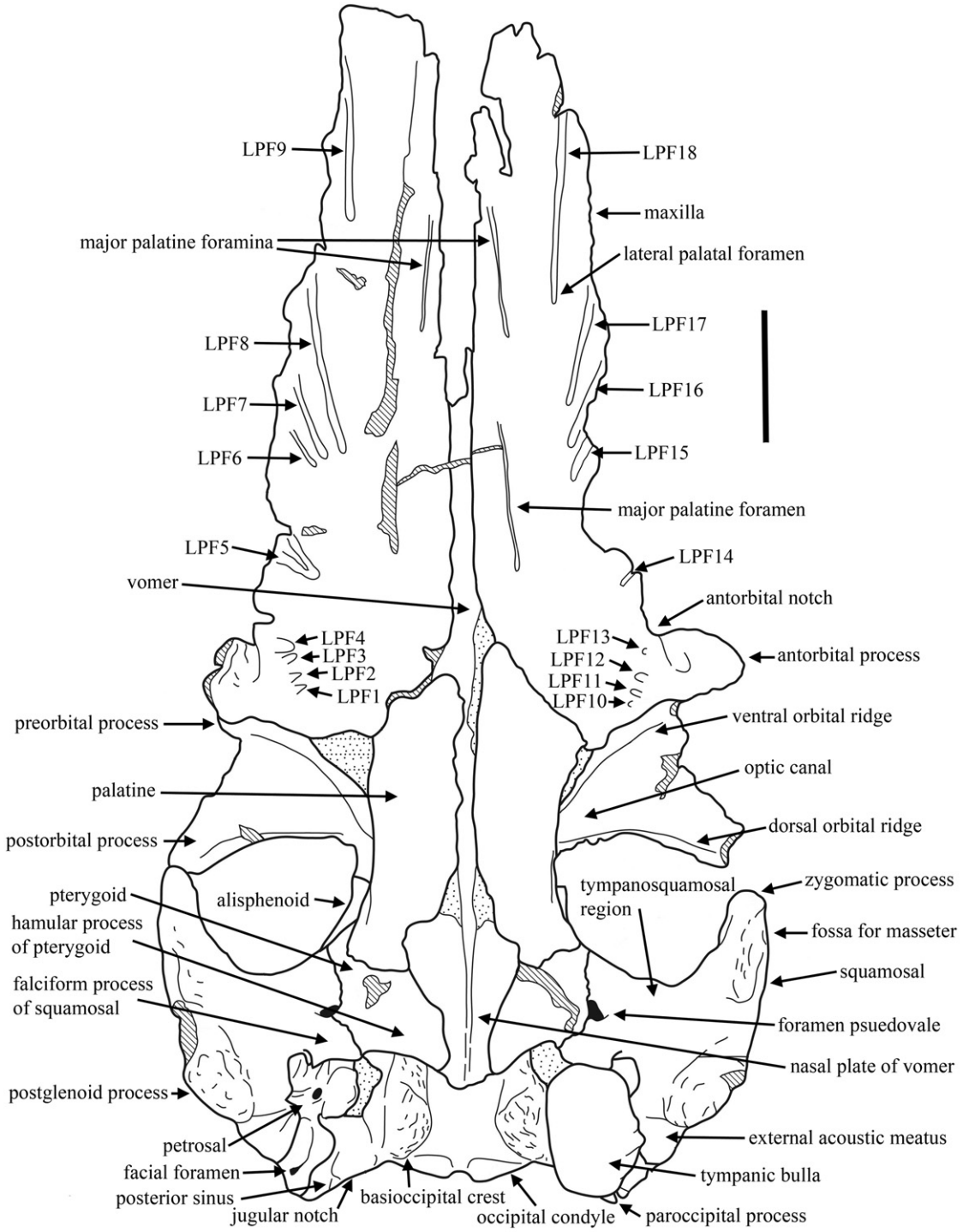

Figure 5. ***Herpetocetus morrowi*** **sp. nov.**, UCMP 124950, illustrated holotype skull in ventral view showing anatomical features. LPF, lateral palatal foramen. Scale bar = 10 cm.

notch on the maxilla; the abrupt termination of the premaxilla near the anterior portion of the nasals and well anterior to the dorsal surface of the frontal; the posterior termination of the ascending process of the maxilla at a level anterior to the parietal; the minimal degree of posterior overlap of the frontal by the parietal; the distinct interorbital constriction exposing both the frontal and parietal on the cranial vertex, and the dorsally open temporal fossae not overhung by the nuchal crests. Apomorphic features

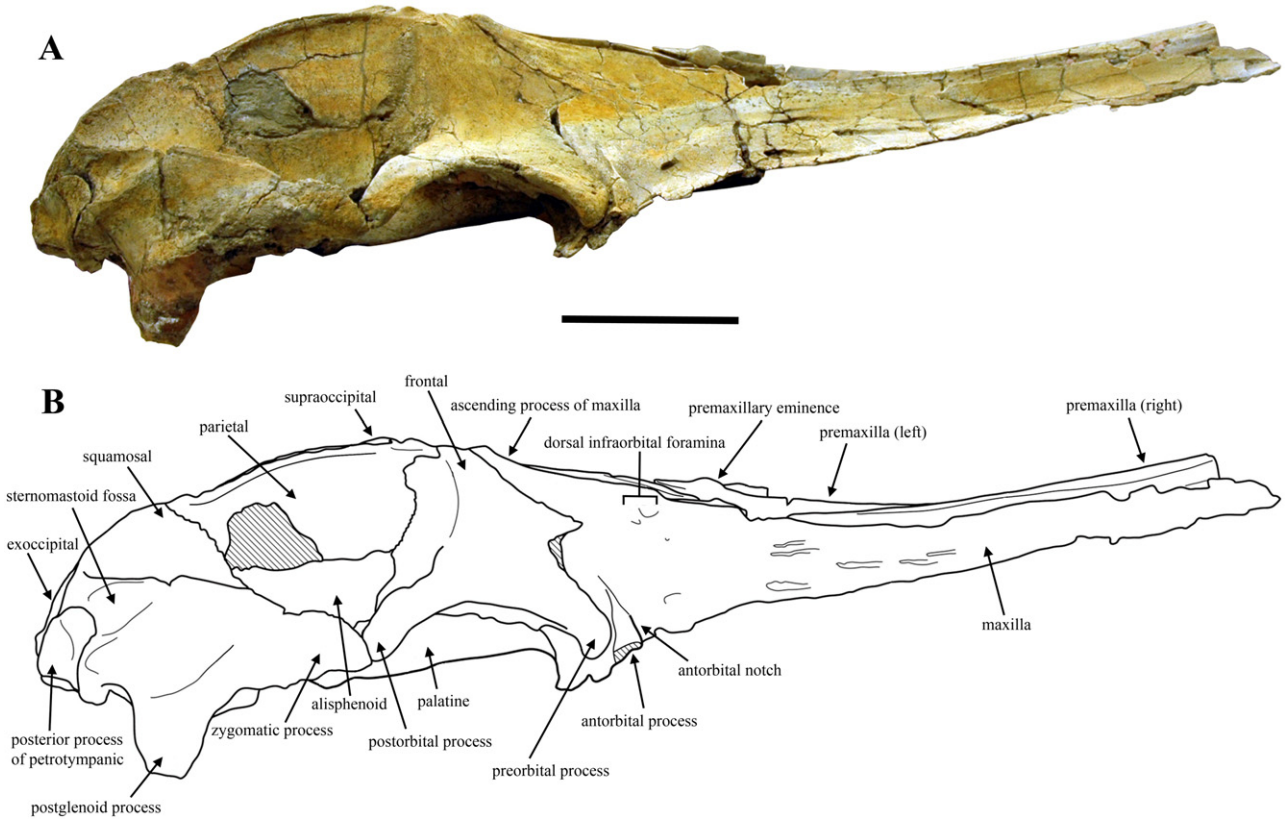

Figure 6. ***Herpetocetus morrowi*** **sp. nov.**, UCMP 124950, holotype skull. A, lateral view; B, illustrated lateral view showing major anatomical features. Scale bar = 10 cm.

include: the anterior extension of the apex of the supraoccipital shield to a level nearly in line with the posterior edge of the supraorbital process of the frontal; the elongated and narrowly triangular ascending process of the maxilla that deeply interdigitates with the anterior cranial elements; and the extremely narrow and elongate nasals that extend posteriorly to terminate in tandem with and be concealed by the overlying ascending processes of the maxillae. Other species of *Herpetocetus* (e.g. *H. bramblei*), as well as *Pi. nana*, have more telescoped skulls in which the dorsal exposure of the parietal and frontal is substantially shorter to nonexistent.

Rostrum: The rostrum of UCMP 124950 is incomplete with the lateral margins of the maxillae and anterior terminations of the maxillae and premaxillae having been lost during diagenesis and/or recovery (Figs 2, 3). Fortunately, both paratype skulls, SDNHM 65781 and SDNHM 130390, have nearly complete rostra (Figs 9, 10). Based on these specimens, the rostrum of *H. morrowi* is known to be long, slender, and spatulate (Figs 12–14). In fact, the rostrum of *H. morrowi* is so long that the length of the functional portion of the palate (the area, in ventral view, from the anterior tip of the premaxilla to the anterior margin of the internal narial fossa along the sagittal plane) makes up approximately 82% of the condylobasal length of the entire skull in SDNHM 130390. This is similar to the condition in *Pi. nana*, but contrasts with the condition in most extant and extinct edentulous mysticetes, which possess relatively shorter palates (e.g. *Parietobalaena palmeri* Kellogg, 1924; *Aglaocetus patulus* Kellogg, 1968; *Caperea marginata*; and *Balaenoptera acutorostrata* Lacépède, 1804).

The anterior termination of the rostrum (i.e. premaxillae) is blunt and rounded, which resembles the condition in *Pi. nana*, but differs from that of *Cep. coronatus* (USNM 489194) in which the distal termination of the elongated rostrum is sharply pointed. In dorsal aspect, the narrow and elongated rostrum of *H. morrowi* has transversely slender maxillae and premaxillae. This distinct attenuation of the rostrum is a feature shared with other small fossil mysticetes, including *Pi. nana*, *Cep. coronatus* (USNM 489194), and *Cet. rathkii* (as reconstructed in Brandt, 1872). Posteriorly, the rostrum of *H. morrowi* is characterized by sharply defined antorbital processes of the maxillae and slender ascending processes

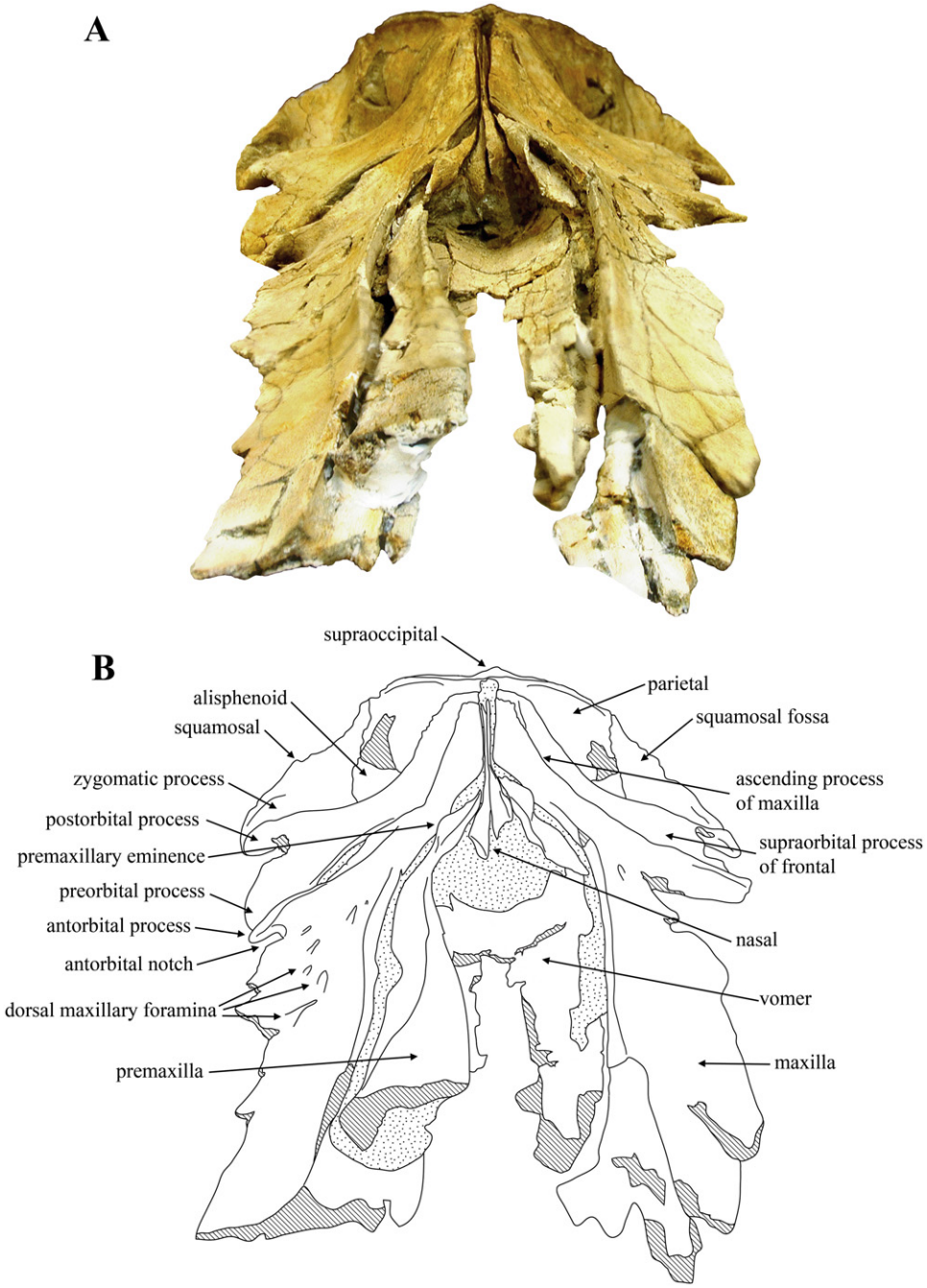

Figure 7. ***Herpetocetus morrowi*** **sp. nov.**, UCMP 124950, holotype skull. A, anterodorsal view; B, illustrated anterodorsal view showing major anatomical features.

of the maxillae that meet at the midline to exclude both the premaxillae and nasals from external contact with the frontals. It is clear that dorsally the maxilla and premaxilla were closely appressed *in vivo* along an unfused suture, as in all edentulous mysticetes. This contrasts with the condition in toothed mysticetes and odontocetes in which the majority of the maxilla/premaxilla suture is fused.

In ventral aspect the maxillae do not meet at the midline on the palate and, instead, there is a continuous sagittal exposure of the vomer. Overall, the palate is surprisingly planar anteriorly, becoming more contoured posteriorly with a broadly rounded mesorostral keel. As thus configured, the palate has minimally concave right and left longitudinal maxillary troughs for the paired baleen racks. Relatively

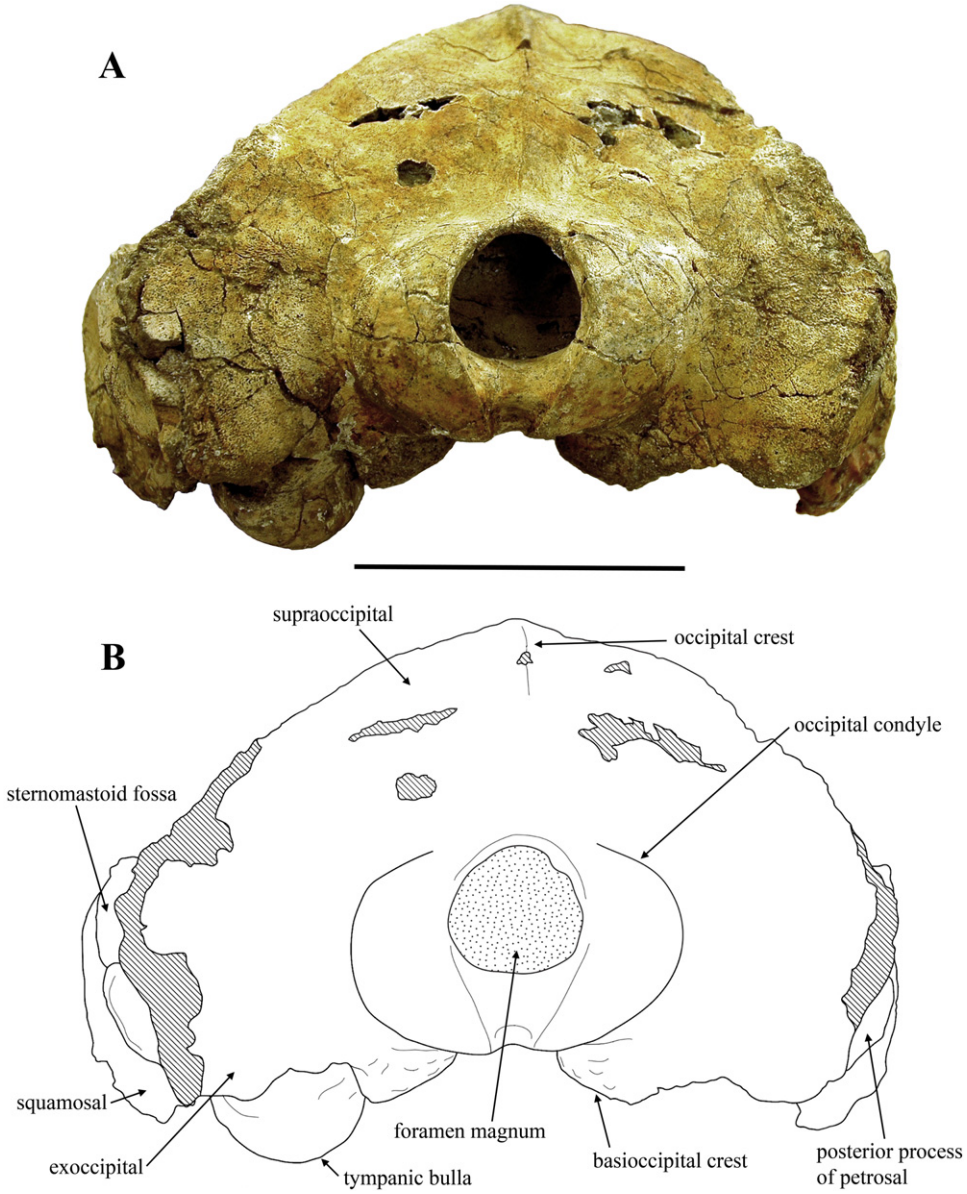

Figure 8. ***Herpetocetus morrowi*** **sp. nov.**, UCMP 124950, holotype skull. A, posterior view; B, illustrated posterior view showing major anatomical features. Scale bar = 10 cm.

planar palates also occur in *Pi. nana* and '*Cetotherium*' *megalophysum* and stand in marked contrast to the palates of extant balaenopteroids and many noncetotheriid Miocene mysticetes (e.g. *Ag. patulus*, *Diorocetus hiatus*, *Pa. palmeri*, and *Pelocetus calvertensis*), which have more prominent ventral mesorostral keels and more strongly concave, longitudinal maxillary troughs.

Viewed laterally (Figs 6, 11), the rostrum has a long and relatively flattened profile for much of its length. It is only at the level of the external narial fossa that the dorsal profile begins to rise toward the cranial vertex.

Cranium: The cranium of *H. morrowi* has a generally quadrate form with the bizygomatic width and condylofrontal length being nearly equal (Figs 2, 12). These cranial proportions are also seen in *Pi. nana* and *Cep. coronatus* and stand in contrast to the distinctly wider crania of fossil and extant balaenopteroids and balaenids. Amongst crown mysticetes, only *Caperea* has a cranium that approaches the quadrate proportions of *Herpetocetus, Piscobalaena*, and *Cephalotropis*. The cranial vertex of *H. morrowi* has a short exposure of both the parietal and frontal, but lacks any trace of a sagittal crest (Figs 2, 3). The temporal crests are weakly developed

Figure 9. ***Herpetocetus morrowi*** **sp. nov.**, SDNHM 65781, paratype skull. A, dorsal view; B, ventral view. Scale bar = 10 cm.

as low, linear swellings on the frontals, which slope gradually from the vertex to the level of the supraorbital processes. The parietal–frontal suture descends posteroventrally from the vertex into the anteromedial corner of the temporal fossa such that the parietal does not overlap the posterior margin of the supraorbital process of the frontal. The parietal–squamosal suture descends nearly vertically towards the temporal fossa and is not raised above the general surface of the temporal wall as a ridge-like linear feature as seen in *Ca. marginata*. The suture also does not coincide with a broad swelling of the parietal and squamosal as seen in *Metopocetus durinasus* Cope, 1896 and *'Cet.' megalophysum* and there is no squamosal cleft. The alisphenoid has a very large exposure on the temporal wall. The temporal fossa is roughly circular, although it is slightly wider transversely than anteroposteriorly elongate. As in other closely related cetotheriids (e.g. *H. transatlanticus*, *H. bramblei*, and *Pi. nana*) and *Ca. marginata*, the lateral margin of the zygomatic process of the squamosal is aligned with the lateral edge of the exoccipital, rather than being distinctly offset laterally from the exoccipital. The squamosal fossa is well developed and extends anteriorly as a continuous (i.e. without a secondary fossa) and linear (i.e. not sinuous) sulcus from the junction of the zygomatic and nuchal crests to the posterior margin of the temporal fossa. The lateral margins of the roughly triangular supraoccipital shield do not overhang the temporal wall. The area of the supraoccipital–exoccipital suture is marked by irregular openings, which probably represent unfused fontanelles. The occipital condyles do not extend posterior beyond the level of the exoccipitals. The postglenoid process is transversely compressed, anterolaterally orientated, and nearly parallel to the longitudinal axis of the zygomatic process, rather than being anteroposteriorly compressed and aligned perpendicular to the sagittal plane, as in most mysticetes. The glenoid fossa thus faces anteromedially and not anteriorly.

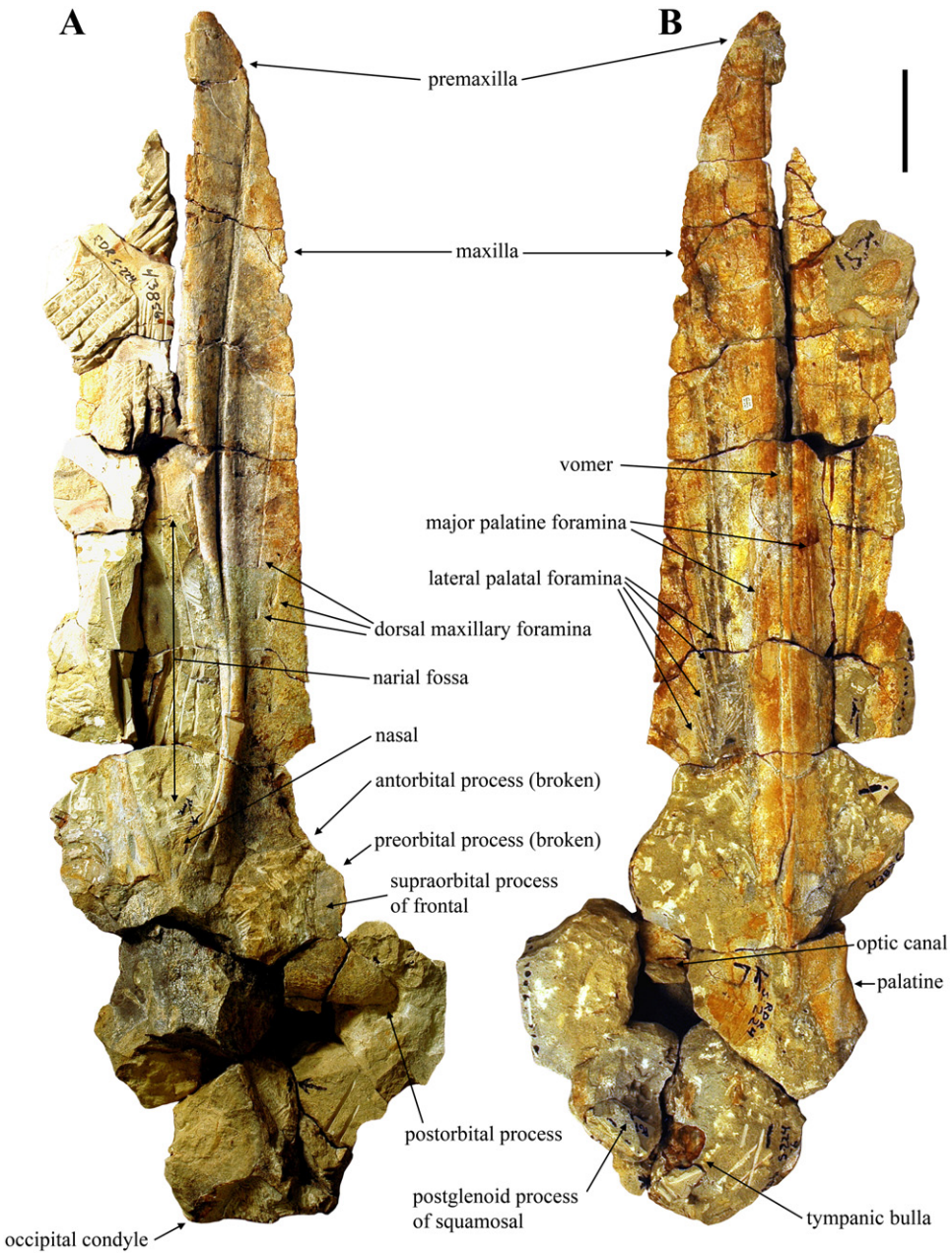

Figure 10. ***Herpetocetus morrowi*** **sp. nov.**, SDNHM 130390, paratype skull. A, dorsal view; B, ventral view. Scale bar = 10 cm.

Premaxilla: Both premaxillae in UCMP 124950 are incomplete and missing their anterior portions. Fortunately, the paratype skulls, SDNHM 65781 and SDNHM 130390, possess nearly complete right premaxillae and based on these specimens the total length of the premaxilla of UCMP 124950 is estimated to have been ~550 mm. The right premaxilla of SDNHM 65781 preserves the external (dorsal) morphology and will serve as the basis for the following description (Fig. 9). The anterior portion of the premaxilla is spatulate and reaches its widest point ~60 mm behind the anterior apex. Here the transverse width measures 48 mm. Transverse measurements taken at 200, 300, 400, 500, and 600 mm behind the anterior apex of the maxilla are 41, 31, 15, 2, and ~1 mm, respectively. Along the margin of the narial fossa the premaxilla remains extremely narrow transversely and tightly appressed to the adjacent maxilla, with which it articulates along a relatively deep and medially convex, unfused lap suture. The

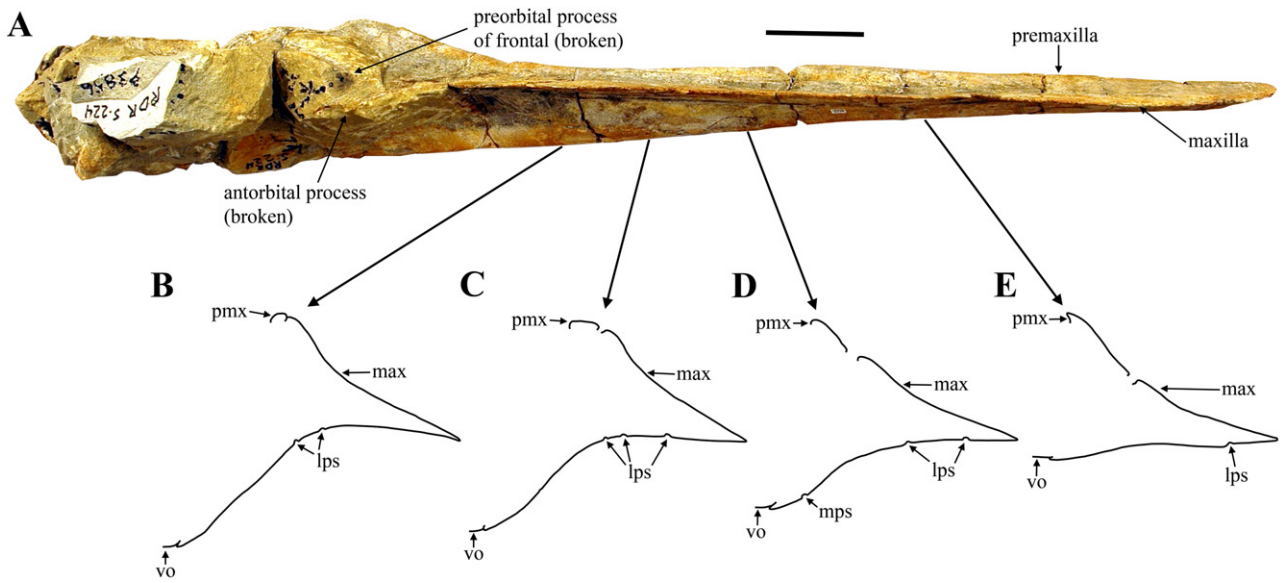

Figure 11. ***Herpetocetus morrowi*** **sp. nov.**, SDNHM 130390, paratype skull. A, lateral view; transverse cross-sections of the right half of the rostrum at B, 716 mm; C, 627 mm; D, 525 mm; and E, 358 mm from the anterior tip of the premaxilla. Abbreviations: lps, lateral palatal sulcus; max, maxilla; mps, major palatine sulcus; pmx, premaxilla; vo, vomer. Scale bar = 10 cm.

posterior 50% of the premaxilla is relatively complete in UCMP 124950 and closely conforms to the general morphology described above for SDNHM 65781. In UCMP 124950, however, the posterior termination of the premaxilla is well preserved and consists of a conspicuous elongate and thickened bony platform that is roughly elliptic in shape, in dorsal aspect, and measures 45 mm anteroposteriorly and 11 mm transversely at its widest point. A distinct, small, and narrowly oval premaxillary eminence is positioned on the anterior portion of each posterior premaxillary platform. The lateral edge of the platform slightly overlaps the medial edge of the adjacent maxilla. Posterior to this premaxillary platform, the premaxilla markedly thins and abruptly terminates between the anterior body of the nasal and the ascending process of the maxilla. Thus, the premaxilla is excluded from external contact with the frontal on the cranial vertex. This arrangement places the posterior termination of the premaxilla anterior to the antorbital notch and well anterior to the posterior termination of the ascending process of the maxilla. In UCMP 124950, this termination of the premaxilla occurs approximately 106 mm anterior to the posterior termination of the ascending process of the maxilla and nasals. A similar arrangement of the premaxilla is seen in *Pi. nana* and '*Cet.*' *megalophysum* (USNM 241531), and serves to clarify the strange architecture of the posterior rostral elements preserved in the holotype of *Met. durinasus* (USNM 8518). With these fossils as a model, it becomes plausible that the paired, narrow bones located behind the fused nasal bones in the holotype of *Met. durinasus* are in fact the posterior ends of the ascending processes of the maxillae and that the premaxillae terminated at a level anterior of where the holotype skull has been broken. This configuration was similarly suggested by Bouetel & de Muizon (2006) based on observations of *Pi. nana*. This anterior placement of the posterior termination of the premaxillae approaches the plesiomorphic condition seen in dorudontines [e.g. *Dorudon atrox* (Uhen, 2004)] and differs from the condition in more divergent mysticetes (e.g. balaenopteroids) in which the ascending process of the premaxilla extends posteriorly in tandem with the adjacent ascending process of the maxilla, and both processes terminate at approximately the same level and often coincident with the posterior margin of the nasals.

Maxilla: The ascending process of the maxilla is bluntly triangular in shape, forming an approximately 30° angle between its lateral and medial margins. The posterior termination of the ascending process reaches to the level of the posterior termination of the slender nasals (Figs 2, 3), which *in vivo* were excluded from dorsal exposure beneath the right and left maxillae, which met at the midline. In UCMP 124950 the lateral margin of the ascending process is relatively linear for ~75 mm as it steeply descends anterolaterally from the vertex. This differs from the more continuously laterally concave lateral margin of the ascending process seen in *Pi. nana*.

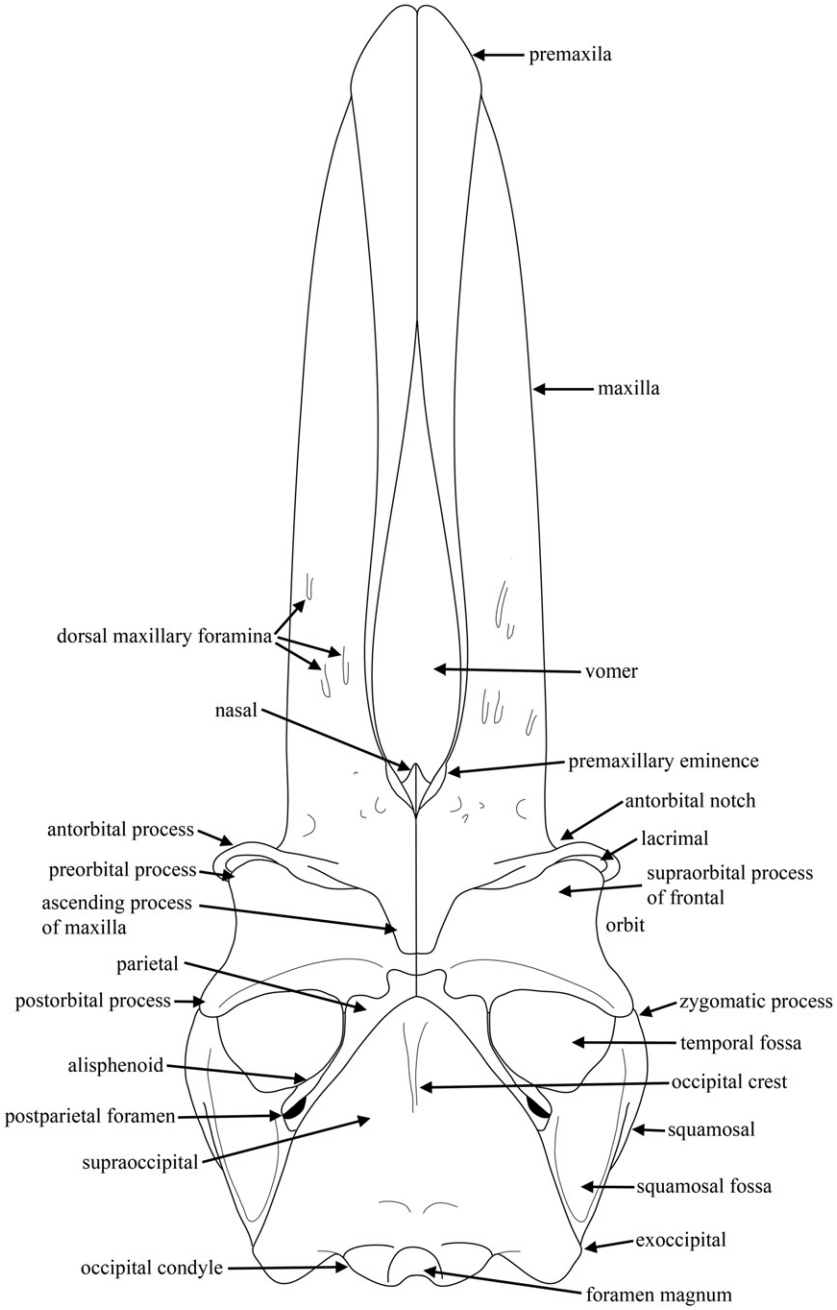

Figure 12. ***Herpetocetus morrowi*** **sp. nov.**, reconstructed skull in dorsal view based on UCMP 124950, SDNHM 65781, and SDNHM 130390 showing anatomical features.

Anterolaterally, the lateral margin of the maxilla becomes transversely orientated as it passes around the anterior border of the supraorbital process of the frontal, transitioning from the ascending process of the maxilla that overlaps the medial portion of the frontal to the infraorbital plate of the maxilla that underlaps the lateral portion of the frontal. In UCMP 124950 the left maxilla has slipped forward, exposing a portion of the large internal infraorbital foramen, the floor of which is coincident with the dorsal (internal) surface of the infraorbital plate of the maxilla.

The distal portion of the antorbital process of the maxilla is well developed and forms an approximately 90° angle with the dorsal plate of the maxilla. The lateral terminus of the antorbital process of the maxilla is narrowly rounded and extends beyond the lateral margin of the preorbital process of the frontal (Figs 2, 3). The antorbital notch is distinct and tightly

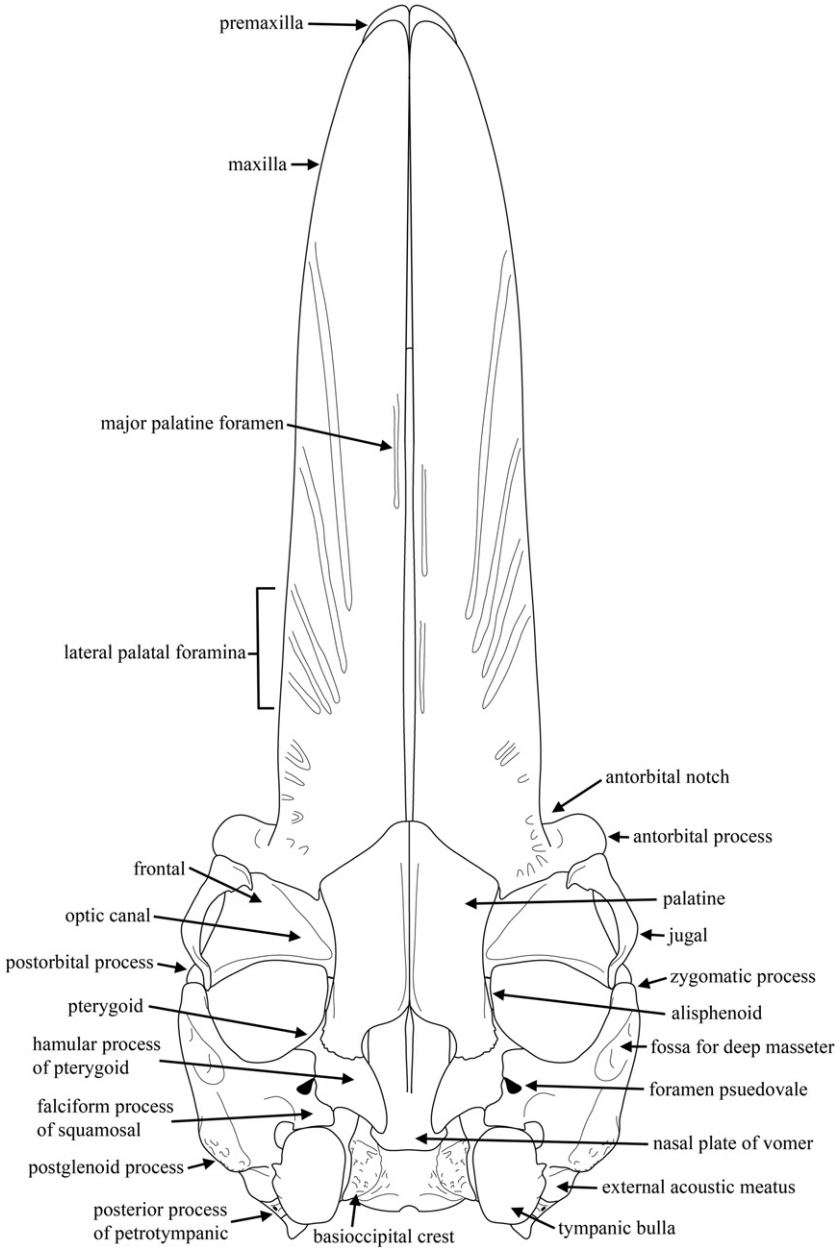

Figure 13. ***Herpetocetus morrowi*** **sp. nov.**, reconstructed skull in ventral view based on UCMP 124950, SDNHM 65781, and SDNHM 130390 showing anatomical features.

constricted anteroposteriorly as in *Pi. nana* and *Cet. rathkii* and unlike the more broadly open antorbital notch in other fossil mysticetes like *Ag. patulus* and *Pa. palmeri*. Medially, the posterior border of the antorbital notch abruptly rises posterodorsally to form a distinct transverse sulcus for passage of the facial nerve.

The external surface of the dorsal plate of the maxilla is extremely narrow in dorsal aspect (Fig. 12), tapers anteriorly, and in UCMP 124950 nowhere measures more than 75 mm wide from the level of the external narial fossa to the anterior terminus. At the anterior terminus of the maxillae in SDNHM 65781 and SDNHM 130390 the lateral and medial margins of the dorsal plate meet to form a sharply acute angle of approximately 8–10° in dorsal view. This attenuation of the maxilla is only approached in specimens of *Cep. coronatus* (e.g. USNM 489194) and *Cetotherium riabinini* Hofstein, 1948 (NMNH-P 668/1), although the line drawings of *Cet. rathkii* published in Brandt (1872: pl. 2, figs 1, 2) suggest that this taxon may also have possessed an acutely attenuated rostrum with

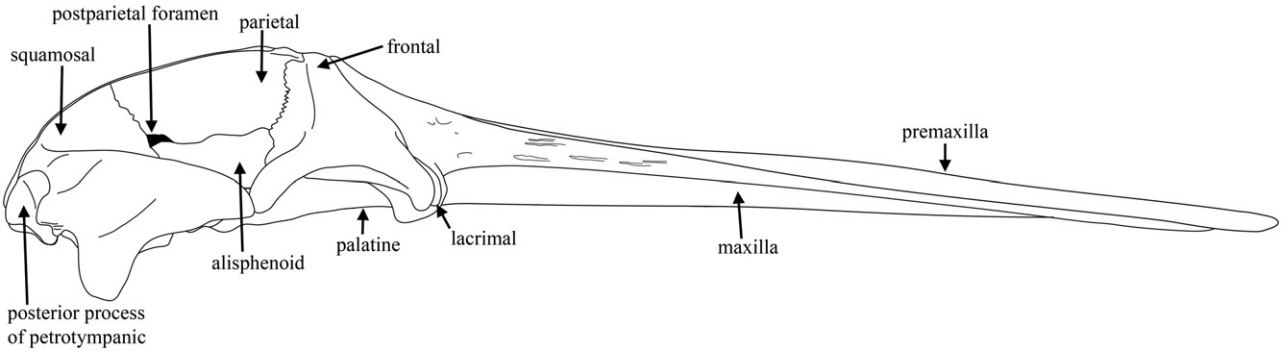

Figure 14. ***Herpetocetus morrowi*** **sp. nov.**, reconstructed skull in lateral view based on UCMP 124950, SDNHM 65781, and SDNHM 130390 showing anatomical features.

transversely narrow maxillae. In contrast, the equally elongate rostrum of *Pi. nana* has maxillae with relatively transversely broader surfaces of the dorsal plate.

In lateral aspect the longitudinal profile of the maxilla of *H. morrowi* gently slopes downward from the cranial vertex, eventually becoming horizontal in orientation, anteriorly (Figs 6, 11, 14). Much of the lateral edge of the maxilla is broken in UCMP 124950, but it is clear that the edge was dorsoventrally thin, as in all other described edentulous mysticetes. In the transverse plane and relative to the horizontal plane, the dorsolateral surface of the dorsal plate of the maxilla slopes approximately 26° from the midline towards the lateral edge at midlength along the rostrum. This is similar to the condition in *Di. hiatus*, *Ag. patulus*, and *Pi. nana*.

The dorsal plate of the maxilla is marked by up to 17 dorsal maxillary foramina (DMF) of various sizes and orientations (Figs 2, 3, 12). In the holotype, ten of these foramina are located on the right maxilla, with the majority being positioned anterior to the nasals. As in *Pi. nana*, a single, large maxillary foramen is consistently present at the level of the anterior margin of the nasals. The following description of the DMF of UCMP 124950 begins with the posteromedially most placed foramen on the right maxilla (DMF1) and proceeds laterally and anteriorly on the right maxilla before proceeding to the left. DMF1 is 6 mm in anteroposterior length and 2 mm in transverse width, and opens dorsally with a short dorsoposteromedially directed sulcus. The first and second foramina are anteroposteriorly separated by a wide bony septum of 7 mm. DMF2 is roughly triangular in shape and is dorsally orientated. In width DMF2 measures 6 mm and is 7 mm in length, with no discernible sulcus. DMF3 is elliptical in shape, is relatively miniscule in size, and is located 20 mm laterally from DMF2. Like DMF2, DMF3 is dorsally orientated and does not possess a sulcus. Anteroposteriorly, the third foramen measures 3 mm anteroposteriorly, and 2 mm mediolaterally. The fourth DMF is positioned 38 mm from the lateral edge of the maxilla, is orientated ventrolaterally, and measures 10 mm anteroposteriorly and 6 mm in dorsoventral height. DMF5 and DMF6 are located anterior to the nasals and near the medial edge of the maxilla, with elongate and anteriorly directed sulci. DMF5 is separated from DMF6 mediolaterally by 6 mm. The sulci of DMF5 and DMF6 are 25 and 30 mm in length and 2 and 3 mm in width, respectively. DMF7 is located 18 mm from the broken lateral edge of the maxilla, is anterolaterally directed, and contains a broad sulcus that measures 24 mm in length and 8 mm in width. Located anteromedially from DMF7, DMF8 is anterolaterally orientated, with a sulcus that measures 32 mm anteroposteriorly and 5 mm mediolaterally. DMF9 is directly anterior to (and orientated similarly to) DMF8. The sulcus of DMF9 is anteriorly incomplete because of a fracture, but is at least 17 mm long and 4 mm wide. The final foramen on the right maxilla (DMF10) has been broken posteriorly by the same fracture that damaged DMF9, leaving only the anteriorly directed sulcus of DMF10 on the dorsal surface of the maxilla. This sulcus is at least 22 mm long and 5 mm wide. DMF11 and DMF12 are both dorsolaterally orientated, lack sulci, and lie on the left maxilla. DMF11 is the more medially positioned of the two foramina, and is similar in shape and location to that of DMF2 on the right maxilla. DMF11 and DMF12 are 8 and 6 mm in length (respectively) and 5 and 3 mm in width (respectively). DMF13 is similar in size to DMF3, measuring 3 mm long and 1 mm wide, but is located further anteriorly. DMF14 is highly damaged, but clearly opens laterally as in DMF4. The width of DMF14 is difficult to determine, but it is estimated to be approximately 10 mm in anteroposterior length. DMF15 is anterolaterally orientated with a

70-mm-long sulcus, and is 7 mm in width. DMF16 and DMF17 are incomplete and present on the broken lateral edge of the maxilla. The associated sulci of both foramina appear to be anterolaterally orientated, but measurements of width and length are unobtainable because of damage.

The ventral plate of the maxilla in UCMP 124950 has been compressed dorsoventrally as a result of diagenetic compaction, which has collapsed the median rostral keel (= palatal keel; mesorostral keel) (Fig. 6). A slight ventrally directed concave curvature towards the midline confirms the presence of a median keel in *H. morrowi*. Fortunately, the palates of the paratype skulls (especially SDSNH 130390) are better preserved. In these specimens the ventral plate of the maxilla is posteriorly sinuous in the transverse plane, but becomes progressively more planar anteriorly (Fig. 11). Thus configured, the palate of *H. morrowi* possessed distinct, yet relatively shallow, longitudinal troughs that housed the baleen racks. Interestingly, the lateral margin of the ventral plate of the maxilla in this new species does not preserve any trace of an alveolar groove as reported in *Pi. nana* (Bouetel & de Muizon, 2006). On the palate of *H. morrowi* the medial margins of the left and right maxillae do not meet at the midline, but are instead separated by the vomer. Posteromedially, the maxillae contact the palatines, which extend anteriorly into the maxillae. This suture in UCMP 124950 was damaged during diagenesis, but it is clearly anteromedially directed with the palatines penetrating farthest anteriorly at the midline. The maxilla–palatine suture in *Pi. nana* is more sinuous with a distinct, anteriorly directed lateral lobe (Bouetel & de Muizon, 2006: fig. 6).

Multiple lateral palatal foramina (LPF) are present on the lateral half of the ventral plate of the maxilla (Figs 4, 5, 13). These foramina are homologous to the foramina associated with vascularization and innervation of the gingival epithelial tissues of the palate from which the baleen racks of modern mysticetes form. The right maxilla contains nine foramina (LPF1–9) with associated sulci, and the left possesses nine as well (LPF10–18). This count is fewer than the expected ~ten to 17 foramina per side observed in modern rorquals, which is probably a result of the incompleteness of the maxilla of UCMP 124950. No open maxillary groove is present on the palate of *H. morrowi*, unlike the condition in balaenids, and the foramina are positioned in a single row, unlike the condition in *Megaptera* and *Eschrichtius*. The posterior-most four lateral palatal foramina on the right maxilla are small with short associated sulci, measuring between 8 (LPF1) and 17 mm (LPF3) in length. These first four foramina are radially orientated, as in species of *Balaenoptera* and stem balaenopteroids (Deméré *et al*., 2008), with sulci orientated at 105, 110, 113, and 87° (LPF1, LPF2, LPF3, and LPF4, respectively) relative to the sagittal plane. LPF5 possesses two anterolaterally orientated sulci. The posterior sulcus of LPF5 measures 21 mm in length and is orientated at 69°; whereas the incomplete anterior sulcus measures at least 28 mm long and is orientated at 35°. LPF6 possesses a sulcus measuring 53 mm in length and an orientation of 29°. LPF7 has a sulcus measuring 77 mm long with an angle of 24° with the sagittal plane. The two anteriormost foramina and sulci on the right maxilla are anterolaterally incomplete in UCMP 124950, and nearly parasagittal in orientation. LPF8 measures at least 115 mm in length and trends at 12° relative to the sagittal plane. The ninth foramen on the right maxilla is the longest of the lateral palatal foramina preserved in UCMP 124950 with a length of at least 183 mm and an orientation of 5°. On the left maxilla, the posterior-most four foramina are also closely spaced and radially arranged. In general, their sulci are shorter than on the right maxilla, with lengths between 3 (LPF10) and 7 mm (LPF11). The orientations of these sulci are also more posteriorly orientated, relatively, with trends of 114, 115, 100, and 114° (LPF10, LPF11, LPF12, and LPF13, respectively). Anteriorly, the lateral palatal foramina and associated sulci are more parasagittally to anterolaterally trending, with angles of 44, 22, 15, 11, and 9° (LPF14, LPF15, LPF16, LPF17, and LPF18, respectively). The sulci of all five anterior foramina are incomplete in UCMP 124950 owing to the loss of the lateral edge of the maxilla during diagenesis.

The right maxilla of the paratype skull, SDNHM 130390, is nearly complete, and preserves the morphology of the anterior lateral palatal foramina, which are not preserved in the holotype skull (Fig. 10). Comparison of the two skulls shows that only a single anterior foramen appears to occur on each maxilla (anterior to foramen no. 8 on the right maxilla and foramen no. 15 on the left maxilla) beyond what is preserved in the holotype skull. In general, the lateral palatal foramina do not occur beyond the approximately posterior-most third of the maxilla in SDNHM 130390. However, the two anterior-most foramina (especially the anterior-most) possess extremely elongate sulci, which extend distally to a position approximately three quarters of the anteroposterior length of the maxilla in ventral view. This extreme elongation of the sulci of the anterior lateral palatal foramina is most likely the result of elongation of the rostrum during postnatal ontogeny after the formation of the lateral palatal foramina. The overall arrangement of the lateral palatal foramina, with radially arranged posterior foramina and parasagittally orientated anterior foramina, is

generally reminiscent of the palate vascularization pattern observed in modern balaenopterids and many extinct mysticetes (e.g. *Ag. patulus*, *Isanacetus laticephalus*, *Pe. calvertensis*, *Pa. palmeri*) and contrasts with the more irregular vascularization patterns seen on the palates of eschrichtiids, balaenids, and neobalaenids (Deméré *et al*., 2008).

Vomer: The vomer forms the floor of the mesorostral canal as in all neocetes and as revealed in CT scans of UCMP 124950 is broadly U-shaped for most of its rostral length where the right and left lateral sheets (laminae laterale) ascend to articulate with the adjacent maxillae. On the palate the vomer is continuously exposed at the midline between the right and left maxillae except posteriorly where it is underlapped by the paired palatines, which meet at the midline. The junction between the paired palatines does not appear to form a distinct median crest, as observed in *H. bramblei* (UCMP 219111). Behind the internal nares, a thin vomerine keel ascends to meet the nasal plate of the vomer. As preserved in UCMP 124950, the nasal plate is transversely broad and extends posteriorly at least as far as the anterior portion of the tympanic bulla and nearly to the level of the posterior terminus of the peribullary sinus fossa. The suture between the nasal plate and the adjacent posterior lamina of the pterygoid is not exposed in any available specimen and cannot be described. An isolated nearly complete vomer and associated presphenoid (SDNHM 42758) preserves a portion of the nasal plate and at least 210 mm of the mesorostral canal. In dorsal view the mesorostral canal is broadly U-shaped and as preserved decreases in width posteriorly from a maximum of 33 mm to a minimum of 20 mm. The prenarial process of the lateral sheet of the vomer attains a maximum transverse thickness of 6 mm. Posteriorly the dorsal margin of the lateral sheet thins to ~2 mm and becomes slightly medially deflected. Ventrally, the right and left lateral sheets of the vomer meet at the midline to form the vomerine crest, which increases in acuity from 80° at the anterior portion of the vomer (as preserved), to 70° at the midpoint of the vomer, to 60° at the posterior portion of the vomer where it underlaps the presphenoid. Distinct, finger-like right and left wings of the vomer are tightly appressed to the laterally concave ventrolateral surfaces of the presphenoid.

Palatine: Both the right and left palatines are preserved in UCMP 124950, with the left palatine being more intact than the right (Figs 4, 5). Diagenetic compaction has crushed and pushed the left palatine upwards approximately 10 mm above the right palatine, damaged the posteromedial edge of both palatines, and opened much of the palatine–maxilla suture. The left and right palatines are separated at the midline by a narrow (~5 mm) exposure of the vomer, and do not contact medially. This contrasts with the condition in *Pi. nana* wherein the palatines are more widely separated at the midline by the ventral, transversely expanded vomerine keel. Although the ventral surface of the left palatine has been slightly distorted, the right palatine is relatively planar and probably preserves the natural form.

In ventral view the lateral margin of the palatine is broadly concave, similar to the condition in *Pi. nana* and unlike the more linear to broadly convex lateral palatine margin in *Cet. rathkii*. The anterior margin of the palatine marked by the palatine–maxilla suture is anteromedially directed and forms an angle of ~45° to the sagittal plane. This is roughly similar to the condition in *Cet. rathkii*, but distinctly different from that in *Pi. nana*, in which the palatine–maxilla suture is more sinuous with a medial, anteriorly concave segment and a lateral, anteriorly convex segment. The ventral surface of each palatine is broadly planar both transversely and longitudinally. Laterally, the palatine contacts and is overridden by the ventral orbital crest of the supraorbital process of the frontal; which nearly excludes the palatines from participating in formation of the orbital fissure. The dorsal edge of the palatines anterior to the ventral orbital crest–palatine contact hangs freely and is not in direct contact with any other cranial elements. The posterior margin of the palatine is moderately complex in morphology and can be subdivided into medial and lateral segments. The medial segment forms the anterior border of the internal nares and extends posterolaterally from the midline towards the root of the hamular process of the pterygoid. This area of the pterygoid is underlapped by the palatine, which extends slightly anterolaterally towards the temporal fossa. The exposure of the palatine–pterygoid suture on the temporal wall runs anterodorsally and is parallel to the lateral exposure of the squamosal–pterygoid and alisphenoid–pterygoid sutures.

Nasal: Post-mortem deformation of the holotype skull has resulted in lateral displacement of the ascending processes of the right and left maxillae to reveal the complete morphology of the nasals. The overall form of the nasals is unique amongst known fossil and living mysticetes and consists of extremely slender posterior segments and expanded and triangular anterior segments (Figs 2, 15). *In vivo* the slender posterior segments were covered by the medial margins of the adjacent ascending processes of the maxillae. Thus concealed, only the triangular anterior segments of the nasals would be dorsally visible, making it appear that the nasals were extremely short, acutely triangular, and confined to an unusually forward position on the rostrum. As

Figure 15. ***Herpetocetus morrowi*** **sp. nov.**, UCMP 124950, nasals of holotype skull in dorsal view. Scale bar = 5 cm.

revealed in UCMP 124950 the slender posterior segment of the left nasal makes up ~60% of the total nasal length (= 155 mm), whereas the broader anterior segment composes only about 40% of the total nasal length. The posterior nasal segment has a transverse width of no more than 2 mm and a dorsoventral height of ~24 mm. Posteriorly, the nasals terminate at the level of the posterior edge of the ascending process of the maxilla. The anterior nasal segment gradually expands anteriorly to a maximum width of ~10 mm before decreasing in width as it tapers anteromedially towards the midline. Together, the anterior segments of the right and left nasals possess a grossly oblanceolate shape, with an acute posterior external termination, a short dorsal sagittal keel, and an acute anterior apex with slightly concave anterolateral margins. This configuration of the anterior margin of the nasals, also seen in the referred skulls of *H. bramblei* (UCMP 219111) and *Herpetocetus* sp. nov. (NSMT-PV 19540), generally parallels the condition in *Pi. nana* and grossly resembles the condition in *Ca. marginata* and *Megaptera novaeangliae*, but differs from the primitive condition seen in *Zygorhiza kochii*, in which the anterior margin of the nasals is posteriorly v-shaped.

The slender posterior segments of the nasals have not been observed in other members of *Herpetocetus*, probably because of incompleteness of specimens (e.g. *H. transatlanticus*) or close juxtaposition of the right and left ascending processes of the maxillae obscuring their features. However, if articulated as in life the maxilla would dorsally override the nasal giving it the appearance of terminating posteriorly at the same level as the short ascending process of the premaxilla, and well anterior to the antorbital notch. It is possible, therefore, that other closely related taxa possess a similar morphology to *H. morrowi*, but it has been obscured by the maxillae. In *Pi. nana* the ascending processes of the right and left maxillae vary in the degree of contact at the midline as seen in different specimens with the result that the posterior segments of the nasals vary in length and width depending upon how far posteriorly the ascending processes of the maxillae extend before meeting at the midline (Bouetel & de Muizon, 2006: fig. 4). In the holotype specimen of *H. transatlanticus* (USNM 182962), the partially preserved frontal clearly shows a deep groove dorsomedially that extends posteriorly to an approximately similar position as the nasal of UCMP 124950. This probably indicates that *H. transatlanticus* also possessed nasals with extremely slender and elongate posterior segments that were obscured from the dorsal surface by the overriding maxillae. Known specimens of *H. bramblei* and *Herpetocetus* sp. nov. (NSMT-PV 19540) either are incomplete or exhibit tightly abutting maxillae, which dorsally obscures the posterior portion of the nasals in these taxa.

Frontal: The supraorbital process of the frontal is depressed below the cranial vertex along a gradually sloping surface as in *Cet. rathkii*, *Di. hiatus*, *Pi. nana*, and fossil and extant balaenids. This differs from the primitive condition in archaeocetes and toothed mysticetes in which the supraorbital processes occur at the same level as the cranial vertex, and also from the more derived condition in balaenopteroids in which the supraorbital processes are abruptly depressed below the cranial vertex. In the latter group the medial portion of the frontal is vertical or nearly so, whereas the lateral portion of the frontal is horizontal or nearly so. In dorsal view, the supraorbital process is roughly quadrate (Figs 2, 3), being moderately wide and long, and similar in form to *Pa. palmeri*, *Cet. rathkii*, and *Pi. nana*. The postorbital process of the frontal contacts the

zygomatic process of the squamosal in line with the apex of the supraoccipital shield, whereas the preorbital process of the frontal overrides the posterolateral portion of the descending process of the maxilla. In *H. morrowi* the preorbital process is more anteroposteriorly expanded and ventrally placed than the postorbital process. Towards the ascending process of the maxilla, and away from the preorbital process, the frontal and maxilla abut, but do not overlap. Near the midline, the ascending process of the maxilla overlaps the anteromedial portion of the frontal as a triangular wedge. Behind this, the frontal has a distinct exposure on the cranial vertex that measures 18 mm in anteroposterior length. An incipient sagittal crest is poorly developed in the holotype and SDNHM 34155. The posterior margin of the frontal contacts the parietal dorsolaterally, and the enlarged alisphenoid ventrolaterally. The sagittal suture between the left and right frontals has relaxed in the UCMP 124950, leading to a slight disarticulation along the midline. This suggests that the suture was not yet tightly fused. Adjacent to the vertex, a lobate process of the parietal penetrates the frontal to create a small, anterior wing (Figs 2, 3). This feature is distinct on the right temporal wall, but has been distorted on the left side post-mortem. A similar lobate anterior parietal wing occurs in *Herpetocetus* sp. nov. (NSMT-PV 19540). Below the small anterior wing in UCMP 124950, the parietal–frontal suture descends steeply as a broadly sinuous feature towards its contact with the alisphenoid, which is located at a level slightly dorsal to the surface of the supraorbital process of the frontal. The frontal–alisphenoid suture measures one-third of the length of the frontal–parietal suture, and is abruptly directed vertically to terminate at the large orbital fissure. As in the holotype of *H. transatlanticus*, a poorly developed temporal crest is positioned on the posteromedial portion of the frontal, originating on the vertex near the parietal–frontal suture and descending to be nearly in line with the posterior third of the orbit before curving posteriorly towards, but never reaching, the postorbital process.

Ventrally, the descending process of the maxilla underlaps the preorbital process of the frontal (Figs 4, 5). The orbit is broad anteroposteriorly, measuring 106 mm from the ventral-most tip of the preorbital process to the postorbital process. A robust ventral orbital ridge is present in UCMP 124950, beginning 48 mm posteromedial to the lateral edge of the preorbital process and terminating near the dorsal extent of the palatine–pterygoid suture. The ventral orbital ridge initially is vertical in orientation at its distal extremity, but reclines posteroventrally as it nears contact with the palatines. The dorsal orbital ridge is less conspicuous than the ventral orbital ridge and has a much lower profile and shorter extent. Unlike the ventral orbital ridge, the dorsal orbital ridge is consistently vertical in orientation and runs mediolaterally, rather than at an angle to the sagittal plane. The ventral and dorsal orbital ridges define the optic canal, which is anteroposteriorly broad distally and proximally constricted. The course of the optic canal emerges from the orbital fissure at an acute angle of ~35° to the sagittal plane and gradually rotates laterally towards its distal termination where the axis of the canal is anterolaterally directed at an angle of ~70° to the sagittal plane. Anterolaterally orientated optic canals are present in other cetotheriids (e.g. *H. bramblei*, *Herpetocetus* sp. nov., *Pi. nana*, and *Cet. rathkii*) and contrast with the condition in balaenopterids, balaenids, and neobalaenids, in which the optic canals are more laterally to posterolaterally orientated.

Parietal: Both parietals are complete in UCMP 124950, except for the posteroventral corners of each, where a roughly rectangular piece of bone appears to be missing (Figs 2, 3, 16). These features may represent parietal fontanelles and, if correctly identified, provide further evidence of the immature nature of the holotype skull. In the holotype skulls of *H. transatlanticus* (USNM 182962) and *H. bramblei* (UCMP 82465) this area is marked by a postparietal foramen (Whitmore & Barnes, 2008); this also characterizes *Herpetocetus* sp. nov. (NSMT-PV 19540). The parietal of *H. morrowi* has a relatively long exposure on both the cranial vertex and temporal wall. As with the frontals, the sagittal suture between the left and right parietals has separated in the holotype specimen, the loosely fused condition suggesting relative immaturity. Dorsally, the parietal is exposed for 12 mm on the cranial vertex before being overridden by the supraoccipital shield. An incipient sagittal crest is present in the holotype and SDNHM 34155. As previously described, the dorsal portion of the parietal intrudes anteriorly into the frontal to create a small anterior wing. This anterior wing, however, does not overlap with the median rostral elements (i.e. nasal, premaxilla, or maxilla) as occurs in extant and most fossil balaenopteroids. Below the anterior wing, the parietal–frontal suture curves first posteriorly, then anteriorly in a sinuous pattern before slightly curving again posteriorly to form a triple junction with the alisphenoid and frontal (Fig. 16). Overall, the parietal–frontal suture is nearly vertical, in contrast with the condition in balaenopteroids and neobalaenids. In *H. morrowi* the relatively long parietal–alisphenoid suture is horizontal along its entire length, and terminates approximately in line with the posterior edge of the temporal fossa, at another triple junction with the alisphenoid and squamosal.

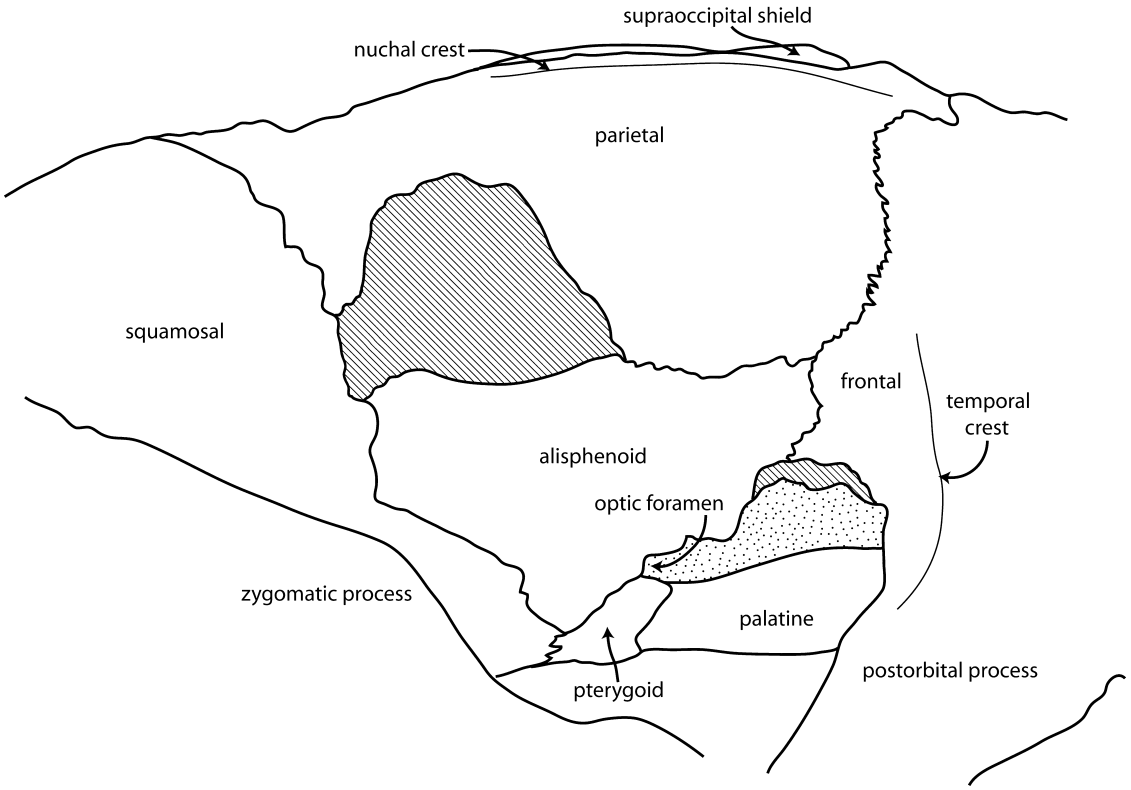

Figure 16. ***Herpetocetus morrowi*** **sp. nov.**, UCMP 124950, illustrated right temporal wall of holotype skull in lateral view showing configuration of anatomical elements.

Viewed anteriorly, the parietal on the temporal wall forms a slight overhang at the nuchal crest. Below the nuchal crest, the parietal is broadly concave, but becomes broadly convex near its ventral margin.

Supraoccipital: The occipital shield is essentially complete in UCMP 124950 with only minor damage near the anterior apex (Figs 2, 3). A pair of irregular openings on either side of the midline in the posterior portion of the supraoccipital may represent fontanelles, as they roughly occur in the region of the neonatal supraoccipital–exoccipital cranial suture (Figs 2, 8). As pointed out by Walsh & Berta (2011) for extant balaenopteroids, the supraoccipital–exoccipital suture initially fuses at its lateral and medial extremities, with final fusion eventually occurring towards the middle. The openings in UCMP 124950, however, may simply represent especially thin areas of the supraoccipital that were broken during diagenesis. The damaged supraoccipital of SDNHM 34155 also shows marginal thinning of bones immediately adjacent to areas of missing bone and may represent the same condition as preserved in UCMP 124950. Furthermore, a partial skull of *Herpetocetus* sp., VMW-65, from the Falor Formation of California possesses paired and similarly placed openings (Boessenecker, 2013). Finally, in a referred skull of *H. bramblei* (UCMP 219111) this area of the occipital shield is marked by very thin bone, where it is preferentially fractured relative to the rest of the braincase. In dorsal view the supraoccipital forms a nearly equilateral triangle, and extends anteriorly to a level in line with the anterior margin of the temporal fossa. This degree of telescoping is greater than seen in *Pi. nana*, *Cet. rathkii*, and *'Cet.' megalophysum*, in which the apex of the supraoccipital terminates at a level distinctly behind the anterior margin of the temporal fossa. This also appears to be the condition in *H. transatlanticus*. A greater degree of telescoping involving an extreme degree of anterior displacement of the apex of the supraoccipital, as well as overlapping of the frontal by the parietal, occurs in extant balaenopterids, balaenids, and neobalaenids.

The apex of the supraoccipital of UCMP 124950 is distinctly triangular, forming an angle of 70° between the right and left nuchal crests. Extending posteriorly from the apex almost to the dorsal rim of the foramen magnum is a low external occipital crest, which is better developed in SDNHM 34155. The external occipital crest is even more pronounced in *H. bramblei* and *Herpetocetus* sp. nov. (NSMT-PV 19540), as well as many of the known skulls of *Pi. nana*. In lateral view the supraoccipital has a

Figure 17. ***Herpetocetus morrowi*** **sp. nov.**, UCMP 124950, basicranium of holotype skull in ventral view. Scale bar = 5 cm.

flexed profile with an anterior portion forming an obtuse angle of 139° with the plane of the cranial vertex (dorsal surface of parietal and frontal) and a steeper, posterior portion forming an angle of 148°. The region of flexure occurs ~67 mm in front of the anterior margin of the foramen magnum. The lateral margin of the supraoccipital, where it forms the lambdoidal suture with the underlying parietal, projects slightly laterally to create a small overhang of the parietal. This minor degree of overhang also occurs in SDNHM 34155 and is reported to be the condition in *H. transatlanticus* and *H. bramblei* (Whitmore & Barnes, 2008). This contrasts with the condition in skulls of *Pi. nana*, *Cep. coronatus*, and '*Cet.*' *megalophysum*, which have a more pronounced lateral overhang of the parietal by the nuchal crest. In extant balaenids, neobalaenids, and especially balaenopterids, the nuchal crest dramatically extends laterally to overhang not only the parietal but the temporal fossa as well.

The nuchal crest of UCMP 124950 is slightly sinuous in dorsal aspect, with an anterior broadly concave segment, a medial broadly convex segment (centred just anterior to the parietal–squamosal–supraoccipital triple junction), and a posterior broadly concave segment. This sinuosity also occurs in SDNHM 34155, as well as *Herpetocetus* sp. nov. (NSMT PV-19450). In contrast, the occipital shields in *Pi. nana* and *H. bramblei* (UCMP 219111) are roughly triangular and appears to lack a marginally sinuous nuchal crest. Furthermore, the apex of the supraoccipital in *Pi. nana* is rounded rather than acutely triangular.

Exoccipital: The supraoccipital–exoccipital suture is tightly fused and indiscernible in UCMP 124950 except, perhaps for the possible fontanelles mentioned above (Figs 2, 8). The lateral and ventral margins of the left exoccipital are damaged, but the right exoccipital is relatively intact except for missing the anterolateral edge of the paroccipital process. Fortunately, a complete left paroccipital process is preserved in SDNHM 34155. Overall, the lateral margin of the exoccipital is relatively squared off in posterior view, which is in contrast to the broadly rounded lateral margins in *Pa. palmeri* and *Cep. coronatus*. In cross-section, the paroccipital process is dorsally, anteroposteriorly broad, but narrows ventrally into a thin sheet. This morphology is grossly similar to that seen in *Cep. coronatus* and contrasts with the more uniformly thin (e.g. *Pa. palmeri*) or uniformly thick (e.g. '*Cet.*' *megalophysum*) paroccipital processes of other mysticetes. The thinness of the ventral segment of the paroccipital process may be linked to the distal expansion of the compound posterior process of the petrotympanic. In ventral aspect, the exposure of the exoccipital of *H. morrowi* is distinctly shortened transversely between the occipital condyle and the composite posterior process of the petrotympanic, and primarily consists of a broad, internally concave, and highly excavated jugular notch (Figs 4, 5, 17). Similar, transversely shortened ventral margins of the exoccipital also appear to occur in *H. bramblei*, *Herpetocetus* sp. nov. (NSMT PV-19540), and *Nannocetus eremus*, and contrast with the condition in *H. transatlanticus* and *Pi. nana*, in which the ventral margin of the exoccipital is distinctly longer and possesses both the jugular notch and the tympanohyal notch. Between the jugular notch and the compound posterior process of the petrotympanic, there is a transversely narrow excavation, which marks the remnant of the posterior sinus. The

posterior sinus of UCMP 124950 is similar to the condition observed in *H. bramblei*, *H. transatlanticus*, *Herpetocetus* sp. nov. (NSMT PV-19540), *N. eremus*, *Pi. nana*, and '*Cet.*' *megalophysum*; but differs from the more pronounced and well-formed posterior sinus of archaeocetes, odontocetes, toothed mysticetes, and eomysticetids.

Basioccipital: The basioccipital in UCMP 129450 is relatively well preserved and characterized by prominent, bulbous basioccipital crests (falcate processes; *sensu* Mead & Fordyce, 2009), separated by a planar exposure of basioccipital approximately 35 mm wide (Figs 4, 5, 17). Although in the holotype the nasal plate of the vomer covers the basisphenoid–basioccipital suture ventrally, CT scans reveal that the suture is closed and fused. This is also the condition in SDNHM 34155 and SDNHM 90484. The basisphenoid–basioccipital suture has been shown to close early in mysticete ontogeny (Walsh & Berta, 2011). In ventral aspect, the basioccipital crests are roughly bulbous in shape in damaged/abraded specimens (e.g. UCMP 129450, SDNHM 90484), but more rhomboid in unabraded specimens (e.g. SDNHM 34155). The anterior margins of the basioccipital crests contact and are partially underlapped by the posterior laminae of the pterygoid. This contact extends transversely from the lateral-most edge of the basioccipital crest to the posterolateral edge of the nasal plate of the vomer, where the basioccipital–pterygoid contact becomes nearly vertically orientated. Anterolaterally, the basioccipital crest is deeply excavated by the peribullary sinus fossa. The sinus does not extend to the posterolateral corner of the basioccipital crest, but instead terminates at a point just behind the midpoint of the longitudinal dimension of the crest. A separate, hemispherical sinus excavates the posterolateral corner of the basioccipital crest. This feature is well preserved in SDNHM 90484, a partial basicranium. Anteriorly, the medial basioccipital wall of the peribullary sinus fossa is continuous with the medial lamina of the pterygoid within the pterygoid sinus fossa.

The occipital condyles are relatively intact in UCMP 129450, and in posterior view each is grossly reniform with rounded margins (Fig. 8). The ventral half of each condyle is transversely wider than the dorsal half. A prominent intercondylar notch separates the occipital condyles on the posteroventral surface of the basioccipital. The foramen magnum is ovate with the ventral portion transversely wider than the dorsal portion. This differs from the condition in *H. bramblei* (UCMP 219111), in which the foramen magnum is nearly circular in shape. Based on ontogenetic age, the occipital condyles protrude more (older) or less (younger) from the surface of the occipital shield on a short, parasagittally directed neck. This ontogenetic variation also affects the anteroposterior positional relationship between the occipital condyles and the exoccipitals, with ontogenetically younger crania possessing condyles that lie anterior to the plane of the exoccipitals, whereas ontogenetically older crania have occipital condyles that posteriorly extend to the level of the exoccipital tips, but not beyond. The ontogenetic series of skulls assigned to *Pi. nana* by Bouetel & de Muizon (2006) display a similar range of variation in development and position of the occipital condyles. Further, this ontogenetic pattern confirms the suggestion by Whitmore & Barnes (2008) that the holotype cranium of *H. transatlanticus*, which possesses occipital condyles closely appressed to the occipital shield and positioned well anterior to the level of the exoccipitals, represents a subadult individual.

Squamosal: Complete squamosals are preserved in UCMP 124950, SDNHM 34155, and SDNHM 65781. In all specimens the squamosal generally has a similar morphology to the squamosals of other herpetocetines as described by Whitmore & Barnes (2008) in being broadly triangular in lateral aspect with a relatively short zygomatic process and a dorsoventrally tall posterior body between the zygomatic crest and the apex of the postglenoid process. The postglenoid process of herpetocetines has rotated from the primitive, transverse orientation in which the glenoid fossa primarily faces anteriorly to assume the derived condition in which the process is more anterolaterally aligned and the glenoid fossa faces anteromedially. It is noteworthy that this anterolateral rotation of the transverse axis of the postglenoid process appears to follow an ontogenetic series, with an almost transversely orientated process in the smallest and most juvenile specimen, SDNHM 125833, and progressively more rotated processes in successively more mature specimens, SDNHM 34155, UCMP 124950, and SDNHM 65781, respectively (Figs 4, 18). Another apparent ontogenetic series observed using the same specimens involves the relative form of the surface of the glenoid fossa, which is transversely and longitudinally convex in less mature specimens (SDNHM 125833 and SDNHM 34155) and transversely and longitudinally planar to slightly concave in more mature specimens (SDNHM 65781). This morphological series is also correlated with expansion and flattening of the distal extremity of the postglenoid process. In SDNHM 125833 and SDNHM 34155 the ventral apex of the postglenoid process distally tapers to a relatively sharp edge, whereas in SDNHM 65781 the ventral apex of the postglenoid process is expanded and flattened to form an approximately lenticular (in ventral view), flattened heel that extends continuously from the posteromedial corner

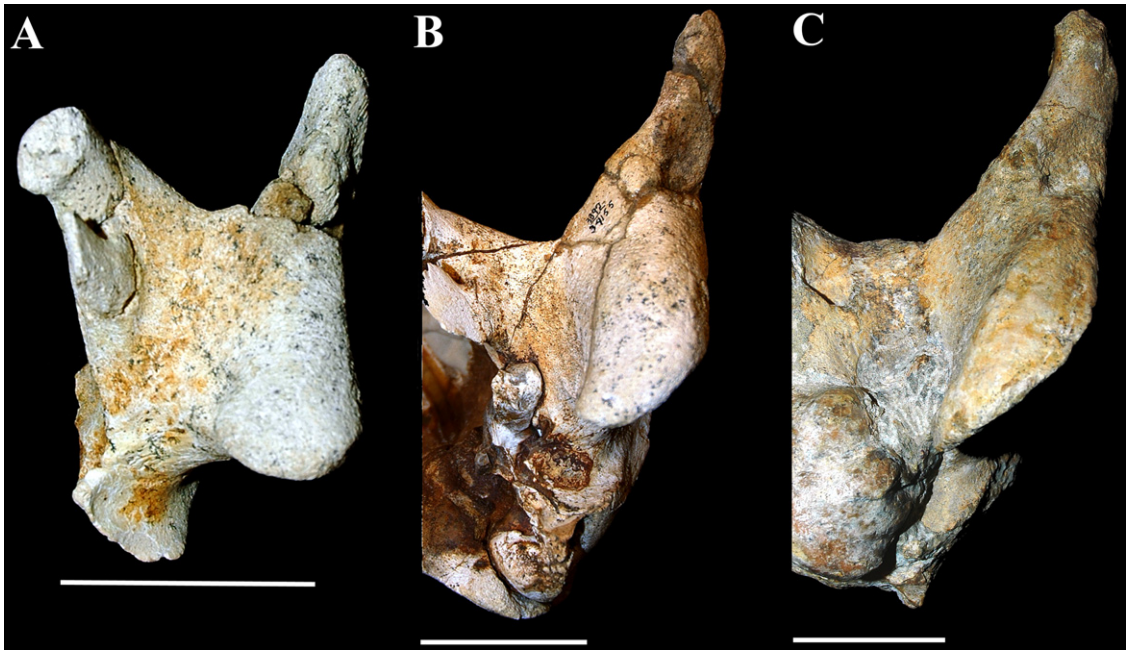

Figure 18. ***Herpetocetus morrowi*** **sp. nov.**, left squamosal in ventral view. A, SDNHM 125833; B, SDNHM 34155; C, SDNHM 65781. Scale bars = 5 cm.

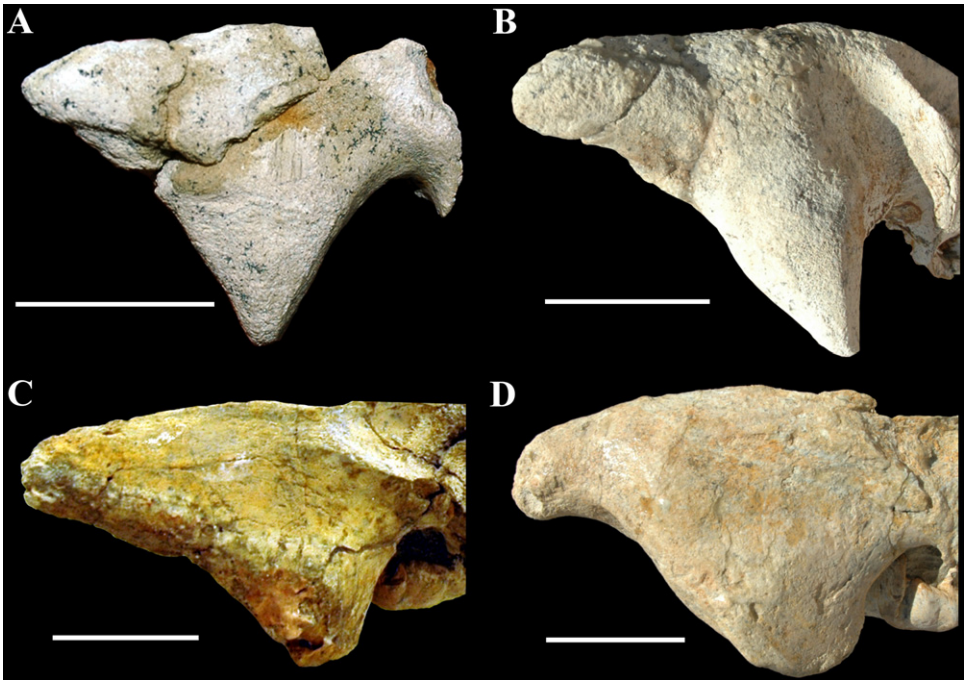

Figure 19. ***Herpetocetus morrowi*** **sp. nov.**, left squamosal in lateral view. A, SDNHM 125833; B, SDNHM 34155; C, UCMP 124950; D, SDNHM 65781. Scale bars = 5 cm.

of the postglenoid process anteriorly around and onto the anterolateral margin of the process (Figs 9, 18–20). The medial margin of this postglenoid heel is sharply defined and separates the nearly vertical surface of the glenoid fossa from the nearly horizontal distal surface of the postglenoid heel.

Anterolateral rotation of the postglenoid process in adult herpetocetines has also resulted in a

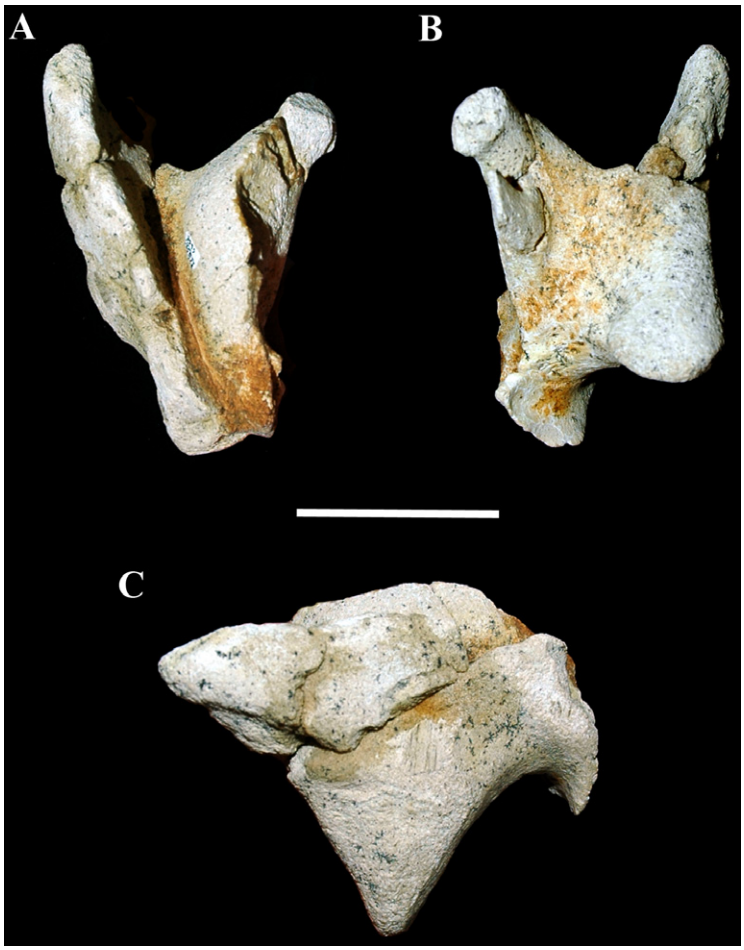

Figure 20. ***Herpetocetus morrowi*** **sp. nov.**, SDNHM 125833, left referred squamosal. A, dorsal view; B, ventral view; C, lateral view. Scale bar = 5 cm.

broad lateral exposure of the external surface of the postglenoid process and has given the posterior portion of the squamosal its broadly triangular appearance. The squamosal morphological series reveals that in juvenile individuals (SDNHM 125833) the posterior border of the postglenoid process assumes the typical, posterior-facing orientation. In this transverse configuration the broad postglenoid process forms the anterior portion of the external auditory meatus and is orientated roughly perpendicular to the lateral surface of the zygomatic process of the squamosal. In successively more mature individuals (SDNHM 34155, UCMP 124950, and SDNHM 65781), the anterolateral rotation of the postglenoid process results in the posterior border of the process now assuming a more lateral orientation. As seen in SDNHM 65781, the surface of the formerly posteriorly facing process no longer forms the anterior portion of the external auditory meatus, but is now positioned roughly in the same plane as the lateral surface of the zygomatic process. As thus configured, the external auditory meatus is bordered anteriorly by the posteromedial corner of the postglenoid process.

The anterior margin of the postglenoid process sharply descends along a roughly uniform sloped glenoid fossa. This differs from *H. bramblei* (UCMP 82465), which has a glenoid fossa that sharply transitions from a moderate ventral slope, anteriorly, to a nearly vertical slope near the distal extremity of the postglenoid process.

The zygomatic process in dorsal aspect is directed anterolaterally, forming an angle with the sagittal plane of ~20–25°. As is true for other herpetocetines, the lateral margin of the zygomatic process aligns with the exoccipital, rather than being distinctly offset laterally from the exoccipital (Figs 2, 3). A similar condition occurs in *Cep. coronatus*. A somewhat different alignment of the lateral margin of the zygomatic process and exoccipital is seen in neobalaenids. In the latter group the zygomatic process is dramatically reduced to the point of being almost indiscernible, and

the lateral surface of the dorsoventrally lengthened postglenoid process is actually displaced medially relative to the lateral surface of the dorsal portion of the squamosal. This dorsal surface of the squamosal, however, does align with the exoccipital to form a laterally convex (not linear) continuous lateral skull border (Fordyce & Marx, 2012).

The squamosal fossa is present, dorsally, and is well demarcated between the braincase wall and the sharply defined zygomatic crest and extends as a narrow fossa from the union of the nuchal and zygomatic crests anteriorly to the posterior rim of the temporal fossa. A very weak subtemporal crest is present in some crania (e.g. SDNHM 65781). The squamosal fossa widens anteriorly, with the anterior transverse diameter of the fossa being roughly twice the posterior diameter. The longitudinal axis of the squamosal fossa, although generally linear, follows a slightly laterally convex arc as it wraps around the squamosal plate of the braincase. Along this longitudinal axis, the floor of the squamosal fossa is also slightly dorsally convex, but is not divided into a distinct dorsally placed posterior subfossa and a more ventrally placed anterior subfossa as in some archaic edentulous mysticetes (e.g. *Eomysticetus whitmorei*). There is no evidence of a squamosal cleft in UCMP 124950 or any of the paratype or referred crania. The overall narrow and elongate aspect of the squamosal fossa is characteristic of herpetocetines, with the exception of *Pi. nana*, which has a squamosal fossa that is relatively larger anteriorly and narrower posteriorly. In other long-snouted mysticetes (e.g. '*Cet.*' *megalophysum*) there is almost no trace of the posterior portion of the squamosal fossa and the anterior portion of the fossa is developed as a hemispherical pocket. In the latter taxon, the dorsal lamina of the squamosal is distinctly swollen laterally on the wall of the braincase and impinges on the squamosal fossa.

As in all herpetocetines, the tympanosquamosal recess is well defined and orientated in the parasagittal plane between the distinctly anterolaterally aligned postglenoid process and the prominent falciform process of the squamosal (Figs 2, 3, 17). The tympanosquamosal recess in *H. morrowi* is transversely broader than in other members of *Herpetocetus* (except NSMT-PV 19540), which have more transversely narrow tympanosquamosal recesses that are tightly constrained by the medial edge of the anterolaterally rotated postglenoid process and the lateral margin of the falciform process. It is noteworthy that the tympanosquamosal recess is essentially absent in *Ca. marginata* and instead this region of the basicranium is marked by a deep and anteroposteriorly elongate ventral crease in the squamosal.

Both the left and right falciform processes are present in UCMP 124950, but neither contains an intact anteromedial edge. In ventral view, the falciform process is transversely broad and somewhat hatchet-shaped. It is divisible into an anterior segment that forms the posterior and ventral rims of the large foramen pseudovale and a posterior segment that extends posteriorly as a triangular projection that is narrowly separated from the tympanic bulla (Fig. 17). In UCMP 124950 this separation, on the left side, measures 2 mm posterolaterally and 6 mm posteromedially. The posterior margin of the falciform process is posteriorly concave to approximate the curvature of the anterior margin of the adjacent tympanic bulla (Figs 2, 3, 17). A similar large and hatchet-shaped falciform process occurs in *H. bramblei* (USNM 219111), *Herpetocetus* sp. nov. (NSMT-PV 19540), *Pi. nana*, and '*Cet.*' *megalophysum* (USNM 205510). In all specimens of *H. morrowi*, the falciform processes have been broken anteromedially, but they probably projected medially to form a relatively broad contact with the pterygoid, as seen in *H. bramblei* (USNM 219111). In UCMP 124950 the squamosal makes up the majority of the foramen pseudovale, with a thin lateral lamina of the pterygoid contributing to the medial rim, and the falciform process forming the lateral edge and floor of the foramen. In general, the foramen pseudovale is roughly triangular in shape and measures 14 mm transversely at the roof of the foramen and 11 mm dorsoventrally at its greatest diameter.

The infundibulum of the external auditory meatus has a relatively uniform diameter both laterally and medially, which differs from the more laterally expanding external auditory meatus of *Cep. coronatus*. As preserved in SDNHM 34155 the infundibulum of the external auditory meatus is formed by the root of the postglenoid process anteriorly and by a thin postmeatal crest posteriorly. This crest is tightly fused to the anterior margin of the expanded 'mastoid process' of the compound posterior process.

Petrosal: In the holotype skull (UCMP 124950) both petrosals and attached tympanic bullae are preserved *in situ*. The right tympanic bulla was removed in order to examine the associated petrosal, which is essentially intact except for an extensive network of diagenetic fractures that penetrate the anterior process (Fig. 17). The right petrosal was not removed from the petrosal fossa (*sensu* Mead & Fordyce, 2009) because of its fragile condition, and consequently the endocranial surface was not available for study. Fortunately, there are two isolated petrosals here referred to *H. morrowi*; SDNHM 38689 (Fig. 21), a complete right petrosal found articulated with a right tympanic bulla, and SDNHM 63690 (Figs 22, 23), an

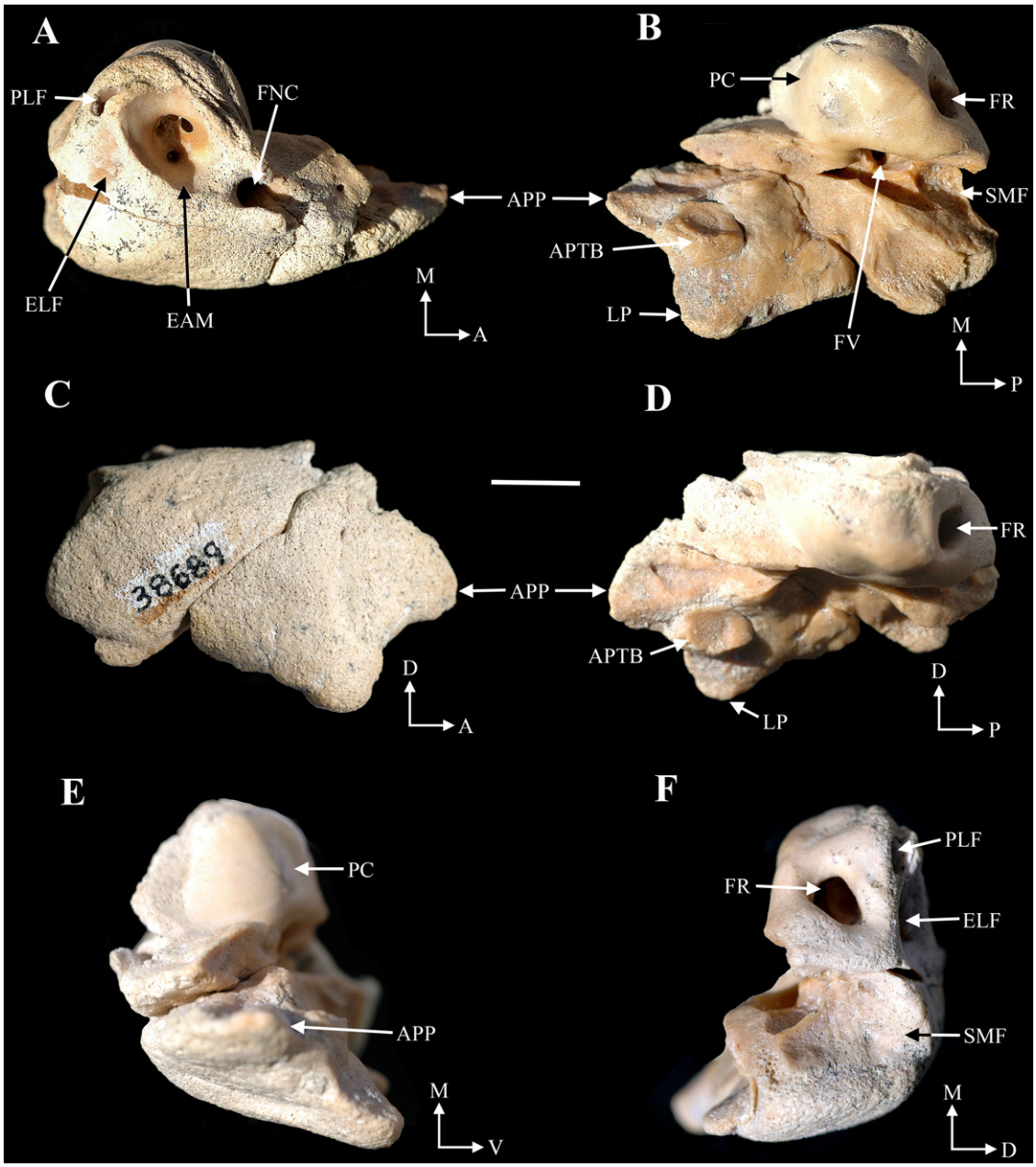

Figure 21. ***Herpetocetus morrowi*** **sp. nov.**, SDNHM 38689, right referred petrosal. A, dorsal view; B, ventral view; C, lateral view; D, medial view; E, anterior view; F, posterior view. Abbreviations: A, anterior; APP, anterior process of the petrosal; APTB, anterior pedicle for attachment of the tympanic bulla; D, dorsal; EAM, external auditory meatus; ELF, endolymphatic foramen; FNC, endocranial opening of the facial nerve canal; FR, fenestra rotunda; FV, fenestra vestibuli; LP, lateral projection of the anterior process; M, medial; P, posterior; PC, pars cochlearis; PLF, perilymphatic foramen; SMF, stylomastoid fossa; V, ventral. Scale bar = 1 cm.

isolated, nearly complete left petrosal. Features of SDNHM 38689 indicate that it is from an immature individual (i.e. small size, shallow and broadly exposed internal auditory meatus, porous surface texture of the suprameatal region, small posterior process, and subdued surface morphology of tympanic bulla). In contrast, SDNHM 63690 appears to be from a more mature individual based on its larger size, well-formed lateral projection of the anterior process, and well-mineralized suprameatal region. The following description of the petrosal of *H. morrowi* is based on features preserved in all three specimens.

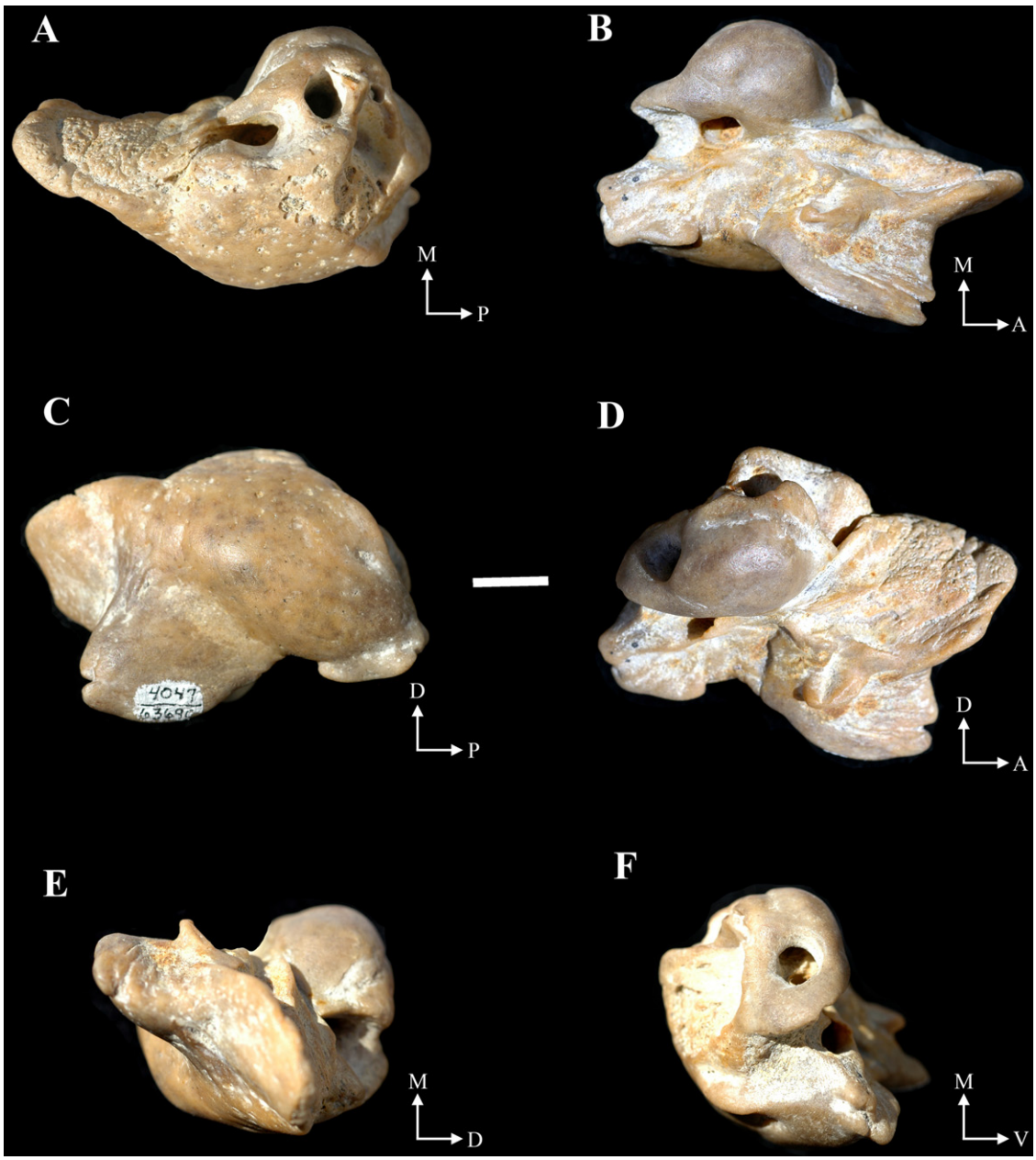

Figure 22. ***Herpetocetus morrowi*** **sp. nov.**, SDNHM 63690, left referred petrosal. A, dorsal view; B, ventral view; C, lateral view; D, medial view; E, anterior view; F, posterior view. Abbreviations: A, anterior; D, dorsal; M, medial; P, posterior; V, ventral. Scale bar = 1 cm.

The right petrosal of UCMP 124950 is large relative to the size of the petrosal fossa, which it almost fills (Figs 4, 5, 17). As articulated with the skull, the anterior process is directed slightly anteromedially toward, but not reaching, the pterygoid sinus fossa. The distal portion of the anterior process is underlapped by the posterior blade of the large falciform process of the squamosal, which remains widely separated from the anterior process throughout its ventromedial curvature. There is no underlapping of the anterior process by the superior lamina of the pterygoid, and in fact the anterior process terminates posterior to the level of the foramen pseudovale. The ventral lateral ridge of the pars cochlearis is tightly articulated with the ventromedial edge of the squamosal from the external acoustic meatus to the posterodorsal edge of the falciform process. The distinct, triangular lateral projection of the anterior process extends ventrolaterally to tightly underlap a portion of the squamosal. The

Figure 23. ***Herpetocetus morrowi*** **sp. nov.**, SDNHM 63690, left referred petrosal; stereophotographic pair in dorsal view. Scale bar = 1 cm.

Figure 24. ***Herpetocetus morrowi*** **sp. nov.**, UCMP 124950, holotype skull in posterolateral view. Scale bar = 5 cm.

compound posterior process is extremely short transversely, but is anteroposteriorly and dorsoventrally expanded distally between the squamosal and exoccipital to create a prominent exposure on the lateral side of the skull (Fig. 24). Anteriorly, the compound posterior process is tightly fused to the postmeatal crest of the squamosal, whereas posteriorly the joint between the posterior process and the exoccipital remains unfused.

The anteroposterior length of the three petrosals as measured from the apex of the anterior process to the posterior rim of the posterior cochlear crest varies from 42 mm in SDNHM 38689, to 48 mm in SDNHM 63690, to 58 mm in UCMP 124950. Some of this size variation appears to be a function of ontogenetic changes, in which the anterior process increases in length more rapidly with age than does the length of the promontorium. Anteroposterior lengths of the three promontoria (measured from the anterior rim of the endocranial opening of the facial canal to the posterior rim of the posterior cochlear crest ranges from 27 mm in SDNHM 38689, to ~29 mm in SDNHM 63690, to 40 mm in UCMP 124950.

Overall, the anterior process of all three petrosals is broad and bluntly triangular in lateral view and distinctly compressed mediolaterally in ventral view. The anterior pedicle for attachment of the tympanic bulla is narrowly elliptical in form, anteroposteriorly orientated, and variably preserved on the epitympanic surface. The groove for the tensor tympani muscle is well developed (especially in SDNHM 63690) as a deeply inset V-shaped fossa medial to the anterior pedicle. None of the petrosals possess an irregular L-shaped anterior edge of the anterior process, a feature present on the left petrosal of *H. transatlanticus* (USNM 182962) and purported by

Fordyce & Marx (2012) to represent an apomorphy shared with *Ca. marginata*. It is likely that this is a polymorphic feature in species of *Herpetocetus* and herpetocetines in general, given the wide range of variation displayed in the available specimens. Furthermore, this 'irregular edge of the anterior process' is formed solely by the anterior process in *Ca. marginata*, but is formed by an interaction between the pars cochlearis and the anterior process in *H. transatlanticus*. This further suggests that the inferred similarities between the shapes of the two anterior processes are not homologous.

Fordyce & Marx (2012) also argued that the lateral projection of the anterior process (= lateral tuberosity) is homologous in *H. transatlanticus* and *Ca. marginata*. The lateral projection in all specimens of *Herpetocetus* examined is constructed as a small, often triangular shelf located lateral to the anterior pedicle of the tympanic bulla and articulating with the squamosal *in vivo*. A distinct flexure separates the root of this projection from the adjacent, dorsolateral surface of the anterior process. In *Ca. marginata* the lateral margin of the anterior process is developed as a greatly elongated and reportedly distinct lateral projection dorsolaterally separated from the main body of the anterior process by a longitudinal groove that articulates with the squamosal (Fordyce & Marx, 2012). Given the distinct difference between the small, triangular lateral projection in species of *Herpetocetus* and the greatly elongated structure and groove of *Ca. marginata*, it appears to be incorrect to suggest that these two morphologies represent the same character state. Fordyce & Marx (2012) also made the distinction that the lateral projection in both *H. transatlanticus* and *Ca. marginata* is positioned anterolateral and not posterolateral to the anterior pedicle. However, the phylogenetic value of this distinction breaks down when the *H. morrowi* petrosal morphological series is examined. In SDNHM 63690 the lateral projection indeed is positioned anterolateral to the anterior pedicle, whereas in SDNHM 34155 the lateral projection is in line with the anterior pedicle, and in SDNHM 38689 it is positioned slightly posterolateral to the anterior pedicle. It is also noteworthy that the anterior process in species of *Herpetocetus* is solidly attached to the entire anterior margin of the pars cochlearis (as it is in essentially all mysticetes), whereas in *Ca. marginata* the wing-like anterior process is only attached to the pars cochlearis via a delicate bony isthmus that connects near the mallear fossa (Ekdale, Berta & Deméré, 2011).

The epitympanic area in *H. morrowi* has a broad and poorly defined mallear fossa and no obvious incudis fossa. As noted by Geisler & Luo (1996) for *Herpetocetus* petrosals from the Yorktown Formation (presumably *H. transatlanticus*), there is no hiatus epitympanicus. However, as also noted by these authors, species of *Herpetocetus* possess a well-developed squamosal flange immediately posterior to the epitympanic area and anterior to the neck of the compound posterior process. A similar feature is present in certain specimens of *H. morrowi*.

The promontorium of *H. morrowi* is globular and anteroposteriorly elongated, being over twice as long as its transverse width (41 and 19 mm, respectively in UCMP 124950). The dorsomedial margin of the promontorium has a distinct promontorial groove, which in more mature specimens clearly demarcates the epitympanic surface of the petrosal from the endocranial surface. The posterior margin of the promontorium is marked by a relatively short posterior cochlear crest that is bluntly triangular in dorsal view. This is also the condition in *H. transatlanticus* and *H. bramblei*. The fenestra cochlea is roughly circular in shape and slightly larger than the fenestra vestibuli (greatest height and length measure 8 and 6 mm, respectively, in UCMP 124950). The fossa for the stapedial muscle lies ventrolateral to the posterior cochlear crest and is wide (11 mm at its greatest transverse width in UCMP 124950) and semiconical to hemispherical in shape, with the apex anteriorly directed toward the fenestra vestibuli. Laterally, the stapedial muscle fossa is separated from the facial nerve sulcus by a low, longitudinal bony septum. The posterior portion of the stapedial muscle fossa is marked by a distinct stylomastoid notch, an indication that the floor of the fossa is not fully ossified. On the posterior surface of the pars cochlearis is a transversely short and roughly square-shaped stylomastoid fossa that does not extend onto the compound posterior process. A large, oval fenestra vestibuli is present on the ventrolateral edge of the pars cochlearis, and measures 4 mm mediolaterally and 6 mm anteroposteriorly in the holotype. The tympanic opening for the facial nerve is positioned posterolateral to the fenestra vestibuli and separated from it by a thin bony septum. The adjacent facial nerve sulcus is relatively short. This is the general condition in mysticete petrosals. In contrast, the tympanic opening for the facial nerve in *Ca. marginata* assumes an entirely novel position well anterior to the fenestra vestibuli and near the anterior margin of the pars cochlearis. As a consequence, the facial nerve sulcus is greatly elongated as it wraps around the anterolateral corner of the promontorium.

The suprameatal area of the petrosal as preserved in SDNHM 63690 lacks any trace of a suprameatal fossa and instead is characterized by a broadly rounded surface that is continuous with a broadly rounded dorsolateral ridge. In the juvenile *H. morrowi* petrosal

(SDNHM 38689), the morphology of the suprameatal region is similar to that in SDNHM 63690, although the area of the dorsolateral ridge is even more rounded. The ventrolateral ridge in SDNHM 63690 is more sharply rounded than the dorsolateral ridge and is set off from the epitympanic region by the longitudinal flexure associated with the lateral projection. This contrasts with the condition in *Herpetocetus* petrosals from the Yorktown Formation (Geisler & Luo, 1996), in which a distinct planar suprameatal fossa is bordered laterally by a sharply angled dorsolateral ridge. Petrosals of *Pi. nana* have a narrow, but more concave suprameatal fossa.

On the dorsal surface of the pars cochlearis of SDNHM 63690 three of the endocranial foramina are roughly aligned with the fenestra cochlea, whereas the fourth foramen (the endolymphatic foramen) is displaced dorsolaterally. From posterior to anterior, the three aligned foramina include a tiny (2 mm), circular perilymphatic foramen, which is separated from the fenestra cochlea by a short bony septum; a larger (5 mm), circular, and deep fundus of the internal auditory meatus; and a larger (~5 mm), oval, and deep endocranial foramen for the facial nerve canal. The facial canal has an anterior fissure for passage of the palatine branch of the facial nerve. Between the internal auditory meatus and the foramen for the facial nerve is a relatively thick (~3 mm) crista transversa that extends nearly to the endocranial surface. The alignment and relative size and shape of these three foramina are similar in petrosals of *Herpetocetus* from the Yorktown Formation and in petrosals of *Pa. palmeri* from the Calvert Formation (Geisler & Luo, 1996). In SDNHM 63690 the endolymphatic foramen lies at the base of a large (7 × 9 mm), diamond-shaped depression positioned dorsolateral to the perilymphatic foramen. The pyramidal process between the perilymphatic foramen and the fundus of the internal auditory meatus is low and unremarkable. It is noteworthy that the morphology of the endocranial surface of the pars cochlearis is slightly different in the juvenile petrosal of *H. morrowi* (SDNHM 38689).

The compound posterior process of the petrotympanic is preserved *in situ* in three specimens including the holotype, as well as SDNHM 34155 and SDNHM 65781. The latter specimen has both petrotympanics in place in the basicranium; however, each is partially concealed by sedimentary matrix. The compound posterior process is best preserved in SDNHM 34155 and can be described as transversely short (~25 mm) and anteroposteriorly wide (40 mm at the widest point). The neck of the process is very narrow (~9 mm) and appears to be primarily square in cross-section. As viewed ventrally, the longitudinal axis of the posterior process forms an angle with the long axis of the pars cochlearis of ~143°. In the holotype this angle is ~154°. The facial nerve sulcus extends onto the compound posterior process as a wide (6 mm) and deep (~7 mm) sulcus that becomes completely floored by bone for the distal 9 mm of its course. As thus configured, the facial nerve canal exits the skull via a circular mastoid foramen approximately 8 mm in diameter (Fig. 24). A similar condition occurs in the holotype skull, wherein the facial nerve canal is completely floored on both of the compound posterior processes. The condition in SDNHM 65781 is equivocal because of breakage.

In lateral view the compound posterior process is broadly expanded on the lateral surface of the skull to form a mastoid process. In the holotype the right mastoid process is broadly rectangle-shaped, measuring 37 mm anteroposteriorly and 58 mm dorsoventrally from its dorsal margin to its posteroventral corner. In SDNHM 34155 these measurements for the left mastoid process are 40 by 49 mm, respectively. Transversely short and laterally expanded compound posterior processes have also been reported in *H. transatlanticus*, *H. bramblei*, *Herpetocetus* sp. nov., *Pi. nana*, *N. eremus*, and *Met. durinasus* (Geisler & Luo, 1996; Bouetel & de Muizon, 2006; Whitmore & Barnes, 2008). As recently discussed by Fordyce & Marx (2012) and Marx *et al.* (2013), *Ca. marginata* also has a laterally expanded compound posterior process. However, the posterior process of *Ca. marginata* is transversely elongated and convex (rather than flattened to concave) on the lateral surface.

Tympanic bulla: Both tympanic bullae are preserved in UCMP 124950 with the left bulla being nearly complete and neither possessing an intact sigmoid process (Figs 17, 25). Several referred tympanic bullae (e.g. SDNHM 34155, 38689, 63691) provide additional morphological details. The right bulla has been removed to reveal the petrosal and petrosal fossa. Anteroposteriorly, the left bulla measures 77 mm, and the anterior lobe measures 50 mm transversely. The transverse width of the posterior lobe cannot be determined because of the missing conical process. The tympanic bulla of *H. morrowi* is several millimetres larger than the holotype tympanic bulla of *H. transatlanticus* (USNM 182962) both transversely and longitudinally.

In ventral view, the bulla has a generally reniform shape, with a narrowly rounded posterior margin and a more bluntly rounded anterior margin. The sigmoid fissure is sharply defined [preserved in SDNHM 38689 (Fig. 26)], whereas the lateral furrow is broad and poorly defined and orientated perpendicular to the longitudinal axis of the bulla. In contrast, the lateral furrow in *Ca. marginata* is sharply defined and orientated oblique to the longitudinal axis. The anterior lobe

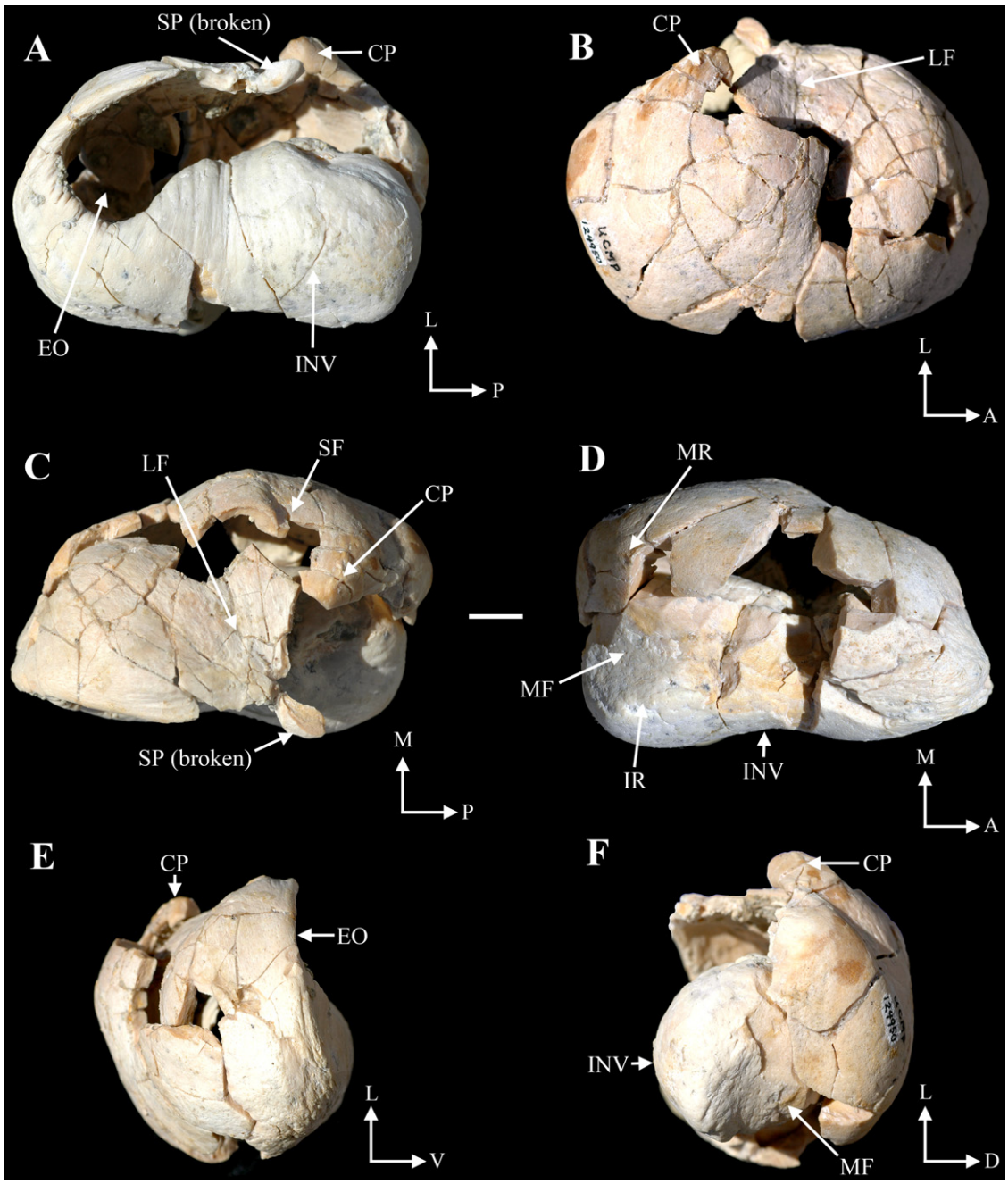

Figure 25. ***Herpetocetus morrowi*** **sp. nov.**, UCMP 124950, right holotype tympanic bulla. A, dorsal view; B, ventral view; C, lateral view; D, medial view; E, anterior view; F, posterior view. Abbreviations: A, anterior; CP, conical process; D, dorsal; EO, Eustachian opening; INV, involucrum; IR, involucral ridge; L, lateral; LF, lateral furrow; M, medial; MF, median furrow; MR, main ridge; P, posterior; SF, sigmoid fissure; SP, sigmoid process; V, ventral. Scale bar = 1 cm.

of the tympanic bulla in *H. morrowi* is relatively long, measuring between 40 and 45% of the total longitudinal length of the bulla. In addition, the anterior margin of the anterior lobe is weakly concave transversely, but is not developed into a conspicuous anterolateral shelf as in many species of *Balaenoptera*.

In dorsal view, the involucrum is characterized by a globular and dorsally expanded dorsal posterior prominence, a derived condition similar to that in *H. transatlanticus*, *Herpetocetus* sp. nov. (NSMT-PV 19540), *N. eremus*, *Pi. nana*, *'Cet.' megalophysum* (USNM 245531), and *'Megaptera' mioceana*. Anterior

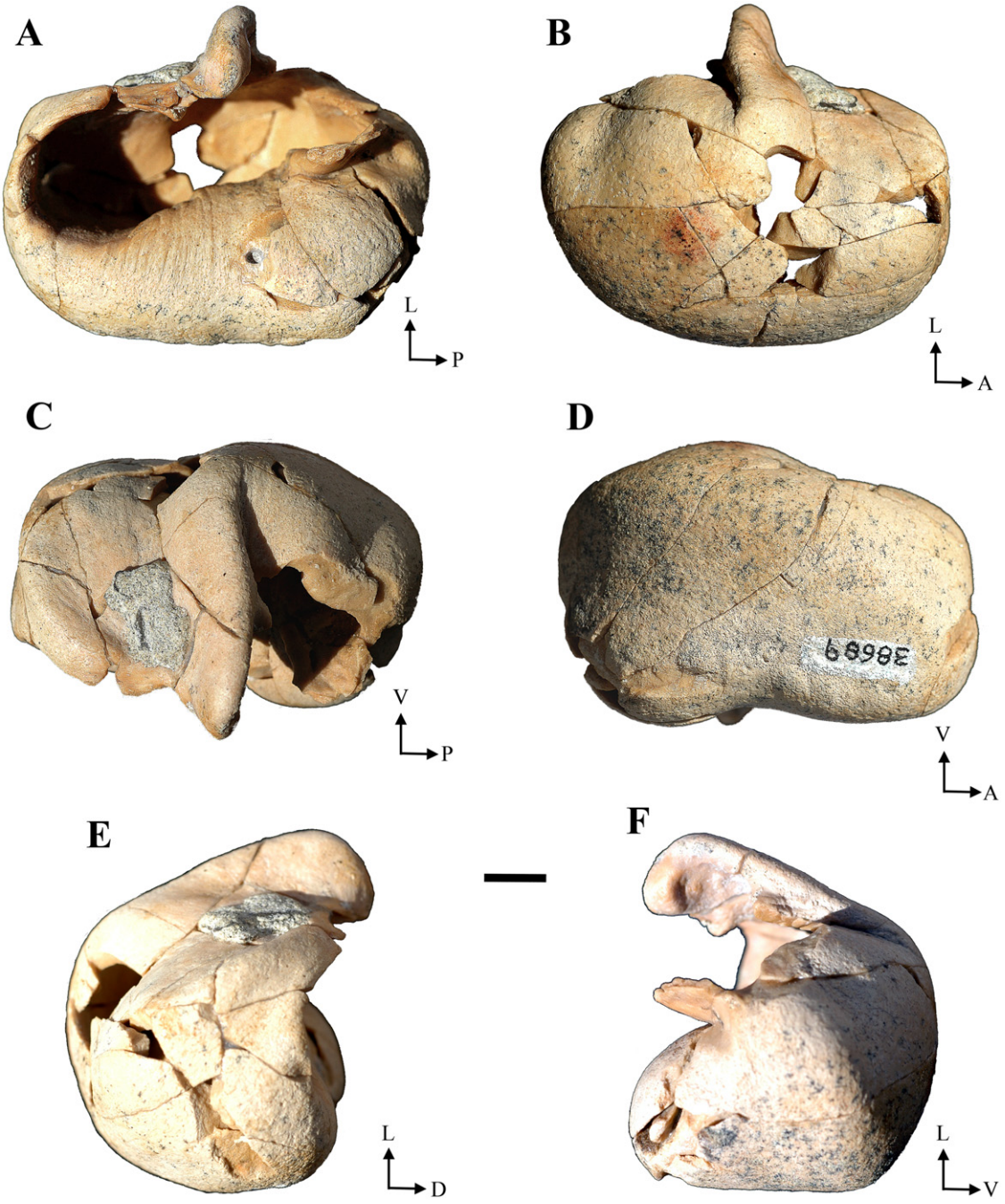

Figure 26. ***Herpetocetus morrowi*** **sp. nov.**, SDNHM 38689, right referred tympanic bulla. A, dorsal view; B, ventral view; C, lateral view; D, medial view; E, anterior view; F, posterior view. Abbreviations: A, anterior; D, dorsal; L, lateral; P, posterior; V, ventral. Scale bar = 1 cm.

to the dorsal posterior prominence, the dorsal surface of the involucrum is crossed by a series of deep transverse creases some of which extend laterally to wrap around the involucral elevation and descend into the tympanic cavity. The Eustachian opening in UCMP 129450 is large, anteriorly broadly rounded, and deeply deflected medially relative to the lateral margin of the involucral elevation. The medial rim of this opening is marked by a series of short (2–3 mm) transverse creases. Medial to these creases, the surface of the involucrum is flattened in a fashion reminiscent of the condition in *Balaenop. acutorostrata* (Ekdale *et al.*, 2011). The anteromedial apex of the involucrum is rounded and not developed

into an anterior spine as occurs in *Pi. nana* (Bouetel & de Muizon, 2006). The conical process in dorsal view is relatively thin and linear compared to that in most other mysticetes, which tend to have conical processes that are thicker and laterally vaulted. Balaenids and neobalaenids also possess linear conical processes, but the processes are even thinner than in species of *Herpetocetus* and typically align with the posterolateral margin of the posterior lobe and are parallel with the longitudinal axis of the bulla. In contrast, the conical process in *Herpetocetus* extends laterally beyond the posterolateral margin of the posterior lobe and forms an angle of ~20° with the longitudinal axis of the bulla. Within the tympanic cavity the posterolateral wall of the bulla is marked by a sharp, linear fold that extends anterodorsally to contact the conical process. This feature has not been observed or reported in any other mysticete bullae. The posterior pedicle is relatively delicate, attaining a maximum transverse diameter no greater than 3 mm. The anterior pedicle is not clearly defined along the thin dorsal margin of the lateral surface of the anterior lobe. The dorsal margin itself is extended dorsally to such a degree as to terminate at a level above the involucrum. In most mysticetes, except balaenids, the dorsal margin of the anterior lobe terminates at a level below the level of the involucrum. As in balaenids and neobalaenids, the medial margin of the involucral ridge of *H. morrowi* when viewed in dorsal profile extends medially to the same level as the medial margin of the main ridge and is not retracted laterally as in balaenopteroids.

In medial aspect, the main ridge is distinctly longer than the involucral ridge and extends in a broad arc from the posterior corner of the bulla to the anterior apex. The main ridge is especially well developed in its posterior half and has a broadly rounded, convex profile in dorsoventral cross-section. Posteriorly, the main ridge is not developed as a posteromedially directed prominence. In contrast, the involucral ridge does possess a posteromedially directed prominence, which in more mature specimens (e.g. SDNHM 34155 and UCMP 129450) is developed as a broad-based pyramidal projection. In medial aspect the axis of the involucral ridge is broadly concave dorsally and converges anteriorly with the more longitudinal axis of the main ridge. In the holotype (UCMP 129450) the anterior apex of the involucral ridge extends beyond the anterior terminus of the main ridge. A distinct median furrow is present in *H. morrowi* and is visible in medial and posterior aspects. The median furrow extends anteriorly to nearly the halfway point between the anterior and posterior margins before it narrows to termination. In this view the bulla of *H. morrowi* closely resembles bullae of *Herpetocetus* sp. nov. (NSMT-PV 19540) and *Pi. nana*.

In posterior view the median furrow between the posterior margins of the involucral and main ridges is broadly concave medially, especially where it approaches the posteromedially directed prominence of the involucral ridge. In the juvenile bulla (SDNHM 38689) the median furrow is a planar surface and lacks the broad concavity of bullae of more mature individuals. The sigmoid process in this view is more dorsally directed than laterally directed and thus projects above the level of the involucrum.

Pterygoid: The pterygoid is relatively small in *H. morrowi* but is well exposed along the ventral and lateral surfaces of the skull (Figs 4, 5, 16, 17). This contrasts markedly with the enormous pterygoid of *Ca. marginata*, but resembles pterygoids in other herpetocetine mysticetes. In UCMP 124950 the lateral exposure of the pterygoid measures 18 mm anteroposteriorly at its dorsal-most edge where it is overlapped by the enlarged alisphenoid to create a horizontally orientated pterygoid–alisphenoid suture. The anterior edge of the pterygoid is underlapped by the palatines along its entire lateral dimension. Posteriorly, the pterygoid broadly abuts the squamosal and forms the thin anterior margin of the foramen pseudovale. The posterior margin of this foramen is formed by the squamosal, with its well-developed, hatchet-shaped falciform process. In *Ca. marginata* the foramen pseudovale lies entirely within the pterygoid and there is no obvious falciform process in the adjacent squamosal.

In UCMP 124950 both the left and right hamular processes retain their original form, but are broken at their anterior contact with the body of pterygoid and displaced dorsally into the overlying pterygoid sinus fossae. The left hamular process is relatively large (~62 mm in anteroposterior length and 45 mm in transverse width), roughly triangular in shape, and was probably anteriorly continuous with the inferior lamina of the pterygoid sinus fossa. The medial margin of the hamular process is medially convex and, as preserved, partially covers the nasal palate of the vomer in ventral view (Fig. 17). The posterolateral margin of the hamular process is posterolaterally concave and extends from the posteromedial margin of the falciform process to the posteriorly directed tip of the hamular process. This configuration is very similar to that seen in the referred skull of *H. bramblei* (UCMP 219111). In contrast, the hamular process of *Pi. nana* appears to be short and transversely narrow. In *Ca. marginata*, the hamular process is poorly defined and consists of a broad and posteriorly convex thickening of the posterior margin of the pterygoid where it floors the internal narial fossa. This configuration is reminiscent of the blunt hamular processes of *Balaena* and *Eubalaena*. In these taxa, however, the hamular

Figure 27. ***Herpetocetus morrowi*** **sp. nov.**, SDNHM 90484, referred basicranium in ventral view. Scale bar = 5 cm.

process is almost entirely covered by the underlying palatine.

Both pterygoid sinus fossae of UCMP 124950 are partially exposed ventrally as a result of the collapse of the left and right hamular processes. The left pterygoid sinus fossa is excavated 8 mm anteriorly beyond the palatine–pterygoid contact and into the pterygoid proper. In SDNHM 90484 this position corresponds to approximately the level of the basisphenoid–presphenoid suture (Fig. 27). The superior lamina of the left pterygoid sinus fossa is well exposed in this specimen and measures 42 mm in width at the level of the pterygoid–squamosal suture and 34 mm in length from the anterior margin of the fossa to the petrosal fossa. The medial lamina is deeply excavated into the pterygoid. This excavation continues posteriorly onto the lateral margin of the basioccipital to form a distinct peribullary sinus fossa. The lateral lamina is shorter than the medial lamina and posteriorly terminates at the anterior rim of the foramen pseudovale. Both the lateral and posterior margins of the lateral lamina are bounded by the squamosal. On the ventral surface of UCMP 124950 a thin posterior lamina extends to the basioccipital crests and contacts the vomer along its entire medial edge. If undamaged, the pterygoid sinus fossa would not be exposed ventrally because of the presence of a broad inferior lamina that is posteriorly continuous with the prominent hamular process. This configuration differs from the condition in '*Cet.*' *megalophysum* in which the pterygoid sinus fossa is more broadly exposed in ventral view. In *Ca. marginata*, the pterygoid sinus fossa is entirely concealed from view by the thickened medial lamina of the pterygoid and the equally thickened pterygoid process of the squamosal.

Alisphenoid: The alisphenoid in the holotype skull is large and roughly rectangular, with an anteroposteriorly elongated (~87 mm long) exposure on the temporal wall (Figs 2, 3, 16). The alisphenoid shares a vertical suture anteriorly with the frontal and is positioned ~11 mm posterior to the anterior edge of the temporal fossa. The alisphenoid forms a horizontal suture with the parietal slightly dorsal to the level of supraorbital process of the frontal. Posteriorly, the alisphenoid–pterygoid suture disappears into a possible fontanelle, which appears to be coincident with the postparietal foramen described in crania of *H. transatlanticus* and *H. bramblei* (Whitmore & Barnes, 2008). The alisphenoid has a long and irregular contact with the squamosal to form an anteroventrally directed suture. The relatively short alisphenoid–pterygoid suture ascends anterodorsally to contact the irregular orbital fissure. The holotype of *H. transatlanticus* also has a large alisphenoid exposure on the temporal wall (erroneously labelled parietal in Whitmore & Barnes, 2008). As reported by Bouetel & de Muizon (2006), adult specimens of *Pi. nana* lack an externally exposed alisphenoid. A very small alisphenoid exposure, however, does occur in subadult specimens of *Pi. nana* (Bouetel & de Muizon, 2006: 335). Immature specimens of *Ca. marginata* also have a small alisphenoid exposure. In contrast, the alisphenoid in the upper Miocene cetotheriid, *Cep. coronatus*, is large and roughly triangular. A large temporal exposure of the alisphenoid generally is considered to represent the pleisiomorphic condition in crown mysticetes. However, given the general pattern of larger alisphenoid exposures in foetal and neonate individuals (Ridewood, 1923), it is possible that this feature in adult cetotheriids may be the result of heterochrony.

Presphenoid: An isolated, nearly complete presphenoid preserved with a partial vomer (SDNHM

42758) measures ~67 mm in length and preserves the complete posterior epiphyseal surface for articulation with the basisphenoid. As in all mysticetes, this articulation was unfused. In dorsal view the presphenoid has a broad, nearly planar endocranial surface that preserves the ventral portion of the sulcus for the optic nerve. This sulcus lies at the posterolateral corner of the presphenoid and is anterolaterally directed at an angle of ~35° to the sagittal plane. Anteriorly, the ventral portion of the ethmoid foramen extends laterally at nearly 90° to the sagittal plane. In ventral view the presphenoid consists of a broad, ventrally directed sagittal ridge that articulated with the nasal plate of the vomer ventrally and the right and left wings of the vomer laterally.

Ethmoid: Portions of the ethmoid are preserved in SDNHM 34155 and SDNHM 42758. In SDNHM 34155 the endocranial surface of the right side of the cribriform plate (i.e. the front of the brain cavity) has a shallow semilunate fossa for the left olfactory lobe of the brain. This fossa is penetrated by a series of cribriform foramina that are grouped into four primary clusters aligned along a dorsomedially orientated arc and separated by delicate bony septa. The right ethmoidal labyrinth is preserved on the anterior surface of the cribriform plate (i.e. the rear of the nasal cavity) and is marked by a series of six ethmoidal cells separated by thin ethmoturbinal bones. Relative to the midfrontal plane, four of the ethmoidal cells are positioned ventrally, one lies within the midfrontal plane, and one lies dorsal to the midfrontal plane. Although incomplete, it is clear that the ethmoturbinals were simple and not folded into the scroll-like structures of terrestrial mammals. Extending ventrolaterally through the ethmoid in the anterior portion of the brain cavity and exiting through the frontal in the medial wall of the optic canal is a slit-like canal that transmits the ethmoidal vessels and nerves. Godfrey, Geisler & Fitzgerald (2013) recently described the ethmoidal anatomy in an Eocene protocetid archaeocete and an extant rorqual mysticete (*Balaenop. acutorostrata*) and suggested that living mysticetes appear to retain a functional olfactory system. Unfortunately, the ethmoid is often not available for study in fossil mysticetes and consequently it is difficult to make meaningful morphological comparisons at this time.

Dentary: The holotype (UCMP 124950) has an associated, nearly complete left dentary, which is missing the anterior ~20% of the horizontal ramus, as well as the majority of the mandibular condyle and the entire angular process (Fig. 28). This represents the second known instance of an associated skull and dentary for a species of *Herpetocetus* with *Herpetocetus* sp. nov. (NSMT-PV 19540), and the first well-described association. In dorsal aspect, the true arc of the lateral curvature of the holotype dentary's horizontal ramus has been distorted because of multiple breaks and some misalignment during preparation. Fortunately, several referred dentaries from the San Diego Formation (e.g. SDNHM 23057, 32138, 35294, 63096, 63257, and 83694) preserve morphological features of the entire dentary of *H. morrowi* (Figs 29–32).

In dorsal view the horizontal ramus of *H. morrowi* is laterally convex, as in all crown mysticetes with the exception of *Eschrichtius robustus*. The degree of curvature is greatest in the posterior quarter of the dentary, especially at the level of the postcoronoid crest. Anterior to this region, the horizontal ramus is relatively straight. In ventral view the posterior portion of the dentary is slightly laterally concave beginning at the level of the coronoid process. Thus, the dentary has an overall sinuous longitudinal profile similar to that seen in balaenopterid mysticetes (Deméré, 1986).

In medial view the distal end of the nearly compete right dentary of *H. morrowi* (SDNHM 63096) is marked by a distinct symphyseal groove, which extends at least 70 mm behind the poorly defined mandibular symphysis (Fig. 29). This symphyseal groove is deepest anteriorly, becoming progressively shallower posteriorly as it merges with a more ventrally placed longitudinal groove that runs posteriorly near the ventromedial margin of the horizontal ramus. This longitudinal groove appears to mark the line of insertion of the mylohyoid muscle (Schulte, 1916). Although clearly defined anteriorly, this mylohyoid groove becomes more subtle posteriorly where it appears to rise dorsally towards the mandibular foramen. Near the dorsomedial margin of the horizontal ramus are a series of approximately nine gingival foramina positioned along the track of the foetal alveolar groove discussed by Ridewood (1923). The distal end of this ossified alveolar groove is marked in SDNHM 63096 by a longitudinal sulcus positioned along the dorsal edge of the dentary that terminates in a distinct, large-diameter foramen. The small-diameter (~1 mm) sulci associated with the more posterior gingival foramina are positioned within 4–10 mm of the dorsal margin and progressively become more anterodorsally inclined from front to back. The most posterior gingival foramen is located within 70 mm of the coronoid process and measures ~3 mm in diameter. On the lateral surface of SDNHM 63096 there are seven mental foramina positioned within 10–14 mm of the dorsal margin. These foramina measure 3–5 mm in diameter and open anteriorly into longitudinal sulci that vary in length from 20–115 mm. Another nearly complete right dentary (SDNHM 63257) has eight mental foramina positioned within 8–11 mm of the dorsal

Figure 28. ***Herpetocetus morrowi*** **sp. nov.**, UCMP 124950, left holotype dentary. A, dorsal view; B, lateral view; C, ventral view; D, medial view (mirrored horizontally) with transverse cross-sections. Scale bar = 10 cm.

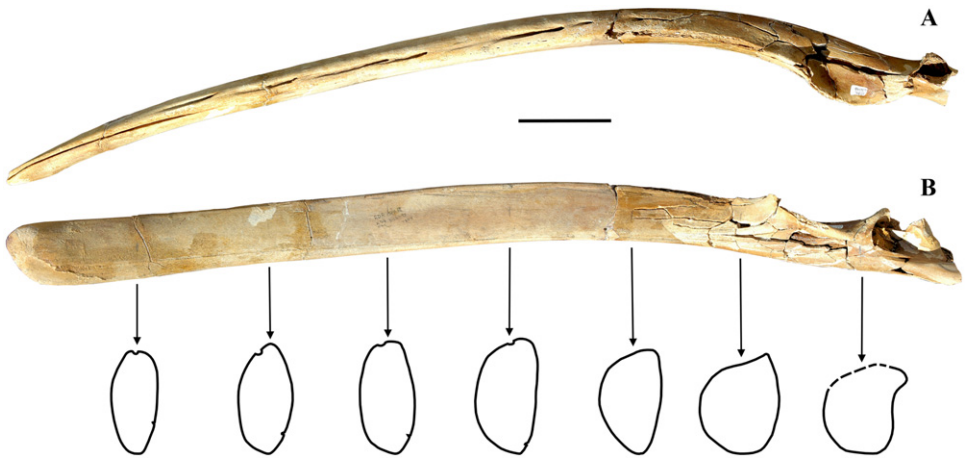

Figure 29. ***Herpetocetus morrowi*** **sp. nov.**, SDNHM 63096, right referred dentary. A, dorsal view; B, medial view with transverse cross-sections. Scale bar = 10 cm.

margin, whereas the holotype left dentary preserves six mental foramina positioned within 4–10 mm of the dorsal margin.

In lateral view the dorsoventral height of the horizontal ramus is nearly uniform from back to front, with a slight increase in dorsoventral height near the anterior end. The shortest dorsoventral height along the horizontal ramus is situated just anterior to the coronoid process where the postcoronoid crest merges with the dorsal margin of the dentary. In SDNHM 32138 and SDNHM 35294, larger referred dentaries from the San Diego Formation, this relative difference in anterior and posterior dorsoventral diameter is more pronounced, which suggests that the distal end

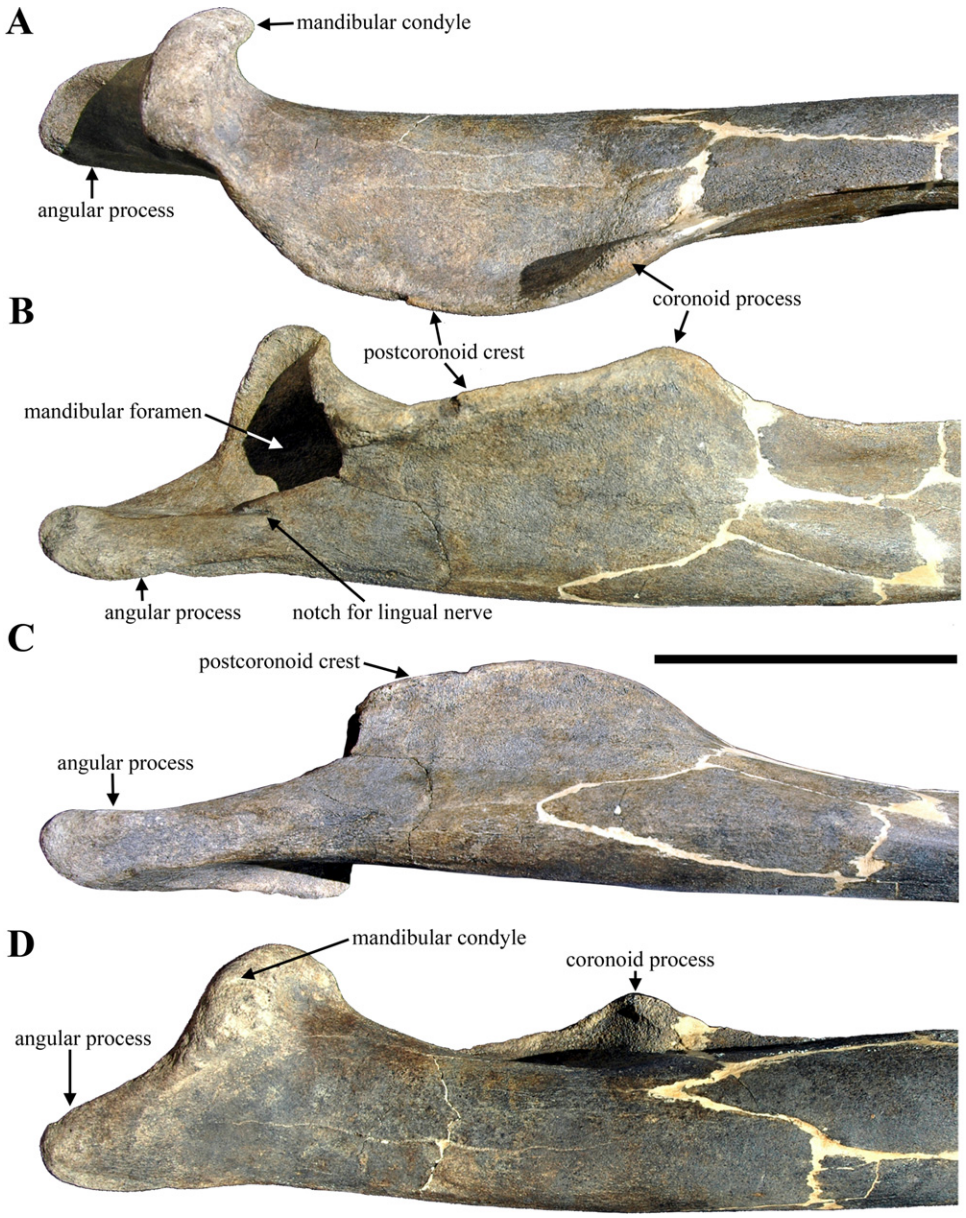

Figure 30. ***Herpetocetus morrowi*** **sp. nov.**, SDNHM 23057, left referred dentary. A, dorsal view; B, medial view; C, ventral view; D, lateral view (mirrored horizontally). Scale bar = 10 cm.

becomes dorsoventrally expanded with developmental age (Fig. 32). This relationship has also been noted in dentaries of Tortonian herpetocetines from California (Boessenecker, 2011a) and is contrary to the condition in balaenopterids, which generally have the maximum dorsoventral diameter positioned just anterior to the coronoid process. Furthermore, the dentary of *Pi. nana* (MNHN SAS 1618) shows a slight dorsoventral expansion at its anterior portion, although it is not nearly to the same degree as the condition observed in *H. morrowi*.

The broadly triangular coronoid process is situated at the anterior end of a long postcoronoid crest from which it is distinguished by a slight, terminal thickening and distinct lateral deflection. In this configuration the coronoid process is comparable to that preserved in the lectotype dentary of *H. scaldiensis*, as well as dentaries of *Pi. nana* and to some extent the dentary of *Cep. coronatus* (USNM 206094). A weakly developed vertical strut descends the lateral side of the coronoid process from the apex to the broadly convex lateral surface of the dentary.

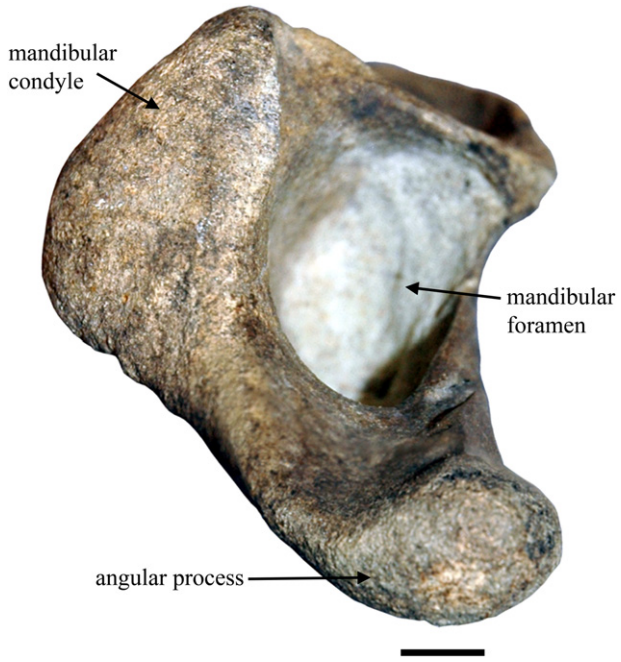

Figure 31. ***Herpetocetus morrowi*** **sp. nov.**, SDNHM 23057, left referred dentary in posterior view. Scale bar = 1 cm.

In UCMP 124950 the curvilinear length of the postcoronoid crest measures 105 mm and extends from the dorsomedial corner of the large mandibular foramen to the apex of the coronoid process. The curvilinear length of the postcoronoid crest in other specimens of *H. morrowi* of comparable size is slightly shorter, with lengths of 90 mm in SDNHM 23057 and SDNHM 83694. In a larger specimen of *H. morrowi* (SDNHM 32138) this measurement is 125 mm. The postcoronoid crest is medially directed at its posterior end, but becomes more vertically directed anteriorly as it ascends in a dorsally convex arc towards the apex of the coronoid process. The middle and anterior portions of the postcoronoid crest are slightly laterally deflected to form the dorsal rim of the concave masseteric fossa. The precoronoid crest is more weakly developed and extends as a low, dorsally concave keel that gradually merges with the dorsal edge of the horizontal ramus.

The mandibular condyle of UCMP 124950 has been nearly completely destroyed, but is clearly directed posterlaterally, as in *Pi. nana* and other herpetocetines described by Boessenecker (2011a). In SDNHM 23057, an isolated left dentary with a complete proximal end, the mandibular condyle is well preserved, offset laterally from the neck of the dentary, and posterolaterally directed (Figs 30, 31). Viewed posteriorly, the articular surface of the mandibular condyle has the shape of a right-angled triangle, with the hypotenuse forming the medial margin of the condyle adjacent to the enlarged mandibular fossa. Viewed laterally, the articular surface of the condyle is orientated ~60° from the horizontal plane. The lateral corner of the mandibular condyle curves anteriorly so that its anterior-most tip is directed in the parasagittal plane. When viewed dorsally, this feature gives the anterior portion of the mandibular condyle a hook-like shape and creates a pocket directly anterior to the condyle. This pocket anterior to the condyle is also present in the holotype left dentary.

Although the angular process is missing from the holotype dentary, several of the referred dentaries of *H. morrowi* do preserve this diagnostic osteological feature (e.g. SDNHM 23057, 35294, and 83694). In these specimens the angular process is well developed as a posteriorly elongated, grossly tubular, bony projection that extends well behind the level of the mandibular condyle (~35 to 45 mm). In his description of *H. scaldiensis*, Van Beneden (1872) called this elongated angular process a 'talon' and likened it to the retroarticular process in the mandible of squamates. It is based on this analogous structure of the angular process that Van Beneden proposed the generic name *Herpetocetus*. Similarly elongated angular processes occur in other herpetocetine mysticetes (Boessenecker, 2011a); although in *Pi. nana* the angular process does not project as far posteriorly. In SDNHM 23057 the ventral surface of the angular process is marked by a distinct longitudinal furrow, which is probably related to insertion of the digastric muscle. This longitudinal furrow is present, but poorly developed in SDNHM 83694. A deep notch is present on the dorsoanteromedial portion of the angular process immediately behind the opening into the large mandibular foramen. This notch is anteromedially directed and is present in all referred *Herpetocetus* specimens from the San Diego Formation, but is absent in *H. bramblei* (UCMP 219079) and *H. scaldiensis* (IRSNB M.379).

A large mandibular foramen is present in UCMP 124950 and referred specimens of *H. morrowi*, and opens posteriorly to exclude the mandibular condyle from reaching the medial side of the dentary. The relative dorsoventral height of the foramen is intermediate between that of nonherpetocetine cetotheres (e.g. *Pa. palmeri*) and that of crown balaenopterids (e.g. *Balaenop. acutorostrata*). In the former, the floor of the mandibular foramen is nearly coincident with the ventral margin of the dentary, whereas in the latter the floor of the foramen is well above the ventral margin. In *H. morrowi* the foramen extends anteriorly only to a level in line with the posterior termination of the precoronoid crest and not beyond. In this respect it resembles the mandibular foramina

Figure 32. ***Herpetocetus morrowi*** **sp. nov.**, SDNHM 35294, left referred dentary in lateral view. Scale bar = 10 cm.

of *H. scaldiensis* (IRSNB M.379) and *Herpetocetus* sp. nov. (NSMT-PV 19540). As discussed by Boessenecker (2011a), the anterior margins of mandibular foramina of Tortonian herpetocetines from California possess a distinct notch, which extends anteriorly to nearly the level of the coronoid process. A shorter anterior notch occurs on the anterior margin of the mandibular foramina in *Pi. nana*.

Cross-sectional profiles of the dentary of *H. morrowi* are generally planoconvex with a planar to weakly convex medial surface and a more strongly convex lateral surface (Figs 28, 29). Near the middle of the horizontal ramus the widest part of the profile is above the midline, whereas in the region of the coronoid process the profile is more nearly circular. Anteriorly, the horizontal ramus is longitudinally rotated such that the medial surface is orientated slightly dorsomedially. A similar condition of longitudinal rotation of the distal portion of the dentary occurs in other herpetocetine mysticetes (Boessenecker, 2011a), as well as in species of *Balaenoptera* (Deméré, 1986). This condition, however, is less extreme than the torsion of the anterior portion of the dentary observed in balaenids.

Postcranial skeleton

Atlas vertebra: The atlas and axis vertebrae are unfused in *H. morrowi*, unlike the condition in balaenids and neobalaenids. The atlas vertebra of UCMP 124950 has been marked #13, which represents a field number and not an inferred order in the vertebral column. The atlas is incomplete and has been broken into two large pieces at the base of the right lamina of the neural arch and the ventrolateral region of the left anterior and posterior articular facets (Fig. 33A, C). Additionally, both transverse processes were damaged during diagenesis, leaving the majority of the left transverse process intact and most of the right missing. There is no evidence of a foramen transversarium on either side. Anteroposteriorly, the atlas is relatively short, measuring 29 mm at its longest point on the left lateral edge, which is a condition distinctly different from the anteroposteriorly long atlases of *Pi. nana* and *Cep. coronatus*.

Viewed anteriorly, the neural spine is relatively low and ridge-like. The neural arch measures 27 mm anteroposteriorly at its thickest point, and exhibits no evidence of postzygapophyses for articulation with the axis. Just dorsal to the anterior articular facet a shallow notch in the left lamina marks the sulcus for passage of the vertebral artery. This configuration differs from that in *Pi. nana*, which has an atlas with laminae that possess an enclosed canal on the ventral portion of each lamina. *Cephalotropis coronatus* (USNM 206094) has a condition similar to that of *H. morrowi*.

The anterior articular facets in UCMP 124950 are reniform in shape, transversely broadest at the midpoint, and shallowly concave. The lateral edges of the articular facets are rounded and do not form a sharp angle with the lateral surface of the centrum. On the posterior surface, the posterior facets for articulation with the axis are transversely thinner than the anterior articular facets, and are broadest in their dorsal-most half. The posterior articular facets are moderately convex and are not sharply offset from the centrum. A steeply ascending and weakly developed facet for articulation with the odontoid process of the axis is present below the neural canal, which separates the left and right posterior articular facets. There is no evidence of a hypophyseal process for articulation with the axis. Hypophyseal processes, however, have been reported in some Miocene mysticetes (e.g. *Pe. calvertensis*; Kellogg, 1965a). In general, the fossa for insertion of the odontoid process is transversely narrower than the spinal canal in UCMP 124950.

Axis vertebra: The axis vertebra (#7) of UCMP 124950 is incomplete, with the right transverse process being dorsoventrally broken at a level approximately 4 mm lateral to the lateral edge of the foramen transversarium (Fig. 33B, D). In general form, the axis is transversely wide and anteroposteriorly compressed, measuring at least 168 mm mediolaterally, 103 mm dorsoventrally, and 15 mm anteroposteriorly. The third cervical vertebra is attached via a thin layer of matrix to the posterior articular facet of the axis, with no visible fusion of bone except at the dorsomedial-most region of the centra. It is unclear whether this fusion is pathological or a result of diagenetic compaction. However, no such fusion is observed in the other vertebrae of UCMP 124950.

In dorsal aspect, the neural arch has been damaged on both the anterior and posterior margins, and the

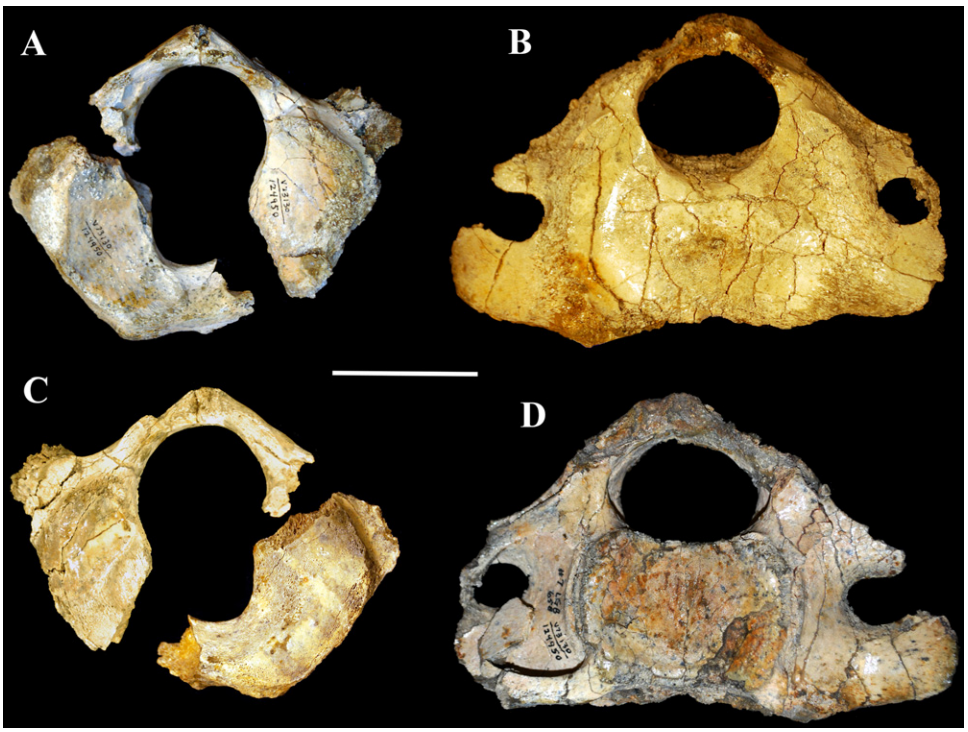

Figure 33. ***Herpetocetus morrowi*** **sp. nov.**, UCMP 124950, holotype cervical vertebrae. A, atlas vertebra, anterior view; B, axis vertebra, anterior view; C, atlas vertebra, posterior view; D axis vertebra and cervical 3, posterior view. Scale bar = 5 cm.

neural spine has been completely abraded away. The neural arch is low and projects dorsoposteriorly to create an ovoid vertebral foramen that measures 46 mm wide and 38 mm tall. It is unclear if the axis possessed zygapophyses because of the lack of complete anterior and posterior margins of the neural arch, as well as the lack of a complete neural arch on the third cervical vertebra.

The anterior articular facets are roughly reniform in shape, are moderately concave, and separated by the odontoid process. Owing to the large width of the odontoid process, the anterior articular facets are broadest dorsally and ventrally, and are narrowest at the midpoint. The ventrolateral margins of the articular facets are laterally convex and are not set apart from the surface of the centrum. This is in contrast to the dorsolateral margins of the articular facets, which are sharp, ridge-like, and project anterior to the surface of the centrum. The odontoid process of the axis is wide and reduced anteroposteriorly. In general form, the odontoid process is smooth and broadly hemispherical in shape with a marked circular depression at its apex. Its ventral surface preserves no discernible facet for articulation with the atlas. The posterior articular facet is obscured by the attached third cervical vertebra.

Both the left and right transverse processes are incomplete in UCMP 124950, although the left transverse process is more complete than the right. As preserved, the transverse processes project posterolaterally and are divisible into dorsal and ventral processes by the well-developed foramen transversarium. This foramen is complete on the right side and configured as a circular opening that measures 15 mm tall and 19 mm wide. The left foramen transversarium is open on its lateral margin, which probably is a feature related to its developmental immaturity.

Other cervical vertebrae: The third cervical is the only other neck vertebra associated with the skeleton of UCMP 124950, and is still articulated with the axis (Fig. 33D). This vertebra is anteroposteriorly thin, measuring 8 mm thick at the centrum. The centrum is nearly elliptic in shape, measuring 74 mm transversely and 50 mm dorsoventrally, and is constricted dorsally and ventrally at the midline. In dorsal view, the posterior surface of the centrum is slightly concave. Both the anterior and posterior epiphyses are present and fused to the centrum, but the epiphyseal sutures are still visible.

The neural canal, although incomplete, is slightly wider than that of the axis (53 mm). Both the left and

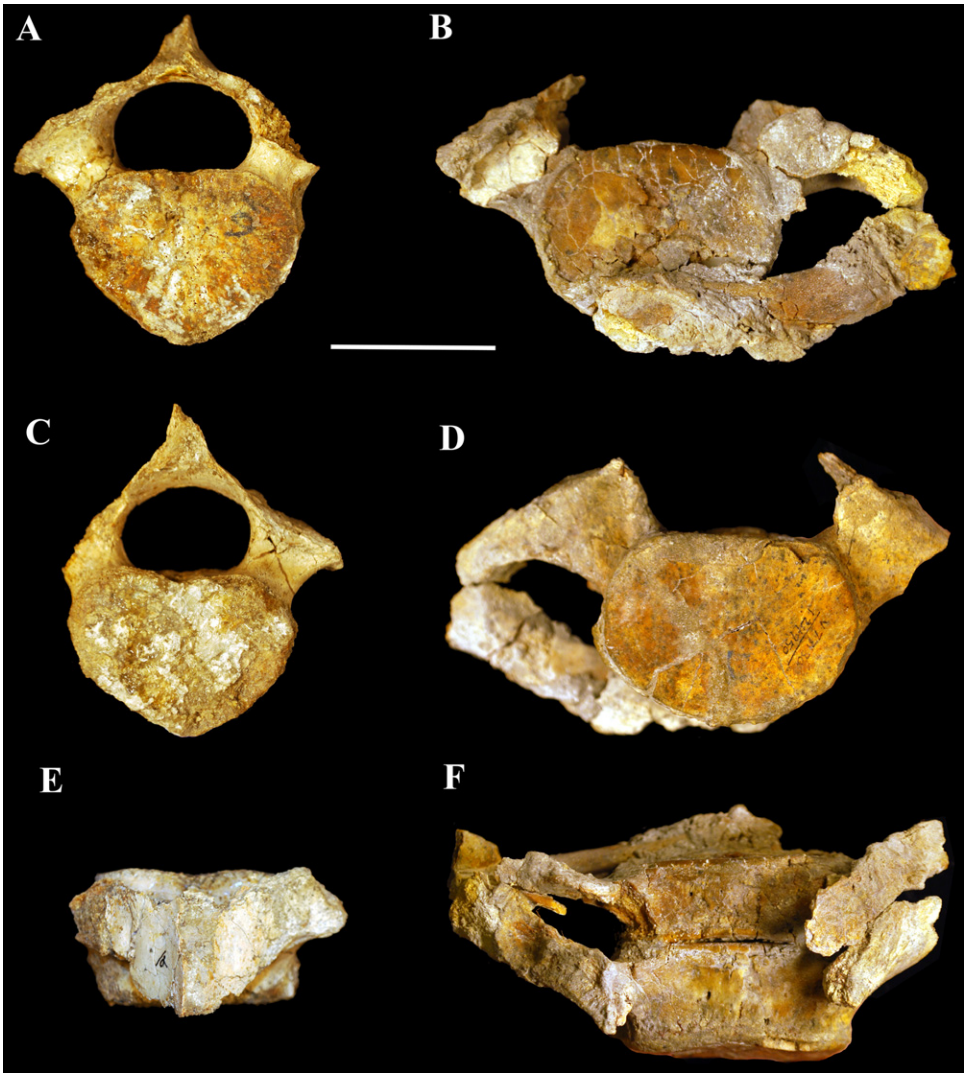

Figure 34. ***Herpetocetus morrowi*** **sp. nov.**, UCMP 124950, holotype thoracic vertebrae. A, vertebra #6, anterior view; B, adjoined vertebrae and rib fragment, anterior view; C, vertebra #6, posterior view; D, adjoined vertebrae and rib fragment, posterior view; E, vertebra #6, dorsal view; F, adjoined vertebrae and rib fragment, dorsal view. Scale bar = 5 cm.

right laminae of the neural arch are broken just above the pedicles. The dorsal surface of the more complete left lamina is tightly adhered, but not fused, to the ventral surface of the neural arch of the axis. The neural spines and zygapophyses have been damaged and lost in UCMP 124950.

The majority of all of the transverse processes of the third cervical vertebra have been lost. The more complete left parapophysis is slender, elongate, and is initially ventrolaterally directed. The parapophysis curves dorsolaterally, suggesting that a large foramen transversarium would have been formed by the parapophysis and the diapophysis, as in *Pi. nana*. The left diapophysis is more slender than the parapophysis, and projects ventrolaterally from the pedicle of the neural arch. Both the right diapophysis and parapophysis are missing.

Thoracic vertebrae: Three thoracic vertebrae were found in association with the skull of *H. morrowi* (Fig. 34). Two of these thoracic vertebrae are connected by matrix, but possess no clear reference field number as is observed for all other vertebrae of UCMP 124950 (Fig. 34B, D, F). The third thoracic vertebra has been marked #6, which represents a field number and not an inferred order in the vertebral column (Figs 1, 34A, C, F). Of the three thoracic vertebrae, the adjoined vertebrae appear to be the most anterior based on the relative anteroposterior

shortness of the centra and the strong anterior deflection of the transverse processes, in dorsal aspect, of the adjoined vertebrae relative to the isolated vertebra. This hypothesis was made via observation of other complete 'cetothere' (both *sensu lato* and *sensu stricto*) vertebral columns (Bouetel & de Muizon, 2006; Kellogg, 1965b), such as those of *Pi. nana* (MNHN SAS 1617) and *Pe. calvertensis* (USNM 11976). A fourth possible thoracic vertebra is associated with UCMP 124950, but its recognition as a thoracic vertebra is questionable and will be addressed with the lumbar vertebrae because of its lack of a clear demifacet for a rib.

The inferred anterior-most thoracic vertebra is the anteroposteriorly shortest, (22 mm centrum length), transversely widest (68 mm centrum width), and dorsoventrally tallest (49 mm centrum height) of the three vertebrae. A second thoracic vertebra is posteriorly attached to the anterior-most thoracic vertebra by matrix. This second thoracic vertebra is considerably longer anteroposteriorly (28 mm centrum length), but is only slightly narrower transversely (67 mm) and shorter dorsoventrally (48 mm). In anterior view the centra of the adjoined vertebrae are roughly elliptic in shape with the dorsal half being slightly wider than the ventral half. The lateral margins of the centra are slightly constricted medially to create an overall concave surface. Both the posterior and anterior epiphyses are fused to the centra in both vertebrae, but the vertebral–epiphysial sutures remain clearly visible. The neural arches and spines of the adjoined vertebrae were lost during diagenesis, leaving only the pedicles and transverse processes intact. The distance between the bases of the left and right pedicles measures 47 mm transversely, which suggests a posterior narrowing of the neural canal relative to the cervical vertebrae. In dorsal aspect, the transverse processes are anterolaterally directed at ~53° relative to the sagittal plane. Both vertebrae are missing the zygapophyses.

The centrum of the proposed posterior-most thoracic vertebra (marked as #6) is nearly twice as long, anteroposteriorly, as the anterior-most thoracic, but is dorsoventrally shorter (46 mm) and transversely narrower (61 mm) than either of the unnumbered adjoined vertebrae. Unlike the other thoracic vertebrae, the centrum of #6 is roughly triangular in shape, with the dorsal half being the widest region and the ventral tip being the narrowest point. The lateral surface of the centrum is less concave than that of the unnumbered adjoined vertebrae and has its greatest curvature ventrally. This concavity occurs on the lateral margin of the centrum until the ventral-most tip, where a raised anteroposteriorly directed ridge is present. Both the posterior and anterior epiphyses are missing from #6, and were probably separated from the centrum during diagenesis. This is also the case for all the lumbar vertebrae and is a reflection of the developmental immaturity of the holotype skeleton. The neural arch of #6 is relatively intact, with only the anterior and posterior margins being damaged. No clear apophysial surfaces are identifiable on #6 because of this damage. In general, the neural arch is low and approximately triangular in shape. This, along with the centrum and pedicles, creates a neural canal that is elliptical in shape, measuring 26 mm tall and 39 mm wide. As was observed in the anterior thoracic vertebrae, this continues the trend of a narrowing neural canal posteriorly along the spinal column. The majority of the distal portion of the neural spine has been lost in #6. Both of the transverse processes are damaged, with the left transverse process being entirely lost and the right being broken at a level ~30 mm from the lateral edge of the neural canal. In dorsal aspect, the right transverse process is anteroposteriorly thicker than the transverse processes of the unnumbered adjoined thoracic vertebrae, and is directed approximately laterally to anterolaterally. The more laterally orientated transverse process of #6 relative to that of the unnumbered adjoined vertebrae suggests that #6 is positioned more distally along the vertebral column.

Lumbar vertebrae: Three lumbar vertebrae are associated with the skull of UCMP 124950 (Figs 1, 35). None of the lumbar vertebrae were found in articulation with each other, but all three have ventrally positioned and ventrolaterally orientated transverse processes, which suggests that they are all posterior lumbar vertebrae. Furthermore, the width and height of the centra are variable between each vertebra, making it unlikely that they were located adjacent to one another in the skeleton. As previously mentioned in the discussion of the thoracic vertebrae of *H. morrowi*, a possible fourth lumbar vertebra was found in association with the skull of UCMP 124950, but its identification as a lumbar vertebra is tentative.

A vertebra, marked as #1, was found immediately posterior to (but not articulated with) the right exoccipital of UCMP 124950 (Figs 1, 35A, B). Classification of this vertebra is uncertain and it may represent either a posterior thoracic vertebra or an anterior lumbar vertebra. The decision to discuss #1 in the description of lumbar vertebrae primarily was based on the lack of clear demifacets for articulation with ribs, as well as on comparisons with the known complete vertebral column of *Pi. nana* (MNHN SAS 1617). The dorsal edges of the transverse processes of #1 are approximately in line with the dorsal edge of the centrum and are horizontal to dorsolateral in orientation. The width of the neural canal, at its broadest, is 31 mm, which is intermediate between

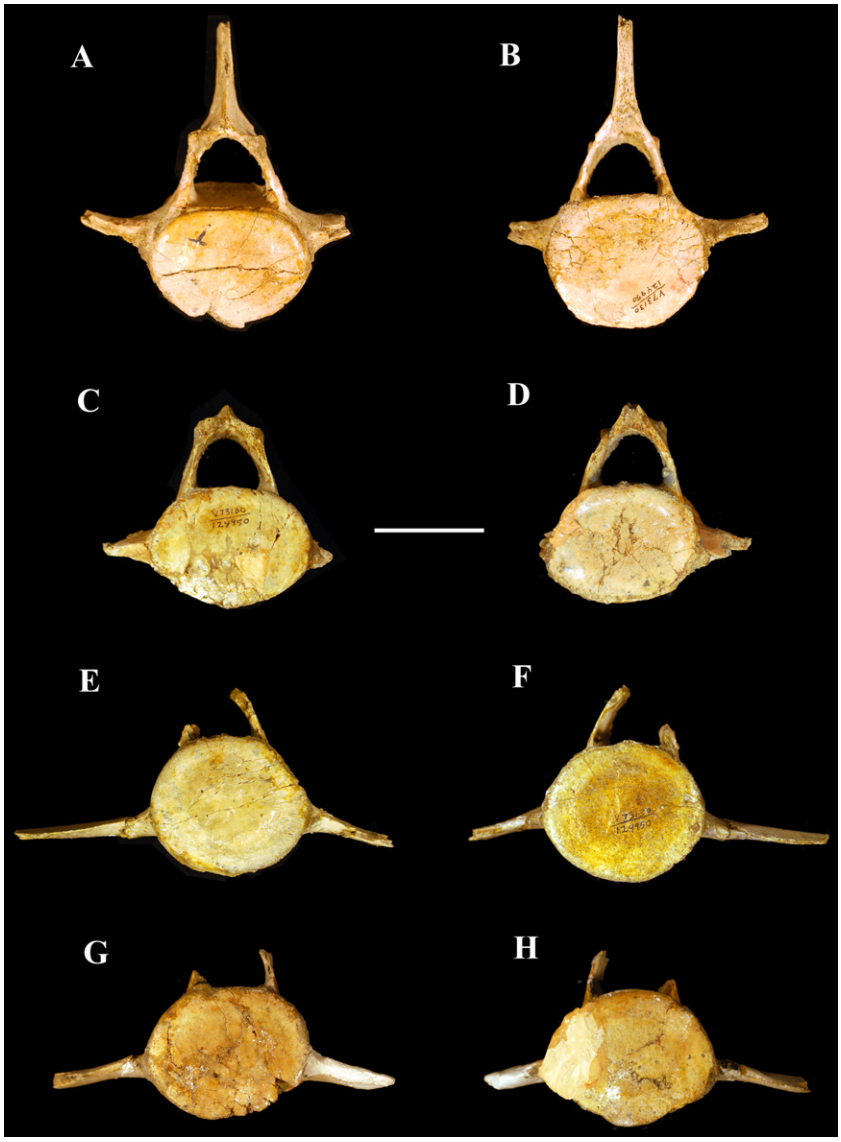

Figure 35. *Herpetocetus morrowi*, UCMP 124950, holotype lumbar vertebrae. A, vertebra #1, anterior view; B, vertebra #1, posterior view; C, vertebra #5, anterior view; D, vertebra #5, posterior view; E, vertebra #2, anterior view; F, vertebra #2, posterior view; G, vertebra #4, anterior view; H, vertebra #4, posterior view. Scale bar = 5 cm.

the wider canal of the posterior-most thoracic (#6) and the narrower canal of the anterior-most lumbar of UCMP 124950. Additionally, the anteroposterior length of the centrum (at 57 mm) is intermediate between that of anterior and posterior vertebrae.

Of the ten total vertebrae found in association with *H. morrowi*, #1 is the most complete with respect to the neural arch and spine. In general, the lateral edges of the transverse processes, the dorsal portion of the neural spine, and the anterior edge of the prezygapophyses of the vertebra were lost during diagenesis. Both the anterior and posterior epiphyses are fused to the centrum but the sutures are still visible. The anterior epiphysis is approximately elliptical in shape, with the widest dimension being at the dorsoventral halfway point (measuring 66 mm wide), and the tallest dimension being in line with the sagittal plane (measuring 51 mm tall). In contrast, the posterior epiphysis appears to be more circular in form than the anterior epiphysis, but its complete form has been ventrally obscured during preparation at UCMP. The centrum measures 57 mm long and is dorsomedially constricted on its ventrolateral surfaces. In lateral view, the ventral surface of the centrum is concavely curved, although to a lesser degree than the ventrolateral surfaces, which creates

the appearance of a slightly anteroposteriorly directed ventral ridge. The spinal canal of #1 is semielliptical in shape, is widest ventrally (at 31 mm wide), and tallest in the sagittal plane (at 29 mm tall). Bounding the spinal canal, the neural arch measures 27 mm long at the base of the pedicles and elongates to 34 mm at the level of the metapophyses. The metapophyses have been anteriorly damaged, and are present as small anterodorsolaterally projecting tubercles. A large, 59 mm tall neural spine is present in #1, but it has been broken dorsally and anteriorly. In lateral view, the neural spine is inclined at 56° relative to the axial plane. The transverse processes are both laterally broken, with the right being more intact than the left. Dorsally, the transverse processes are lateral to posterolateral in orientation at 81° relative to the sagittal plane, and measure 25 mm anteroposteriorly at the proximal edge. In anterior view the transverse processes are slightly dorsolateral in orientation, inclining at 70° relative to the sagittal plane. With respect to position, the transverse processes are located in line with the dorsal edge of the centrum.

With regards to the three lumbar vertebrae that are unequivocal in classification, the vertebra marked as #5, as a reference to field notation, is the most anterior positioned on the vertebral column (Figs 1, 35C, D), although it is clearly not as anteriorly located as #1. Both the anterior and posterior epiphyses are fused to the centrum of #5, but not enough fusion has occurred to obscure the vertebral–epiphysial sutures. The anterior epiphysis has been damaged ventrally, but is clearly elliptical in shape (measuring 67 mm wide and 50 mm tall). The posterior epiphysis is similarly elliptical, and has been damaged medially, dorsolaterally, and ventrolaterally. With respect to centrum length, #5 is the shortest of the three lumbar vertebrae at 63 mm, which continues the general trend of anterior to posterior centrum lengthening in the vertebrae of *H. morrowi*. This trend was also noted in the descriptions of other cetotheres, such as Kellogg (1965a) and Bouetel & de Muizon (2006). The centrum of #5 has been crushed ventrally during diagenesis, which has obscured the morphology of the ventral and ventrolateral surfaces. Both the left and right transverse processes have been damaged proximally, with the right transverse processes being more laterally complete than the left. In anterior view, the transverse processes are positioned at approximately the dorsoventral halfway point on the centrum, and are laterally orientated. The orientation and anteroposterior length of the transverse processes in dorsal aspect are indeterminable in #5 because of the incompleteness of the specimen. The neural arch of #5 is the most complete of the three lumbar vertebrae, but has been damaged dorsoposteriorly and anteriorly. Anteroposteriorly, the neural arch measures 38 mm long at the base of the pedicles. Both metapophyses have been destroyed with only the most proximal portions remaining, although it is clear that they were approximately dorsoanterior in orientation. The neural spine has been lost during diagenesis in #5. In general, the spinal canal is semielliptical in shape, measuring 25 mm tall and 30 mm wide at the base. The spinal canal is thus wider than that of the other lumbar vertebrae and narrower than that of #1, of all thoracic vertebrae, and of all cervical vertebrae in UCMP 124950.

The vertebra marked as #2 for field notation reference is a posterior lumbar vertebra because of its ventrally positioned, and deflected, transverse processes (Figs 1, 35E, F). In general, the vertebra is missing the majority of the neural arch and the entirety of the neural spine. The right transverse process is complete but has been broken and repaired proximally, which has distorted its orientation in anterior view. Conversely, the left transverse process has been broken laterally, but maintains its natural orientation. Both epiphyses are fused to the centrum in #2, with the suture between the anterior epiphysis and the centrum being less visible, and thus more highly fused, than that of the posterior epiphysis. The anterior and posterior faces of the centrum are nearly circular in shape, with the widest point being at approximately the halfway point (measuring 66 mm wide) and the tallest point being in line with the sagittal plane (measuring 59 mm tall). The centrum of #2 is intermediate in length (at 63 mm anteroposteriorly) between the longer #4 and shorter #5, and is longer than the more anteriorly positioned #1. Similarly, the spinal canal is intermediately wide (measuring 26 mm transversely at the ventral base of the spinal canal) between the wider #5 and #1, and the narrower #4. The neural arch has been broken at the pedicles in #2 and is therefore only describable with respect to its anteroposterior length at the base, which measures 37 mm. The transverse processes are positioned just ventral to the dorsoventral halfway point on the centrum. The right transverse process projects 57 mm laterally and measures only 4 mm dorsoventrally, making the transverse processes of #2 shorter than all other lumbar vertebrae in UCMP 124950. In anterior view, the left transverse process is reclined ventrolaterally at 112° relative to the sagittal plane. An accurate recording of transverse process orientation in dorsal view could not be taken on #2 because of the previously described damage to the more complete right transverse process and relatively incomplete left transverse process, but it is clear that they are orientated laterally to slightly anterolaterally.

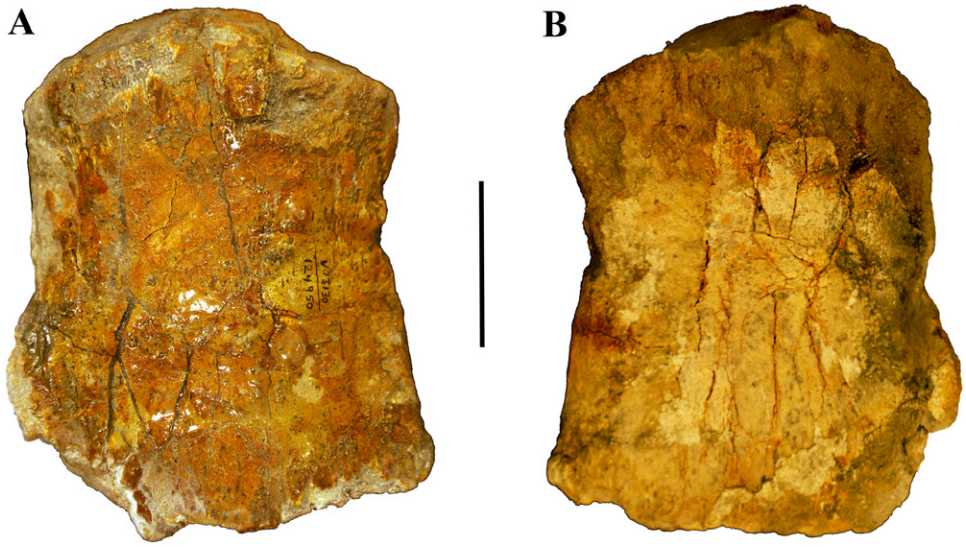

Figure 36. ***Herpetocetus morrowi*** **sp. nov.**, UCMP 124950, left (?) holotype humerus. A, internal view; B, external view. Scale bar = 5 cm.

The lumbar vertebra labelled #4 is the most posteriorly positioned of the lumbar vertebrae (Figs 1, 35G, H). This inference is made based on the lengthening of the centrum beyond the posterior edge of the neural spine relative to the other lumbar vertebrae, the relatively narrower spinal canal, and the laterally shortened transverse processes. The centrum of #4 is noticeably longer than that of the other lumbar vertebrae, measuring 68 mm anteroposteriorly, and extends posteriorly 20 mm beyond the posterior edge of the pedicles for the neural arch. Both the posterior and anterior epiphyses are fused to the centrum, with the margin between the anterior epiphysis and the centrum being nearly indiscernible, and the suture between the posterior epiphysis and the centrum being readily visible. The anterior epiphysis is roughly circular in shape, but is slightly wider than it is tall (at 67 mm wide and 54 mm tall). With respect to the other lumbar vertebrae of UCMP 124950, the lateral surfaces of centrum #4 are the most inflated, but still retain a slight mediolateral constriction ventrally and ventrolaterally. The neural arch has been lost during diagenesis and only the proximal portions of the pedicles remain. Transversely between the pedicles, the spinal canal measures 25 mm wide at the base and is therefore the narrowest of all of the vertebrae found in association with UCMP 124950. The transverse processes of #4 are laterally short, with the nearly complete right transverse process measuring 41 mm mediolaterally. In anterior aspect, the transverse processes are positioned slightly ventral to the dorsoventral halfway point of the centrum, and are deflected 104° ventrolaterally relative to the sagittal plane. Viewed dorsally, the transverse processes are roughly rectilinear in shape, are slightly anterposteriorly longer at the lateral edges, and are orientated anterolaterally at 83° relative to the sagittal plane.

Ribs: A single, relatively complete rib and seven rib fragments were found in association with UCMP 124950. The rib fragments are damaged to the point that they preserve almost no useful morphological features. Although the isolated right rib was unmarked at the time of study, field photographs taken at the time of collection of UCMP 124950 clearly show this rib to be field element #8 (Fig. 1). The rib is anteroposteriorly flattened and has been broken distally. Its capitulum and tuberculum are distinct, although the articular surfaces of both are eroded and damaged. In anterior view, the proximal portion of the rib (neck, capitulum, and tuberculum) is nearly rectilinearly angled with the body. The anterior surface of the shaft is convexly curved, whereas the posterior surface is flattened, except for the region just distal to the tuberculum, which is shallowly concave. Near the proximal-most point of the body, #8 measures 24 mm transversely and is 11 mm anteroposteriorly. Further down the shaft, at the broken distal edge, the rib narrows to 21 mm transversely and measures only 10 mm anteroposteriorly. A distinct ridge is present on the dorsolateral edge of the rib, making it thin and blade-like.

Humerus: A single humerus (left?) is associated with the skull of UCMP 124950 (Figs 1, 36). This poorly mineralized humerus has been badly damaged and is missing the proximal epiphysis. The diaphysis is transversely flattened, with the proximal end being transversely thicker than the distal end (66 and

46 mm, respectively). Conversely, the humerus is anteroposteriorly widest distally (122 mm) and is constricted halfway along the proximal–distal height of the diaphysis, making the anterior and posterior margins concave. From the distal to the proximal end, the humerus measures 142 mm in height, albeit this does not reflect the true height of the humerus because of the incompleteness of both the distal and proximal margins. The radial facet is flat, elliptical in shape, and elongate anteroposteriorly. The ulnar facet has been largely destroyed, but appears to be anteroposteriorly shorter than the radial facet, and continues onto the posterior edge. The general proportions of this incomplete humerus appear to roughly conform to those of *Pi. nana*. The latter taxon has a mean humerus : radius length ratio of 0.7:1.0 (Bouetel & de Muizon, 2006), suggesting that *H. morrowi* had similar forelimb proportions.

Phylogenetic relationships of *Herpetocetus morrowi*

Methods

A phylogenetic analysis was performed using parsimony in the computer application PAUP* 4.0b10 (Swofford, 2003). The data matrix (see Supporting Information Appendix S3) consists of 30 taxa (28 ingroup taxa and two outgroup taxa [see Supporting Information Appendix S1]), which are coded for 130, equally weighted morphological characters (see Supporting Information Appendix S2). Twenty-five characters were ordered and all other characters were unordered. Minimum branch lengths of zero were automatically collapsed. Coding of multistate taxa was treated as an uncertainty, and starting trees were obtained via stepwise addition. During searches, the branch swapping algorithm utilized was tree-bisection-reconnection (TBR). The considered ingroup taxa included an eomysticetid (*Eomysticetus whitmorei*), 17 purported 'cetotheriids' (*Aglaocetus moreni*, *Ag. patulus*, *H. bramblei*, *H. morrowi*, *Herpetocetus* sp. nov. (NSMT-PV 19540), *H. transatlanticus*, *Cep. coronatus*, *'Cet.' megalophysum*, *Cet. rathkii*, *Cophocetus oregonensis*, *Di. hiatus, Met. durinasus*, *'Met.' vandelli*, *Mi. elysius*, *N. eremus*, *Pe. calvertensis*, and *Pi. nana*), five balaenopteroids (*Balaenop. acutorostrata*, *Eschrichtius robustus*, *Megaptera miocaena*, *Meg. novaeangliae*, and *Parabalaenoptera baulinensis*), and five balaenoids (*Ca. marginata*, *Balaena mysticetus*, *Balaenula astensis*, *Eubalaena glacialis*, and *Peripolocetus vexillifer*). The outgroup taxa considered were two toothed mysticetes (*Aetiocetus weltoni* and *Janjucetus hunderi*). A bootstrap analysis was run in PAUP* using 1000 bootstrap replicates and ten random step-wise addition pseudoreplicates per replicate. Bremer support values (Bremer, 1994) were calculated using TNT v. 1.1 (Goloboff, Farris & Nixon, 2008) using the traditional search option and retaining suboptimal trees up to ten steps longer than the shortest tree based on 10 000 replicates. Analyses were run under both accelerated transformation and delayed transformation optimization regimes, with unequivocal apomorphies only being considered as those that occur at nodes under both regimes.

Results

The parsimony analysis conducted for the described data set recovered five most parsimonious trees, with the shortest trees recovered having lengths of 348 steps (consistency index of 0.4785, retention index of 0.6533, and rescaled consistency index of 0.3126). The strict consensus of the most parsimonious trees (Fig. 37) recognized the following monophyletic groups: Chaeomysticeti, crown Mysticeti, Cetotheriidae, Herpetocetinae, Cetotheriinae, Balaenoidea, Balaenidae, Neobalaenidae, Balaenopteroidea, Eschrichtiidae, and Balaenopteridae.

Chaeomysticeti

A well-supported (bootstrap = 95%; Bremer support = 5) edentulous mysticete clade occurs in the most parsimonious trees and is diagnosed by 12 unequivocal characters: premaxillary–maxillary suture on the rostrum unfused (char. 7); supraorbital process anteroposteriorly narrow and very elongate transversely (char. 29); temporal crest extending far onto dorsal surface of supraorbital process of the frontal (char. 33); anterior wing of parietal–frontal suture absent (char. 36), shape of nuchal crests straight in dorsal aspect (char. 39); exoccipital width 70–80% of zygomatic width (char. 44); palate with median keel dividing it into right and left concave surfaces (char. 48); relatively straight dorsal involucral surface of the tympanic bulla in medial view (char. 71); straight horizontal ramus of the dentary in dorsal aspect (char. 106); coronoid process finger-like and laterally deflected (char. 108); mandibular condyle with two major axes of curvature (char. 115); and mineralized teeth absent in adults (char. 119). Of these characters five can be considered unambiguous synapomorphies, which are herein defined as those characters that have a consistency index of 1.0. These unambiguous synapomorphies are characters 7, 48, 108, 115, and 119. This clade includes all edentulous mysticete taxa.

Crown Mysticeti

A monophyletic crown Mysticeti is well supported by the analysis (bootstrap = 90%; Bremer support = 4) and is diagnosed by seven unequivocal characters: dorsal profile of rostrum in lateral aspect not step-like with narial fossa gently ascending posteriorly

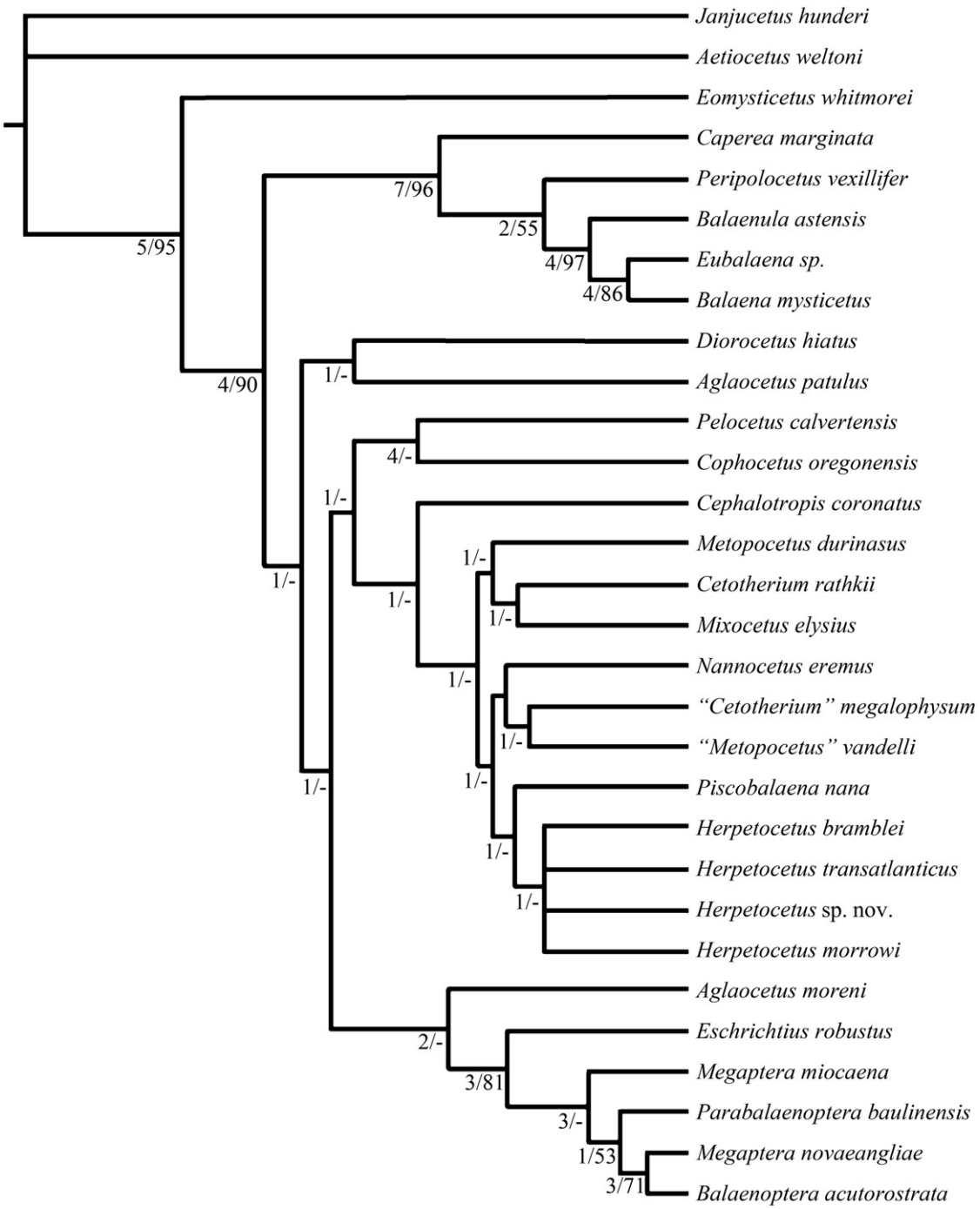

Figure 37. Phylogram showing the strict consensus of five most parsimonious trees (348 steps, consistency index = 0.4785, retention index = 0.6533) recovered during analysis. Numerical values to the left of nodes are Bremer support values and bootstrap support values, respectively. Nodes that received a bootstrap score of less than 50% are denoted with '-'.

(char. 5); nasal length moderately long, 10–17% of condylobasal length (char. 10); length of exposure of cranial vertex short in dorsal aspect (char. 31); supraorbital process of the frontal gradually sloping from vertex (char. 32); main ridge of tympanic bulla long and extending to anterior margin of bulla (char. 64); posterior cochlear crest on the petrosal present as medially extending shelf adjacent to fenestra cochlea

(char. 85); and fenestra cochlea larger than fenestra vestibuli (char. 94). Three of these characters can be considered unambiguous synapomorphies. These are characters 5, 32, and 64. Within the strict consensus of all most parsimonious trees, all edentulous mysticetes, except for *Eo. whitmorei* fell within crown Mysticeti.

Balaenoidea

Balaenoidea is very well supported (bootstrap = 96%; Bremer support = 7) in all of the most parsimonious trees and is diagnosed by 16 unequivocal characters: rostrum moderately arched dorsoventrally (char. 1); rostrum transverse width broad, 20–24% of condylobasal length (char. 2); dorsal profile of cranium in lateral aspect low or flat-lying (char. 8); nasal length short, 0–10% of condylobasal length (char. 10); nasals very broad, width 51–79% of length (char. 11); anterior margin of nasals v-shaped, apex anteriorly directed (char. 13); posterior-most edge of nasals anterior to supraorbital process of frontal (char. 17); ascending process of premaxilla anterior to supraorbital process of frontal (char. 21); position of posteromedial corner of maxilla anterior to supraorbital process of frontal (char. 22); posteromedial corner of maxilla developed as 90° corner (char. 24); apex of occipital shield in line with supraorbital process of frontal (char. 37); anterior-most margin of palatines not exposed at midline (char. 53); tympanic bulla rhomboid in shape (char. 62); conical process of tympanic bulla uniformly thin (char. 70); medial torsion of anterior portion of dentary present (char. 109); and up to six cervical vertebrae fused (char. 124). Of these characters four can be considered unambiguous synapomorphies. These are characters 17, 62, 70, and 124. Balaenoidea contained the families Neobalaenidae and Balaenidae, and included *Cap. marginata*, *Pe. vexillifer*, *Balaenula astensis*, *Eubalaena* sp., and *Balaena mysticetus*.

Balaenidae

A monophyletic Balaenidae is well supported by the analysis (bootstrap = 97%; Bremer support = 4) and is diagnosed by four unequivocal characters: squamosal fossa reduced or absent (char. 41); glenoid fossa and zygomatic process depressed below bulk of basicranium (char. 43); glenoid fossa directed ventrally (char. 46); and tympanic bulla dorsoventrally compressed (char. 63). Of these characters, two can be considered unambiguous synapomorphies. These are characters 43 and 63. This clade consisted of *Balaenula astensis*, *Eubalaena* sp., and *Balaena mysticetus*.

Balaenopteroidea

A moderately well-supported (bootstrap = 81%; Bremer support = 3) Balaenopteroidea occurred in all most parsimonious trees and is diagnosed by six unequivocal characters: nasal width very broad, 51–79% of length (char. 11); supraorbital process of frontal abruptly deflected below vertex (char. 32); anterior margin of occipital shield straight (char. 38); squamosal fossa reduced to absent (char. 41); neck of dentary recurved (char. 105); and mandibular foramen small with maximum height of foramen < 50% of height of neck (char. 107). Two of these characters (characters 32 and 105) can be considered unambiguous synapomorphies. Balaenopteroidea included both Eschrichtiidae and Balaenopteridae, and included *Eschrichtius robustus*, *Meg. miocaena*, *Pa. baulinensis*, *Meg. novaeangliae*, and *Balaenop. acutorostrata*.

Balaenopteridae

Balaenopteridae is moderately supported (bootstrap = 71%; Bremer support = 3) and is diagnosed by four unequivocal characters: nasal length short, 0–10% of condylobasal length (char. 10); nasal width extremely broad, > 80% of nasal length (char. 11); posterior half of nasals attenuated relative to anterior half (char. 18); and lateral margins of nasals anteriorly divergent (char. 19). Of these characters, none can be considered unambiguous. Balaenopteridae consisted of *Meg. novaeangliae* and *Balaenop. acutorostrata* within the strict consensus tree.

Cetotheriidae

A monophyletic Cetotheriidae is very weakly supported (Bremer support = 1), but was recovered in all most parsimonious trees. This clade was diagnosed by seven unequivocal characters: transverse width of rostrum at midpoint narrow, 11–19% of condylobasal length (char. 2); glenoid fossa directed anteromedially (char. 46); posterior sinus present (char. 61); crista transversa high and reaching cerebral surface of pars cochlearis (char. 93); internal opening for vestibulocochlear nerve subequal to internal opening for facial nerve (char. 97), posterior process of petrosal well exposed on lateral wall of skull (char. 103); and angular process of dentary protrudes slightly posterior to posterior edge of mandibular condyle (char. 118). Of these characters, only a single character (character 118) can be considered unambiguous. Cetotheriidae consisted of twelve taxa: *Cep. coronatus*, *Met. durinasus*, *Cet. rathkii*, *Mi. elysius*, *N. eremus*, *'Cet.' megalophysum*, *'Met.' vandelli*, *Pi. nana*, *H. bramblei*, *H. morrowi*, *Herpetocetus* sp. nov., and *H. transatlanticus*. These taxa can be further subdivided into two subfamilies, Cetotheriinae and Herpetocetinae, with only *Cep. coronatus* being excluded from both. Subfamily Cetotheriinae, here, is composed of *Cet. rathkii*, *Met. durinasus*, and *Mi. elysius*. Herpetocetinae is composed of *N. eremus*, *'Cet.' megalophysum*, *'Met.' vandelli*, *Pi. nana*, *H.*

bramblei, *H. morrowi*, *Herpetocetus* sp. nov., and *H. transatlanticus*. Within Herpetocetinae, *Pi. nana* is sister to *Herpetocetus*; and *N. eremus*, '*Cet.*' *megalophysum*, and '*Met.*' *vandelli* group closer to each other than they do to *Pi. nana* or *Herpetocetus*. Furthermore, the structure of this tree suggests that '*Cet.*' *megalophysum* and '*Met.*' *vandelli* are improperly diagnosed and belong to, perhaps, novel genera or a single inclusive genus.

Discussion

The past 10 years has witnessed a resurgence in research focused on the systematics and evolutionary history of Mysticeti. Although the resulting published phylogenies share a number of similarities, no consensus currently exists with regards to the phylogenetic placement of certain species, genera, and clades. All studies recognize a monophyletic Balaenidae and most also recognize a monophyletic Balaenopteridae (e.g. Rychel, Reeder & Berta, 2004; McGowen, Spaulding & Gatesy, 2009; Yang, 2009; Bisconti, 2010; Marx, 2010). The monospecific nature of crown Eschrichtiidae and crown Neobalaenidae render these taxa monophyletic by default. Disagreement in the phylogenetic literature primarily originates from the placement of family-level clades and the topology of deep parts within the mysticete tree. A monophyletic pairing of Balaenopteridae plus Eschrichtiidae to form Balaenopteroidea typically is recovered in studies based on morphological characters (Deméré *et al*., 2005), and although molecular studies typically find a similar result, Balaenopteridae is often recovered as a paraphyletic group with *Eschrichtius robustus* nested within the traditional balaenopterids (Rychel *et al*., 2004; McGowen *et al*., 2009). Morphological studies generally also find a monophyletic Balaenoidea (Balaenidae plus Neobalaenidae) (Bisconti, 2012; Churchill, Berta & Deméré, 2012), whereas molecular studies typically place Neobalaenidae as sister to balaenopteroids (McGowen *et al*., 2009; Slater *et al*., 2010). However, one recent morphological study (Marx, 2010) placed neobalaenids closer to balaenopterids and far removed from balaenids, whereas another study by Fordyce & Marx (2012) went so far as to hypothesize that the extant neobalaenid, *Ca. marginata*, is actually a member of the formerly completely extinct and monophyletic Cetotheriidae. This proposal of *Ca. marginata* as a living cetotheriid will be discussed more fully below.

The inclusion of fossil mysticetes in phylogenetic studies results in expanded tree topologies with increased taxonomic diversity and the inclusion of a number of extinction-pruned mysticete lineages. The taxonomic membership and phylogenetic placement of these extinct lineages varies amongst published studies with certain groups either falling outside of or inside of crown Mysticeti. Deméré *et al*. (2005) recovered a monophyletic Chaeomysticeti, with an early diverging eomysticetid lineage and a stem, paraphyletic grouping of *Isanacetus*-group and *Cetotherium*-group cetotheres (*sensu* Kimura & Ozawa, 2002) positioned outside of crown Mysticeti. A clade consisting of *Mi. elysius* and *Cet. rathkii* (= Cetotheriidae *sensu stricto* of others) was recognized within the 'cetotheres,' whereas crown Mysticeti consisted of a monophyletic Balaenoidea (Balaenidae + Neobalaenidae) and a monophyletic Balaenopteridae (Eschrichtiidae + Balaenopteridae). The latter group included several late Miocene and Pliocene fossil taxa.

Bouetel & de Muizon (2006) recovered a roughly similar topology with a diverse grouping of stem chaeomysticetes positioned outside the crown, which consisted of monophyletic Balaenoidea and Balaenopteroidea. Within their stem chaeomysticete group, Bouetel & de Muizon (2006) recovered a monophyletic Cetotheriidae (*sensu stricto*), which they defined as containing the following taxa: *Mi. elysius*, *N. eremus*, *Cet. rathkii*, *Met. durinasus*, *Herpetocetus sendaicus* (= *Herpetocetus* sp. nov. of this study), and *Pi. nana*.

The study by Steeman (2007) was the first to propose a more inclusive crown Mysticeti that contained all fossil and living chaeomysticetes with the exception of a stem eomysticete clade. Within the crown, Steeman (2007) recognized three higher level monophyletic groups including an early diverging, traditional balaenoid clade and a clade containing a newly recognized, monophyletic Cetotheroidea and a redefined, monophyletic Balaenopteroidea. Cetotheroids included a monophyletic Cetotheriidae (*Cephalotropis*, *Piscobalaena*, *Cetotherium*, *Metopocetus*, *Herpetocetus*, and *Nannocetus*), a monophyletic Eschrichtiidae, and a stem cetotheroid group consisting of '*Cet.*' *megalophysum* and '*Mesocetus*' *argillarius*. Balaenopteroids consisted of a puzzling assortment of early and middle Miocene *Isanacetus*-group cetotheres (*sensu lato*) divided amongst three monophyletic groups, one of which was sister to a monophyletic Balaenopteridae. The decision by Steeman (2007) to name many of these familial-level clades appears to have been premature, as subsequent studies by other authors have not supported these clades.

Bisconti (2008) examined a large number of fossil and living mysticetes in a phylogenetic analysis based on 165 morphological characters. The resulting phylogenetic hypothesis recovered a monophyletic Chaeomysticeti consisting of a stem eomysticetid lineage sister to a diverse crown Mysticeti. As in the phylogeny of Steeman (2007), Bisconti (2008) recovered a monophyletic Balaenoidea at the base of the crown. Balaenoids were sister to a successive

series of *Isanacetus*-group 'cetotheres' plus *Titanocetus sammarinensis*, which in turn was sister to an unnamed clade consisting of a monophyletic Cetotheriidae (*Cet. rathkii*, *Mi. elysius*, and *Met. durinasus*), a monophyletic Eschrichtiidae (*Eschrichtius robustus* and *Eschrichtoides gastaldii*), and a monophyletic Balaenopteridae (includes crown balaenopterids plus an assortment of extinct late Miocene and Pliocene taxa). It is noteworthy that both Steeman (2007) and Bisconti (2008) recovered a monophyletic group composed of cetotheriids (*sensu stricto*) and eschrichtiids to the exclusion of balaenopterids.

Deméré *et al*. (2008) in a total evidence analysis based on a number of fossil and living mysticetes recovered a low diversity crown Mysticeti that excluded all *Isanacetus*-group and *Cetotherium*-group cetotheres and instead contained only balaenids, neobalaenids, eschrichtiids, and balaenopterids. Within the cetotheres was a clade consisting of *Cet. rathkii* and *Mi. elysius*, whereas within the crown, neobalaenids were found to be sister to balaenopteroids to the exclusion of balaenids.

Marx (2010) included 53 fossil and living mysticete taxa in a phylogenetic analysis based on 150 morphological characters. Like Steeman (2007) and Bisconti (2008), Marx (2010) recovered a stem eomysticetid clade that was sister to a more inclusive crown Mysticeti containing all remaining fossil and living chaeomysticetes. Within crown Mysticeti, Marx (2010) recognized an early diverging balaenid clade that was well removed from neobalaenids. A series of early and middle Miocene *Isanacetus*-group cetotheres was positioned between balaenids and a more crownward clade containing a monophyletic Cetotheriidae (*Mi. elysius*, *Pi. nana*, *Metopocetus* spp., *Cet. megalophysum*, *Aulocetus latus*, *N. eremus*, *H. transatlanticus*, and *Cet. rathkii*) and an unnamed clade of neobalaenids + eschrichtiids + balaenopterids.

Bisconti (2012) recently described *Miocaperea pulchra*, the first known fossil neobalaenid, from the upper Miocene of Peru, and included it within a phylogenetic analysis. Like most studies that include fossil taxa, the study of Bisconti (2012) placed all fossil edentulous mysticetes except the stem eomysticetids within crown Mysticeti. In addition, he recovered an early diverging Balaenoidea (balaenids + neobalaenids) and a successive series of fossil-filled clades sister to a crown Balaenopteroidea. Included in the more stemward clades was a monophyletic Cetotheriidae that consisted of *Mi. elysius*, *Cet. rathkii*, *Pi. nana*, and *Met. durinasus*. Unlike his earlier analysis in which eschrichtiids were sister to cetotheriids, Bisconti (2012) recovered a monophyletic Balaenopteroidea consisting of balaenopterids and eschrichtiids.

In the present study, a stem chaeomysticete lineage of eomysticetids is sister to a diverse crown Mysticeti with an early diverging and monophyletic Balaenoidea and later diverging and monophyletic Cetotheriidae and Balaenopteroidea. The few *Isanacetus*-group cetotheres included in this analysis are divided between one clade (*Ag. patulus* + *Di. hiatus*) placed sister to Balaenopteroidea and Cetotheriidae and a second clade (*Co. oregonensis* + *Pe. calvertensis*) positioned sister to Cetotheriidae.

Only a few of these published phylogenies consider the evolutionary relationships of species of *Herpetocetus*. However, those that do consistently place *Herpetocetus* within a monophyletic Cetotheriidae that typically also contains *Cet. rathkii*, *Met. durinasus*, *Pi. nana*, *N. eremus*, and *Mi. elysius*. Bouetel & de Muizon (2006) proposed that *Piscobalaena* and *Herpetocetus* formed a clade with the following successive cetotheriid sister taxa: *Met. durinasus*, *Cet. rathkii*, *N. eremus*, and *Mi. elysius*. In contrast, Whitmore & Barnes (2008) considered *Nannocetus* and *Herpetocetus* to be sister taxa, placing them in a newly named taxon, Herpetocetinae. Unfortunately, Whitmore & Barnes (2008) did not include *Pi. nana* in their study. Furthermore, Whitmore & Barnes (2008) proposed that herpetocetines were sister to a more diverse group of cetotheriid mysticetes, which they assigned to a redefined Cetotheriinae consisting of *Cetotherium*, *Metopocetus*, *Amphicetus*, *Heterocetus*, *Mesocetus*, *Cephalotropis*, *Mixocetus*, and *Plesiocetopsis*. Except for *Cetotherium*, *Metopocetus*, *Cephalotropis*, and *Mixocetus*, the remaining taxa (all from the Belgian Miocene) are generally not diagnosable because each is based on an amalgamation of unassociated skeletal elements. The noncladistic analysis of Whitmore & Barnes (2008) also concluded that the cetotheriine and herpetocetine mysticetes constitute a more inclusive and redefined Cetotheriidae (*sensu stricto*).

The comprehensive study of Marx (2010) did not recover a monophyletic Herpetocetinae (*sensu* Whitmore & Barnes, 2008), but instead found *N. eremus* to be the sister taxon of a clade composed of *Cet. rathkii* and *H. transatlanticus*. In a more recent study, however, Fordyce & Marx (2012) did recover a monophyletic Herpetocetinae, but the genus *Herpetocetus* was found to be paraphyletic, with *N. eremus* more closely related to *H. transatlanticus* to the exclusion of *H. bramblei*. Most surprising was the recovery of *Ca. marginata* nested between *Pi. nana* and a herpetocetine clade within a redefined Cetotheriidae, which contained *Met. durinasus* and *Cet. rathkii* as stem taxa.

The present study recovered a monophyletic Cetotheriidae that is divisible into two main lineages; one consisting of a redefined Cetotheriinae containing

Cet. rathkii, *Mi. elysius*, and *Met. durinasus* and a second consisting of a redefined Herpetocetinae containing a monophyletic group of *Pi. nana* and species of *Herpetocetus*, and a sister clade consisting of *N. eremus* and '*Cet.*' *megalophysum*. The plasticity of the herpetocetine lineage is partly a result of the small sample size and poor preservation of the *N. eremus* hypodigm.

DISCUSSION

The hypodigm of *H. morrowi* consists of numerous specimens, which collectively, preserve a majority of the more diagnostic osteological elements of the skeleton of this Late Pliocene diminutive mysticete. In this regard, the hypodigm of *H. morrowi* is broadly comparable with the large sample of specimens of *Pi. nana* from the upper Miocene of Peru (Bouetel & de Muizon, 2006) and provides a solid basis for understanding the anatomy of herpetocetine cetotheriids. This is especially true for the skull of *H. morrowi*, which preserves functionally significant and ontogenetically informative features of the cranium, rostrum, petrotympanic complex, and dentary.

As with other members of the cetotheriid clade, the skull of *H. morrowi* possesses an elongate and spatulate rostrum attached to a grossly quadrate cranium. The external narial fossa is placed well anterior to the antorbital notch and the level of telescoping is intermediate between that of balaenopteroids and more stemward cetotheres. The posterior rostral elements (maxillae, premaxillae, and nasals) form a deeply V-shaped interdigitation with the frontals. However, the cranial bones are not as anteriorly telescoped as they are in extant mysticetes. Instead, the parietal–frontal and parietal–squamosal sutures are nearly vertical and both the frontal and parietal are exposed in a relatively long intertemporal constriction on the cranial vertex in front of the triangular occipital shield. The temporal fossa is open dorsally and not overhung by a laterally flared nuchal crest and the parietal does not overlap with any portion of the maxilla. Like all herpetocetines, the elongated right and left ascending processes of the maxilla of *H. morrowi* meet proximally at the midline behind the nasals and the posterior portions of the premaxillae terminate well anterior to the posterior termination of the maxillae.

The cranial vertex of *H. morrowi* provides a good model for interpreting the enigmatic cranial morphology of some problematic fossil mysticetes [e.g. *Met. durinasus*, *'Cet.' megalophysum*, and MR 401 (the partial cranium assigned by Van Beneden, 1886, to '*Mesocetus*' *longirostris*)]. In the fragmentary holotype specimens of these taxa there are only two, and not three, sets of posterior rostral bones preserved and previous studies have proposed different interpretations of the homology of these bones. Some authors suggest that only the nasals and premaxillae are preserved (Kellogg, 1965b), whereas other authors have suggested that it is the nasals and maxillae that are preserved (Bouetel & de Muizon, 2006; Whitmore & Barnes, 2008). As revealed in the holotype skull of *H. morrowi*, the proximal portions of the nasals in certain cetotheriids become extremely narrow and are overridden by and hidden beneath the medial margins of the ascending processes of the maxillae. In turn, both the nasals and maxillae terminate posteriorly in the frontal at essentially the same level on the vertex. The proximal portions of the premaxillae, however, actually terminate well anterior to the posterior termination of the maxillae and nasals at the level of the posterior margin of the external narial fossa. Based on these findings it seems likely that the two sets of posterior rostral bones preserved in *Met. durinasus*, *'Cet.' megalophysum*, and MR 401 represent the nasals and maxillae.

Comparison with *Caperea marginata*

Given the recent proposal that *Ca. marginata* is a living fossil and a member of the herpetocetine clade (Fordyce & Marx, 2012; Marx *et al*., 2013), it is relevant to discuss this enigmatic living species in relation to the new fossil species of *Herpetocetus*. Although there are some morphological similarities shared between *Ca. marginata* and herpetocetines, there are also many similarities shared between *Ca. marginata* and extant and extinct balaenids (Bisconti, 2012). The essential question is whether these similarities represent homologous similarities or analogous similarities (i.e. are they the result of common ancestry or of convergence) and, if homologous similarities, are they synapomorphies or symplesiomorphies? Of course there is also the possibility that the proposed similarities actually represent errors in assessment of morphology. In the case of *Ca. marginata* with its many autapomorphic features, this is a real challenge. A case in point is the orientation of the postglenoid process of the squamosal.

Fordyce & Marx (2012) proposed that the very unusual postglenoid process of *H. transatlanticus* is homologous with the equally unusual postglenoid process of *Ca. marginata*. These authors argued that in both taxa the postglenoid process is rotated from a strictly transverse orientation to a more anterolateral orientation and, thus, the glenoid fossae in both taxa face anteromedially. However, we argue that the herpetocetine postglenoid process greatly differs from that of *Ca. marginata* and that many of the observed similarities are superficial. In herpetocetines, including *H. transatlanticus*, the postglenoid

process is distinctly compressed anteroposteriorly and the original transverse axis of the process is strongly rotated anterolaterally so that instead of facing posteriorly to form the anterior border of the external auditory meatus, the posterior surface of the postglenoid process is actually in line with the lateral margin of the zygomatic process of the squamosal. In this configuration the posterior surface of the postglenoid process faces posterolaterally and only the original posteromedial corner of the process is left to form the anterior border of the external auditory meatus. This clearly is not the case in *Ca. marginata* in which the posterior surface of the postglenoid process faces posteriorly to slightly posterolaterally (similar to the plesiomorphic condition) and is still largely transversely orientated. In addition, the posterior surface of the postglenoid process forms a distinct angle with the lateral margin of the zygomatic process. Further, the nearly vertically orientated articular surface of the glenoid fossa in herpetocetines clearly faces anteromedially, whereas in *Ca. marginata* the more horizontally orientated and posteroventrally reclined articular surface of the glenoid fossa faces anteroventrally. Finally, the orientation and shape of the postglenoid process has been shown to change throughout ontogeny in *H. morrowi*, which suggests that the configuration of the postglenoid process in the holotype specimen of *H. transatlanticus*, a relatively young individual (as suggested by Whitmore & Barnes, 2008), should not be considered the adult morphology. Therefore, the comparison of the postglenoid process of the holotype specimen of *H. transatlanticus* with *Ca. marginata* in Fordyce & Marx (2012) is questionable, and should instead be made with adult specimens of *Herpetocetus*.

The condition of the postglenoid process in species of *Herpetocetus* represents a synapomorphy shared with *N. eremus* and *Pi. nana*, whereas the condition in *Ca. marginata* is generally autapomorphic or symplesiomorphic and shared with most other mysticetes. This is not to say that the postglenoid process in *Ca. marginata* is not unusual. In fact, like almost every aspect of its anatomy the postglenoid process in *Ca. marginata* is marked by autapomorphic features. Perhaps most striking is the medially and anteriorly displaced position of the postglenoid process in relation to the zygomatic process of the squamosal. Viewed posteriorly, it is clear that the body of the postglenoid process takes a distinct medial step at the level of the external auditory meatus such that the lateral margin of the zygomatic process is positioned well lateral to the lateral margin of the postglenoid process (see figures in Fordyce & Marx, 2012). Viewed ventrally, the medial displacement of the postglenoid process is clearly evident in the relative positions of the longitudinal axes of the body of the postglenoid process and the anterior apex of the zygomatic process. This configuration does not occur in any other known mysticete (including species of *Herpetocetus*), with the exception of the extinct neobalaenid, *Miocaperea pulchra*. Correlated with the medial displacement of the postglenoid process in *Ca. marginata* is the presence of a deep ventral squamosal crease that occupies the region of the basicranium, which in almost all other mysticetes (including herpetocetines) is occupied by a generally transversely broad tympanosquamosal recess. Fordyce & Marx (2012) also contend that both taxa possess a homologous ventromedially orientated postglenoid process, when viewed posteriorly. Although, when viewed posteriorly, the postglenoid processes in both taxa possess a similar, but analogous, ventromedially orientated ventral corner, this same feature also occurs in species of *Eubalaena*.

The pterygoid is another relevant bone in comparing *Ca. marginata* with extinct herpetocetine mysticetes. *Ca. marginata* has, arguably, the most bizarre pterygoid of any known mysticete. It is enormous and lacks many of the common landmarks of mysticete pterygoids. Like balaenids, the hamular process is reduced to a mere thickening of the posterior margin of the pterygoid and is not developed as a distinct, triangular projection. However, unlike in balaenids, the pterygoid is broadly exposed on the basicranium in *Ca. marginata* and not largely underlapped by the posterior blade of the palatine. Species of *Herpetocetus*, by contrast, have a relatively small exposure of the pterygoid and a distinct, triangular hamular process that is not underlapped by the palatine.

Fordyce & Marx (2012) suggested several homologies between the petrosal of *Ca. marginata* and *H. transatlanticus*. First, these authors noted an irregular, L-shaped anterior edge of the anterior process of the petrosal in both *Ca. marginata* and *H. transatlanticus* (Fordyce & Marx, 2012: character 85). This feature, however, appears to be polymorphic in species of *Herpetocetus*, as it does not clearly appear in specimens of *H. morrowi*. Furthermore, the configuration of the L-shaped anterior edge differs between *Ca. marginata* and *H. transatlanticus*, in that it is formed solely in the anterior process (i.e. only formed by a single structure) in the former, but is formed by the intersection of the anterior process and pars cochlearis (i.e. formed by two structures) in the latter. This suggests that any observed similarity in the shape of these features is purely superficial and should not be considered as homologous (and therefore not useful for determining evolutionary relationships).

A second petrosal synapomorphy for *Ca. marginata* and species of *Herpetocetus* suggested by Fordyce & Marx (2012) is a broad, elongate, shelf-like lateral projection of the petrosal (Fordyce & Marx, 2012:

character 92). As discussed in the description of the petrosal of *H. morrowi*, the lateral projection of the petrosal in all known species of *Herpetocetus* is small and roughly triangular in shape. However, the lateral margin of the anterior process of *Ca. marginata*, as suggested by Fordyce & Marx (2012), is anteroposteriorly elongate and marked a distinct lateral projection that is shelf-like and separated from the remainder of the anterior process by a groove. If this feature can be considered the lateral projection, then it runs for approximately the entire length of the lateral margin of the anterior process, unlike in species of *Herpetocetus*. The morphology of the lateral projections in these two taxa, therefore, is clearly different, not only in size, but also in shape. Finally, Fordyce & Marx (2012) discussed the supposedly similar placement of the lateral projection (being positioned anterolaterally to the anterior pedicle on the anterior process) in *H. transatlanticus* and *Ca. marginata*. However, a morphological (and perhaps ontogenetic) series of petrosals referred to *H. morrowi* shows that the position of the lateral projection relative to the anterior pedicle is either highly variable or changes with ontogenetic age (see discussion of the morphology of the petrosal of *H. morrowi*).

Intraspecific variation in the skull of *Herpetocetus morrowi*

One of the inherent problems faced by systematic palaeontologists is how to deal with morphological variation in the recognition and diagnosis of fossil species. As in extant organisms, morphological variation within a given population is expressed as intraspecific variation amongst individuals of the same ontogenetic age, amongst individuals of different ontogenetic ages, and between individuals of different sexes. As vertebrate palaeontologists often have only a few specimens available for study for any given taxon, it is not unusual for specimens representing each of these different expressions of intraspecific variation to be assigned to different species. This problem of the biological meaning of morphological variation lies at the core of the age-old conundrum of taxonomic lumping vs. taxonomic splitting. It needs to be borne in mind that just as failure to recognize intraspecific variation can lead to overestimates of palaeobiodiversity and related phylogenetic errors, failure to recognize interspecific variation can lead to underestimates of palaeobiodiversity and errors in phylogeny. Thus, when the opportunity arises to study a relatively large suite of vertebrate fossil specimens of a single species, it is cause for celebration.

A good example of ontogenetic variation within *H. morrowi* is seen in the morphological series of squamosals starting with the smallest and most juvenile specimen, SDNHM 125833, and followed by the progressively more mature specimens, SDNHM 34155, UCMP 124950, and SDNHM 65781, respectively. When viewed as an ontogenetic series, these specimens reveal variation in the degree of anterolateral rotation of the postglenoid process, wherein the almost transversely orientated process in SDNHM 125833 becomes progressively more anterolaterally rotated in successively more mature specimens. Anterolateral rotation of the postglenoid process has also resulted in a broad lateral exposure of the external surface of the postglenoid process in adult herpetocetines, which has given the posterior portion of the squamosal its broadly triangular appearance (Fig. 24). In juvenile individuals (SDNHM 125833) the posterior surface of the postglenoid process is orientated roughly perpendicular to the lateral surface of the zygomatic process of the squamosal and forms the anterior margin of the external auditory meatus. In successively more mature individuals (SDNHM 34155, UCMP 124950, and SDNHM 65781) the anterolateral rotation of the postglenoid process results in the posterior surface of the process assuming a more lateral orientation wherein this surface no longer forms the anterior margin of the external auditory meatus, but instead is positioned roughly in the same plane as the lateral surface of the zygomatic process. This same squamosal morphological series also reveals that the relative form of the articular surface of the glenoid fossa, which is transversely and longitudinally convex in less mature specimens (SDNHM 125833 and SDNHM 34155), becomes transversely and longitudinally planar to slightly concave in more mature specimens (SDNHM 65781). Further, the apex of the postglenoid process in juvenile individuals tapers distally to a relatively sharp edge, whereas in more mature individuals (SDNHM 65781), the apex of the postglenoid process is expanded and flattened to form an approximately lenticular (in ventral view), flattened heel that extends continuously from the posteromedial corner of the postglenoid process anteriorly around and onto the anterolateral margin of the process (Figs 18, 19).

The exoccipital also preserves an instructive morphological series that probably translates into an ontogenetic series. The occipital condyles in SDNHM 90484, SDNHM 31455, and UCMP 124950 are relatively broad and closely appressed to the adjacent planar surfaces of the exoccipitals, whereas the occipital condyles in SDNHM 65781 (a developmentally more mature individual) are more well defined and set off from the exoccipitals by a distinct neck. This same degree of morphological variation was used by

Whitmore & Barnes (2008) to propose that the holotype skulls of *H. transatlanticus* and *N. eremus* represented immature individuals, whereas the holotype skull of *H. bramblei* (with its well-defined occipital condyles) was suggested to represent a mature individual.

The variable degree of development of the anterior and posterior processes of the petrosal in *H. morrowi* appears to represent yet another ontogenetic series, with juvenile specimens (SDNHM 38689) possessing an anteroposteriorly short anterior process and distally short and narrow posterior process, whereas more mature specimens (UCMP 124950 and SDNHM 63690) display a relatively longer anterior process and more distally elongated and wider posterior process. Bisconti (2001) noted a similar ontogenetic series in the petrosals of juvenile and adult fin whales (*Balaenoptera physalus* Linnaeus, 1758).

Temporomandibular anatomy and feeding ecology

Inferring fossil mysticete feeding strategies based on osteological features alone has proven to be a perplexing problem. Modern mysticete bulk feeding can be categorized into three general strategies: active lunge feeding (balaenopterids), passive skim feeding (balaenids and neobalaenids), and lateral suction feeding (*Eschrichtius*). In general, feeding strategies in fossil mysticetes have been assumed based on morphological similarities and phylogenetic relationships with modern mysticete groups. However, the unique craniomandibular morphology of *Herpetocetus* greatly differs from that in extant mysticetes, thus limiting the effectiveness of this direct, comparative approach in delimiting function. Fortunately, the *H. morrowi* hypodigm includes several well-preserved dentaries and basicrania that provide sufficient morphological detail to allow for a more biomechanically focused functional analysis of jaw mechanics and feeding strategy in this diminutive Pliocene mysticete.

The angular process of the dentary in *Herpetocetus* is posteriorly elongate, indicating an increased importance of the action of the pterygoid, masseter, and digastric muscles (Figs 30, 38, 39). Several *H. morrowi* dentaries (SDNHM 23057 and SDNHM 83694) display distinct ridges along the angular process that are interpreted in this study to represent osteological correlates of insertion areas for several of the muscles involved in feeding. Along the lateral edge of the angular process, a shallow, dorsoventrally orientated, semicircular ridge extends to approximately the halfway point along the anteroposterior axis of the angular process (Figs 30, 38, 39). Using published accounts of a foetal specimen of *Balaenoptera borealis* Lesson, 1828 by Schulte (1916) and information gained through dissection of a neonate *Eschrichtius robustus* by the authors, this ridge is here interpreted to mark the posterior-most insertion point for the superficial masseter. The dorsal-most extent of the insertion for the superficial masseter in *H. morrowi* is demarcated by a low pedestal directly medial to the anterior-most extent of the mandibular condyle. No muscle attachment scars were noted for the anterior-most part of the superficial masseter insertion. The deep portion of the masseter does not appear to have any well-defined muscle attachment scars on the dentaries of *H. morrowi*. However, it is likely that this muscle filled the area immediately dorsal to the superficial masseter and the remainder of the masseteric fossa.

A distinct pair of ridges, one medial and one lateral, is visible on the ventral surface of the angular process (Figs 30, 38, 39). The ridges run in parallel anteroposteriorly until approximately the level of the anterior border of the mandibular foramen. These ridges and the intervening ventral surface between them, are here interpreted as the osteological correlate for the insertion of the digastric muscle.

The medial surface of the angular process is flattened to slightly concave with longitudinally orientated crests on the dorsal and ventral sides of the concavity. The dorsal crest runs approximately from the ventromedial border of the mandibular foramen, posterolaterally, to a position just lateral of the posterior-most edge of the angular process before terminating. The ventral crest is equivalent to the ridge forming the medial margin of the insertion of the digastric muscle. These crests and concavity are interpreted as the insertion point for the medial pterygoid muscle.

The temporalis muscle inserts onto the coronoid process, as in all mammals. SDNHM 23057 bears a distinct muscle attachment scar, which spans the majority of the pre- and postcoronoid crests, as well as the coronoid process. Posteriorly, this scar is narrow and is exposed along the medial edge of the precoronoid crest. As it approaches the position of the coronoid process, the scar becomes more expanded and dorsally positioned before narrowing again along the postcoronoid crest. The majority of the temporalis therefore inserts onto the coronoid process, but is probably present as a thin sheet of muscle along the pre- and postcoronoid crests.

The temporomandibular joint of most species of modern mysticetes, with the exception of balaenids and neobalaenids, is nonsynovial and fibrocartilaginous (Schulte, 1916; Pivorunas, 1977; and Lambertsen, Ulrich & Straley, 1995). A discrete joint capsule is instead replaced with an interarticular pad consisting of a fibrocartilaginous mass. This mass

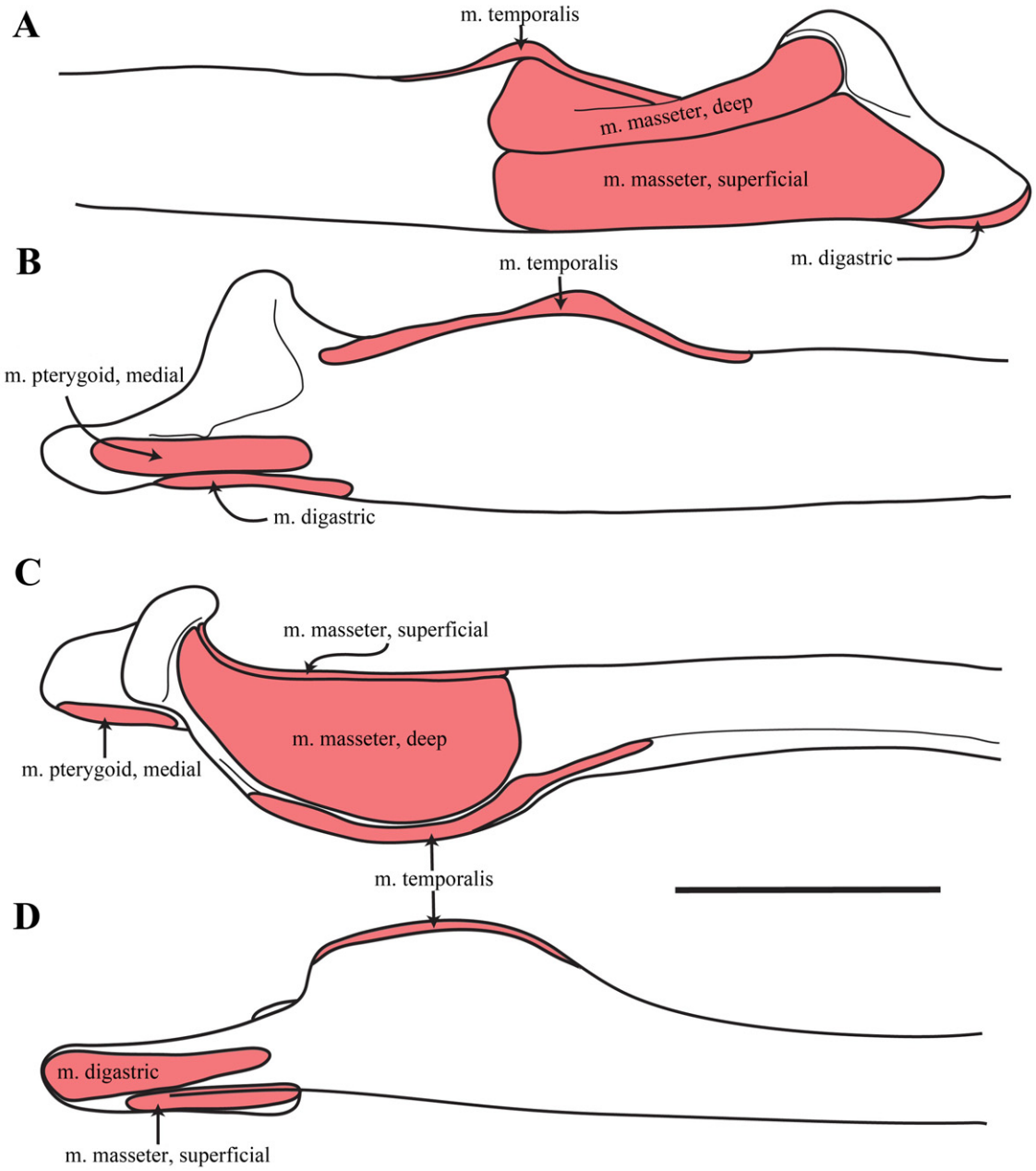

Figure 38. ***Herpetocetus morrowi*** **sp. nov.**, SDNHM 23057, illustrated left dentary showing hypothesized insertion points of the mandibular musculature. A, lateral view; B, medial view; C, dorsal view; D, ventral view. Scale bar = 10 cm. Abbreviation: m, muscle.

originates from the glenoid fossa and surrounds the mandibular condyle. The lack of a synovial articulation coupled with the elastic mandibular symphysis permits lateral motion of the dentaries at the symphysis and at the temporomandibular joint in balaenopterids and eschrichtiids (omega-rotation of Lambertsen *et al.*, 1995). This lateral movement is another manner in which oral volume can be maximized. Interestingly, the shape and orientation of the postglenoid process in *H. morrowi* impedes omega-rotation by physically blocking the posterior portion of the mandible from moving laterally. Furthermore, the posteriorly elongate angular process, coupled with the constriction of the size of the glenoid fossa posteriorly by the postglenoid process and tympanic bulla in *H. morrowi*, inhibits abduction (delta-rotation of Lambertsen *et al.*, 1995) of the mandible to the same degree as seen in modern mysticetes.

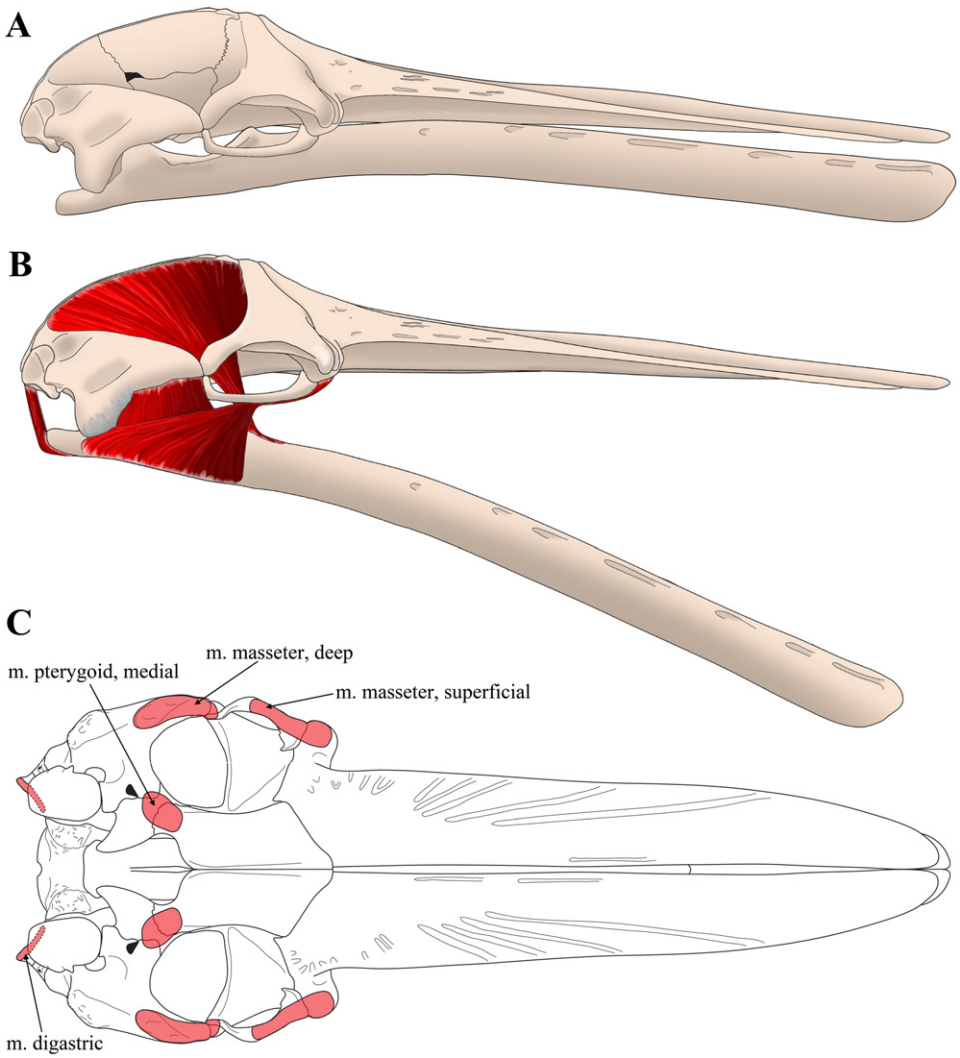

Figure 39. ***Herpetocetus morrowi*** **sp. nov.**, reconstructed skull and mandible based on UCMP 124950, SDNHM 65781, SDNHM 130390, SDNHM 63096, SDNHM 23057, and UCMP 219111. A, lateral view of articulated skull and mandible with mandible adducted; B, lateral view of articulated skull and mandible with mandible abducted and hypothesized musculature configured; C, ventral view of skull showing hypothesized origination points of mandibular musculature. Abbreviation: m, muscle.

Manipulation of dentaries in articulation with skulls suggests that *H. morrowi* could not abduct its dentary to greater than approximately 25° relative to the lateral edge of the maxilla. This indicates that oral volume was not increased as in balaenopteroids, but shifted towards restricted gape and decreased oral volume – counterintuitive to the notion of bulk feeding, and indicating that this puzzling anatomy was positively selected for a separate function. However, it should be noted that the only movement that is not impeded by the temporomandibular arrangement observed in *Herpetocetus* is rotation of the dentary about its longitudinal axis (alpha-rotation of Lambertsen *et al*., 1995). In fact, the inability of *Herpetocetus* to undergo omega-rotation may enhance alpha-rotation by providing a relatively fixed axis for the dentary to rotate about. Furthermore, both the superficial portion of the masseter and the medial pterygoid have large insertion areas on the dentary. Although these muscles are often associated with adduction and elevation of the dentary, they also contribute to alpha-rotation. Therefore, *H. morrowi* probably had greater torque with respect to alpha-rotation, and possibly even greater control of this movement.

Although deduction of feeding strategy is difficult in fossil mysticetes because of a lack of clear osteological correlates for specific feeding structures, it is possible to exclude certain feeding strategies given the previously mentioned observations on the

temporomandibular region of *H. morrowi*. The balaenopterid strategy of lunge feeding involves temporally discrete intervals of active engulfment of large volumes of prey-laden water while swimming forward. This is accomplished by gaping the mouth up to 90° and distending the ventral throat pouch, which inflates like a parachute and is lined by the flaccid tongue. Oral volume is further enhanced in modern balaenopterids by having a broad, flat rostrum. *Herpetocetus morrowi*, however, displays morphologies that limit the volume of prey-filled water that it is possible to intake during feeding (maximum oral volume). The rostrum of *H. morrowi*, although flattened as in balaenopterids, is noticeably attenuate and therefore limits the width of gape anteriorly (with a ratio of rostrum length to width of approximately 3.1:1 at the midpoint). As previously mentioned, *H. morrowi* was also unable to achieve the degree of delta-rotation or omega-rotation that is exhibited by modern balaenopterids during feeding. Owing to the fact that no soft tissue features are available for this taxon, it is impossible to know whether *H. morrowi* possessed rows of ventral throat grooves. However, it is unlikely that *H. morrowi* utilized lunge feeding, as it clearly has evolved a feeding apparatus that has diverged from maximizing oral volume.

Balaenoids employ passive, skim feeding to filter planktonic organisms from the water column. During skim feeding, balaenids employ hydrodynamic and hydraulic pressure to push water over the baleen and through the oral cavity in a semicontinuous manner (Werth, 2004). Skim feeding is therefore accomplished in balaenoids by swimming into prey-rich water with the mouth open for extended periods of time. The rostrum in balaenoids is highly arched to accommodate long baleen plates and the glenoid fossa is depressed far below the palate. By contrast, *H. morrowi* probably possessed exceptionally short baleen because of its flattened palate, broad median palatal keel and elevated glenoid fossa. Furthermore, the anterior opening of the oral cavity in *H. morrowi* is relatively small because of a narrow rostrum and the incapability of the mandible to achieve a high degree of delta rotation. From this insight, it can be inferred that *H. morrowi* was poorly adapted for bulk feeding from its anterior end, as in the manner of balaenopterids (El Adli & Boessenecker, 2011; Gol'din, Startsev & Krakhmalnaya, 2013). In fact, the largest feeding surface in *H. morrowi* occurs laterally because of the overall length of the rostrum.

Eschrichtius robustus is the only known modern mysticete to employ lateral suction feeding in order to obtain nourishment. In this feeding strategy, grey whales dive to the sea floor, roll to their side, and open their mouth to draw in sediment containing benthic invertebrates (Nerini, 1984). *Eschrichtius robustus* utilizes rapid depression and retraction of the tongue to create an influx of pressure in the oral cavity, which pulls water and sediment into the mouth. However, *E. robustus* has been observed using alpha-rotation of its mandible (and therefore its lower lips) to manipulate sediment into and out of its mouth during suction feeding.

The rostrum of *E. robustus* is slightly arched and relatively narrow compared with balaenopterids. *Eschrichtius robustus* also possesses the shortest baleen plates amongst extant mysticetes. Furthermore, *E. robustus* possesses two deep ventral throat grooves, which accommodate expansion of the throat during suction feeding. Although soft tissue features, such as the presence or absence of ventral throat grooves, are unavailable, several parallels can be drawn between the morphologies observed in *H. morrowi* and in *E. robustus*. As previously mentioned, the baleen plates of *H. morrowi* were probably exceptionally short, even more so than in *E. robustus*. While feeding, *E. robustus* employs a level of delta-rotation of the mandible that is not only possible, but probably enhanced in *H. morrowi*. The morphology of the posterior end of the dentary of *H. morrowi* suggests that it could employ a high degree of torque with regards to alpha-rotation, which could be utilized in manipulation of sediment, as in *E. robustus*. The posterior elongation of the angular process in *H. morrowi* also increases the force associated with adduction by increasing the length of the in-lever. This factor may be important for closing the jaws when the oral cavity is filled with heavy sediment. Finally, to compensate for the large amount of pressure on the rostrum associated with expelling water through the baleen, *E. robustus* and *H. morrowi* display a high level of interdigitation of the rostrum with the cranium.

Although it is difficult to deduce mysticete feeding strategies directly from osteological features, the high degree of specialization observed in the temporomandibular region of *H. morrowi* makes it possible to narrow down the possible options. Clearly *H. morrowi* has many features that appear optimal for lateral suction feeding, as in *E. robustus*. This is not to say that *H. morrowi* necessarily fed from the sea floor, like *E. robustus*, as it is also equally plausible that *H. morrowi* fed laterally from vertical surfaces on the continental shelf or from within kelp forests (Fig. 40). It is also possible that *H. morrowi* employed a novel strategy that has not previously been documented in mysticetes. However, without modern comparative taxa or soft tissue morphologies available it is most reasonable to assume, given the morphology of the skull and dentary, that *H. morrowi* employed lateral suction feeding as its primary strategy of obtaining nourishment.

Figure 40. Artistic reconstruction of ***Herpetocetus morrowi* sp. nov.** in the late Pliocene Pacific Ocean off southern California. The fish depicted in the upper left is a sheephead (*Semicossyphus* sp. Ayres, 1854), known from otoliths and isolated teeth from the San Diego Formation (illustration by Robert Boessenecker).

Suction feeding was hypothesized as the dominant feeding behaviour in the cetotheriid *Cet. riabinini* (Gol'din *et al*., 2013) based on particular features of the skull (e.g. narrow rostrum) in addition to some functional similarities with suction-feeding ducks. However, many of these features were attributed to suction feeding based on analogy rather than biomechanics. Given this hypothesis, it is therefore possible that the rather extreme morphology of *H. morrowi* is a more derived version of morphology observed in earlier cetotheriids like *Cet. riabinini*.

The extinction of *Herpetocetus*

It is interesting to note that although both *E. robustus* and *H. morrowi* probably employed a similar feeding strategy, only the former taxon survived into the present time. Boessenecker (2013) demonstrated that species of *Herpetocetus* survived at least to the Early to Middle Pleistocene, making *Herpetocetus* the only extinct genus of mysticete currently known from the Pleistocene. Numerous extinction and dispersal events of marine mammals occurred during the Pliocene–Pleistocene transition of the eastern North Pacific. This included the extinctions of species of the lipotid dolphin *Parapontoporia* Barnes, 1984; temperate latitude monodontids, a number of archaic porpoises (Phocoenidae) and balaenopterids, and species of the benthic feeding walrus, *Valenictus* Mitchell, 1961. In concert with these extinctions, this period was characterized by the adaptive radiation of delphinids and the dispersal of non-*Callorhinus* otariids, harbour seals (*Phoca*), elephant seals (*Mirounga*), sea otters (*Enhydra*), and grey whales (*Eschrichtius*) into the region (Boessenecker, 2011b, 2013).

Despite this turnover in Pliocene–Pleistocene marine mammals, the youngest known fossil specimen of *Herpetocetus* documents a middle Pleistocene extinction of the *Herpetocetus* lineage in the eastern North Pacific, which is long after the extinction of the Pliocene marine mammal fauna (Boessenecker, 2013), attesting to a surprisingly recent disappearance of this archaic mysticete. Pyenson & Lindberg (2011) demonstrated that the carrying capacity for *E. robustus* dropped several times throughout the Pleistocene as a result of high-amplitude eustatic sea-level changes that began in the middle Pleistocene, causing reduction in continental shelf area and, therefore, intermittent loss of optimum benthic foraging habitat. These authors speculate that *E. robustus* therefore employed a more generalized feeding strategy, which allowed the grey whale to survive extinction during middle and late Pleistocene low sea levels. The highly specialized temporomandibular morphology of species of *Herpetocetus* and its consequential inhibition of abduction of the mandible beyond 25° prohibited species of *Herpetocetus* from utilizing such active bulk feeding as a viable alternative feeding strategy during periods of minimal shelf area in glacial maxima during the middle Pleistocene. Therefore, it is reasonable to hypothesize that habitat loss, as a consequence of Pleistocene glaciation, provides a plausible hypothesis for the disappearance of this relatively long-lived genus and the ultimate extinction of a highly successful lineage of baleen whales. Thus, an era in mysticete evolutionary history concluded, ushering in the time of a completely modern mysticete fauna.

ACKNOWLEDGEMENTS

The authors would like to recognize the life and accomplishments of Jared R. Morrow for his contributions to sedimentary geology and for his tireless efforts to educate a new generation of geologists and palaeontologists. Jared's endeavours to help his students in any way possible did not go unnoticed or unappreciated. He is greatly missed. The authors would like to thank L. G. Barnes, G. Calvano, R. A. Cerutti, J. Pitt, B. O. Riney, and P. J. Sena for collection of the invaluable specimens of *H. morrowi* examined in this study. D. J. Bohaska, M. B. Goodwin, R. J. Hilton, P. A. Holroyd, C. W. Potter, N. D. Pyenson, and K. A. Randall are thanked for allowing us to study specimens under their care. Scripps Mercy Hospital is thanked for helping to produce CT images of UCMP 124950 and SDNHM 65781. The authors benefited from discussions with A. C. Dooley, E. G. Ekdale, D. C. Fisher, R. E. Fordyce, J. H. Geisler, P. D. Gingerich, F. G. Marx, C. H. Tsai, M. D. Uhen, and J. A. Wilson. This study was partially funded by an NSF grant to T. A. Deméré. Finally, the authors would like to thank S.J. Godfrey and an anonymous reviewer for their thorough and constructive comments on this manuscript. R. W. Boessenecker was supported during a portion of this study by a University of Otago Doctoral Scholarship. J. J. El Adli was partially supported during a portion of this study by a University of Michigan Department of Earth and Environmental Sciences Departmental Fellowship.

REFERENCES

Abel O. 1938. Vorlaeufige mitteilungen ueber die revision der fossilen mystacoceten aus dem Tertiaer Belgiens. *Bulletin du Musée royal d'Histoire naturelle de Belgique* **14:** 1–34.

Ayres WO. 1854. Description of new fishes from California. *Proceedings of the California Academy of Natural Sciences* **1:** 3–22.

Barnes LG. 1984. Fossil odontocetes (Mammalia: Cetacea) from the Almejas Formation, Isla Cedros, Mexico. *Paleobios* **42:** 1–46.

Bisconti M. 2001. Morphology and postnatal growth trajectory of rorqual petrosal. *Italian Journal of Zoology* **68:** 87–93.

Bisconti M. 2008. Morphology and phylogenetic relationships of a new eschrichtiid genus (Cetacea: Mysticeti) from the Early Pliocene of northern Italy. *Zoological Journal of the Linnean Society* **153:** 161–186.

Bisconti M. 2010. New description of *'Megaptera' hubachi* Dathe, 1983 based on the holotype skeleton held in the Museum für Naturkunde, Berlin. *Quaderni del Museo di Storia Naturale di Livorno* **23:** 37–68.

Bisconti M. 2012. Comparative osteology and phylogenetic relationships of *Miocaperea pulchra*, the first fossil pygmy right whale genus and species (Cetacea, Mysticeti, Neobalaenidae). *Zoological Journal of the Linnean Society* **166:** 876–911.

Boessenecker RW. 2011a. Herpetocetine (Cetacea: Mysticeti) dentaries from the Upper Miocene Santa Margarita Sandstone of Central California. *Paleobios* **30:** 1–12.

Boessenecker RW. 2011b. New records of the fur seal *Callorhinus* (Carnivora: Otariidae) from the Plio-Pleistocene Rio Dell Formation of Northern California and comments on otariid dental evolution. *Journal of Vertebrate Paleontology* **31:** 454–467.

Boessenecker RW. 2013. Pleistocene survival of an archaic dwarf baleen whale (Mysticeti: Cetotheriidae). *Die Naturwissenschaften* **100:** 365–371.

Boessenecker RW. In press. A new marine vertebrate assemblage from the Late Neogene Purisima Formation in Central California, part II: pinnipeds and cetaceans. *Geodiversitas*.

Boessenecker RW, Geisler JH. 2008. New material of the bizarre whale *Herpetocetus bramblei* from the latest Miocene Purisima Formation of Central California. *Journal of Vertebrate Paleontology* **28:** 54A.

Bouetel V, de Muizon C. 2006. The anatomy and relationships of *Piscobalaena nana* (Cetacea, Mysticeti), a Cetotheriidae ss from the early Pliocene of Peru. *Geodiversitas* **28:** 319–395.

Brandt J. 1843. De Cetotherio, novo balaenarum familiae genere. *Bulletin de l'Académie Impériale des Sciences de Saint Pétersbourg* **2:** 145–148.

Brandt J. 1872. Über eine neue Classification der Bartenwale (Balaenoidea) mit. *Bulletin de l'Académie Impériale des Sciences de St.-Pétersbourg* **17:** 113–124.

Bremer K. 1994. Branch support and tree stability. *Cladistics* **10:** 295–304.

Brisson MJ. 1762. *Regnum animale in classes IX.: distributum, sive synopsis methocica sistens generalem animalium distributionem in classes IX, & duarum primarum classium, quadrupedum scilicet & cetaceorum, particularem divisionem in ordines, sectiones, genera & species*. apud T. Haak.

Churchill M, Berta A, Deméré TA. 2012. The systematics of right whales (Mysticeti: Balaenidae). *Marine Mammal Science* **28:** 497–521.

Cope ED. 1896. Sixth contribution to the knowledge of the Miocene fauna of North Carolina. *Proceedings of the American Philosophical Society* **35:** 139–146.

Deméré TA. 1986. The fossil whale, *Balaenoptera davidsonii* (Cope 1872), with a review of other Neogene species of Balaenoptera (Cetacea: Mysticeti). *Marine Mammal Science* **2:** 277–298.

Deméré TA, Berta A, McGowen MR. 2005. The taxonomic and evolutionary history of fossil and modern balaenopteroid mysticetes. *Journal of Mammalian Evolution* **12:** 99–143.

Deméré TA, McGowen MR, Berta A, Gatesy J. 2008. Morphological and molecular evidence for a stepwise evolutionary transition from teeth to baleen in mysticete whales. *Systematic Biology* **57:** 15–37.

Dollo L. 1909. The fossil vertebrates of Belgium. *Annals of the New York Academy of Sciences* **19:** 99–119.

Ekdale EG, Berta A, Deméré TA. 2011. The comparative osteology of the petrotympanic complex (ear region) of extant baleen whales (Cetacea: Mysticeti). *PLoS ONE* **6:** e21311.

El Adli JJ, Boessenecker RW. 2011. The musculature of the temporomandibular region in the Mio-Pliocene baleen [whale] genus *Herpetocetus* and its inference for feeding strategy. *Journal of Vertebrate Paleontology* **31:** 104A.

Fordyce RE, Marx FG. 2012. The pygmy right whale *Caperea marginata*: the last of the cetotheres. *Proceedings of the Royal Society B* **280:** 20122645.

Geisler JH, Luo Z. 1996. The petrosal and inner ear of *Herpetocetus sp.* (Mammalia: Cetacea) and their implications for the phylogeny and hearing of archaic mysticetes. *Journal of Paleontology* **70:** 1045–1066.

Godfrey SL, Geisler JH, Fitzgerald EMG. 2013. On the olfactory anatomy in an archaic whale (Protocetidae, Cetacea) and the minke whale *Balaenoptera acutorostrata* (Balaenopteridae, Cetacea). *The Anatomical Record* **296:** 257–272.

Gol'din P, Startsev D, Krakhmalnaya T. 2013. The anatomy of *Cetotherium riabinini* Hofstein, 1948, a baleen whale from the late Miocene of Ukraine. *Acta Palaeontologica Polonica*. doi: http://dx.doi.org/10.4202/app.2012.0107

Goloboff PA, Farris JS, Nixon KC. 2008. TNT, a free program for phylogenetic analysis. *Cladistics* **24:** 774–786.

Gray JE. 1864. Notes on the whalebone-whales; with a synopsis of the species. *The Annals and Magazine of Natural History* **14:** 345–353.

Hatai K, Hayasaka S, Masuda K. 1963. Some fossil tympanics from the Mizuho period of northern Japan. *Saito Ho-on Kai Museum of Natural History, Research Bulletin* **32:** 5–17.

de Heinzelin J. 1955. Considérations nouvelles sur le Néogène de l'Ouest de l'Europe. *Bulletin de la Societé belge de Géologie* **64:** 463–476.

Hofstein ID. 1948. Pachyostosis in fossil whales. *Zbirnyk Prats Z Paleontologii I Stratygrafii, Instytut Geologichnych Nauk URSR* **1:** 65–75.

Kellogg R. 1924. Description of a new genus and species of whalebone whale from the Calvert Cliffs, Maryland.

Proceedings of the United States National Museum **63:** 1–14.

Kellogg R. 1929. A new cetothere from southern California. *Bulletin, University of California Publications in Geological Sciences* **18:** 449–457.

Kellogg R. 1965a. Fossil marine mammals from the Miocene Calvert Formation of Maryland and Virginia. *United States National Museum Bulletin* **247:** 1–45.

Kellogg R. 1965b. A new whalebone whale from the Miocene Calvert Formation. *United States National Museum Bulletin* **247:** 1–45.

Kellogg R. 1968. A sharp-nosed cetothere from the Miocene Calvert. *United States National Museum Bulletin* **247:** 163–173.

Kimura T, Ozawa T. 2002. A new cetothere (Cetacea: Mysticeti) from the early Miocene of Japan. *Journal of Vertebrate Paleontology* **22:** 684–702.

Lacépède BGE. 1804. *Histoire naturelle des Cetaces*. Paris: Chez Plassan.

Laga P, Louwye S, Geets S. 2001. Paleogene and neogene lithostratigraphic units (Belgium). *Geologica Belgica* **4:** 135–152.

Lambertsen RL, Ulrich N, Straley J. 1995. Frontomandibular stay of Balaenopteridae: a mechanism for momentum recapture during feeding. *Journal of Mammology* **76:** 877–899.

Lesson RP. 1828. *Histoire Naturelle, Générale et Particulière des Mammifères et des Oiseaux Découverts depuis 1788 jusqu'à nos Jours. Complément des oeuvres de Buffon, ou historie naturelle des animaux rares découverts par les naturalistes et les voyageurs depuis la mort de Buffon. Tom. 1 Cétacés*. Paris: Baudoin Frères, 1–442.

Linnaeus C. 1758. *Systema naturae. 10th ed., vol. 1.* Holmiae.

Louwye S, Laga P. 1998. Dinoflagellate cysts of the shallow marine Neogene succession in the Kalmthout well, northern Belgium. *Bulletin of the Geological Society of Denmark* **45:** 73–86.

Louwye S, Marquet R, Bosselaers M, Lambert O. 2000. Stratigraphy of an Early-Middle Miocene sequence near Antwerp in northern Belgium (southern North Sea Basin). *Geologica Belgica* **13:** 269–284.

Marx FG. 2010. The more the merrier? A large cladistic analysis of mysticetes, and comments on the transition from teeth to baleen. *Journal of Mammal Evolution* **18:** 77–100.

Marx FG, Buono MR, Fordyce RE, Boessenecker RW. 2013. Juvenile morphology: a clue to the origins of the most mysterious of mysticetes? *Die Naturwissenschaften* **100:** 257–261.

McGowen MR, Spaulding M, Gatesy J. 2009. Divergence date estimation and a comprehensive molecular tree of extant cetaceans. *Molecular Phylogenetics and Evolution* **53:** 891–906.

Mead JG, Fordyce RE. 2009. The therian skull: a lexicon with emphasis on the odontocetes. *Smithsonian Contributions to Zoology* **627:** 1–248.

Mitchell ED. 1961. A new walrus from the Imperial Pliocene of southern California: with notes on odobenid and otariid humeri. *Los Angeles County Museum Contributions in Science* **44:** 1–28.

Mitchell ED. 1989. A new cetacean from the Late Eocene La Meseta Formation Seymour Island, Antarctic Peninsula. *Canadian Journal of Fisheries and Aquatic Sciences* **46:** 2219–2235.

Mourlon M. 1876. *Etudes stratigraphiques sur les Dépots Miocènes supérieurs et Pliocènes de Belgique*. Brussels: Imprimeur de l'Académie royale de Belgique.

Nerini M. 1984. A review of gray whale feeding ecology. In: Jones, ML, Swartz, SL, Leatherwood, S, eds. *The Gray Whale*. San Diego: Academic Press, Inc., 423–450.

Oishi M, Hasegawa Y. 1994. Diversity of Pliocene mysticetes from eastern Japan. *Island Arc* **3:** 436–452.

Pilleri G, Siber H. 1989. Neuer spättertiärer cetotherid (Cetacea, Mysticeti) aus der Pisco Formation Perus. *Beiträge zur Paläontologie der Cetaceen Perus:* Bern: Hirnanatomisches Institut, Ostermundigen, 108–115.

Pivorunas A. 1977. The fibrocartilage skeleton and related structures of the ventral pouch of balaenopterid whales. *Journal of Morphology* **151:** 299–313.

Powell CL II, Barron JA, Sarna-Wojcicki AM, Clark JC, Perry FA, Brabb EE, Fleck RJ. 2007. Age, stratigraphy, and correlation of the late Neogene Purisima Formation, Central California Coast Ranges. *U.S. Geological Survey Professional Paper* **1740:** 1–32.

Pyenson ND, Lindberg DR. 2011. What happened to gray whales during the Pleistocene? The ecological impact of sea-level change on benthic feeding areas in the North Pacific Ocean. *PLoS ONE* **6:** e21295.

Rasband WS. 1997. *ImageJ*. Bethesda, MD: US National Institutes of Health. Available at: http://imagej.nih.gov/ij/

Ridewood WG. 1923. Observations on the skull in foetal specimens of whales of the genera *Megaptera* and *Balaenoptera*. *Philosophical Transactions of the Royal Society of London, Series B* **211:** 209–272.

Rychel AL, Reeder TW, Berta A. 2004. Phylogeny of mysticete whales based on mitochondrial and nuclear data. *Molecular Phylogenetics and Evolution* **32:** 892–901.

Schulte W. 1916. Anatomy of a foetus of *Balaenoptera borealis*. *Memoir of the American Museum of Natural History* **1:** 389–502.

Slater GJ, Price SA, Santini F, Alfaro ME. 2010. Diversity versus disparity and the radiation of modern cetaceans. *Proceedings of the Royal Society B* **277:** 3097–3104.

Steeman ME. 2007. Cladistic analysis and a revised classification of fossil and recent mysticetes. *Zoological Journal of the Linnean Society* **150:** 875–894.

Swofford DL. 2003. *PAUP*: phylogenetic analysis using parsimony* (**and other methods*), v. 4.0 b10. Sunderland, MA: Sinauer Associates.

Uhen MD. 2004. Form, function, and anatomy of *Dorudon atrox* (Mammalia, Cetacea): an archaeocete from the middle to late Eocene of Egypt. *University of Michigan Papers on Paleontology* **34:** 1–222.

Van Beneden P. 1872. Les baleines fossiles d'Anvers. *Bulletins de l'Academie royale des Sciences, des Lettres et des Beaux – Arts de Belgique* **2:** 6–20.

Van Beneden PJ. 1882. Description des ossements fossiles des environs d'Anvers: III. (Planches) Genres: *Megaptera*, *Balaenoptera*, *Burtinopsis* & *Erpetocetus*. *Annales du Musée Royal d'Histoire Naturelle de Belgique* **7:** 1–90.

Van Beneden PJ. 1886. Description des ossements fossiles des environs d'Anvers: V. (Planches) Genres: *Amphicetus*, *Heterocetus*, *Mesocetus*, *Idiocetus* & *Isocetus*. *Annales du Musée Royal d'Histoire Naturelle de Belgique* **13:** 1–139.

Walsh BM, Berta A. 2011. Occipital ossification of balaenopteroid mysticetes. *The Anatomical Record: Advances in Integrative Anatomy and Evolutionary Biology* **294:** 391–398.

Werth AJ. 2004. Models of hydrodynamic flow in the bowhead whale filter feeding apparatus. *Journal of Experimental Biology* **207:** 3569–3580.

Whitmore F, Barnes L. 2008. The Herpetocetinae, a new subfamily of extinct baleen whales (Mammalia, Cetacea, Cetotheriidae). *Virginia Museum of Natural History Special Publication* **14:** 141–180.

Yang X. 2009. Bayesian inference on cetacean phylogeny based on mitochondrial genomes. *Biologia* **64:** 811–818.

SUPPORTING INFORMATION

Additional Supporting Information may be found in the online version of this article at the publisher's web-site:

Appendix S1. Specimens utilized.
Appendix S2. Character list.
Appendix S3. Character-taxon data matrix.